Broadband Linearization Technologies for Broadband Radio-over-Fiber Transmission Systems

Ran Zhu

A Thesis

In the Department

of

Electrical and Computer Engineering

Presented in Partial Fulfillment of the Requirements

For the Degree of

Doctor of Philosophy (Electrical and Computer Engineering) at

Concordia University

Montreal, Quebec, Canada

August, 2015

© Ran Zhu, 2015

CONCORDIA UNIVERSITY
SCHOOL OF GRADUATE STUDIES

This is to certify that the thesis prepared

By: Ran Zhu

Entitled: Broadband Linearization Technologies for Broadband Radio-over-Fiber Transmission Systems

and submitted in partial fulfillment of the requirements for the degree of

Doctor of Philosophy (Electrical and Computer Engineering)

complies with the regulations of the University and meets the accepted standards with respect to originality and quality.

Signed by the final examining committee:

_____ Chair
Dr. L. Wang

_____ External Examiner
Dr. J. Azana

_____ External to Program
Dr. C. Wang

_____ Examiner
Dr. M. Mehmet Ali

_____ Examiner
Dr. R. Paknys

_____ Thesis Supervisor
Dr. J.X. Zhang

Approved by: _____
Dr. A.R. Sebak, Graduate Program Director

August 28, 2015 _____
Dr. A. Asif, Dean
Faculty of Engineering & Computer Science

ABSTRACT

Broadband Linearization Technologies for Broadband Radio-over-Fiber Transmission Systems

Ran Zhu, Ph.D.

Concordia University, 2015

Wireless access networks consist of three sections, i.e., back-haul, front-haul, and wireless transmission, where the front-haul transmission systems are to distribute radio frequency (RF) signals to antenna towers. For current low-capacity wireless access, RF signals over coaxial cables, digital fiber-optic transmission, microwave point-to-point transmission, and narrowband radio-over-fiber (RoF) transmission have been used for the front-haul transmission systems. However, with the increase of demand of high capacity wireless access and also use of massive multiple-input and multiple-output (MIMO) antennas, low-cost, simple and broadband front-haul transmission systems are required in current 4G and in particular the future 5G wireless.

RoF transmission system, which is based on optical subcarrier modulation, combines the advantages of both optical fiber and radio transmission, where the optical fiber has low loss, low cost, extremely high capacity, lightweight, and immunity to electromagnetic interference, and the radio transmission simplifies remote radio units (RRUs) at antenna towers. Furthermore, radio transmission based front-haul is transparent to RF signal frequency and wireless protocol, i.e., upgradable, in addition to simplified RRUs.

Unfortunately, RoF is an analog optical transmission, and it is well known that any analog transmission is susceptible to nonlinear distortion. To be more specific, nonlinear distortion is the major limit for RoF transmission. In fact, all inline functional optical and electrical components used in RoF transmission systems may induce the nonlinear distortion. Specifically in RoF based front-haul systems, two key functions, i.e., RF

power amplification and optical subcarrier modulation, are the main factors in introducing nonlinear distortions. The nonlinear distortions from RF power amplifiers (PAs) have been studied for decades. Therefore, the nonlinear distortions from the optical subcarrier modulation are the main concern in this thesis. The nonlinear distortions include harmonic distortions (HDs) and intermodulation distortions (IMDs). For narrow band RF signals, the HDs can be suppressed by RF filtering, but it may be impossible for the IMDs to be filtered out. For broadband RF signals, both HDs and IMDs could fall in the passband of RF signals and introduce crosstalk, and therefore both of them are required to be suppressed, i.e., linearization required.

In the past decades, linearization for RF PAs has been investigated extensively, mainly focusing on signal processing based linearization, i.e., digital linearization. Unfortunately, the digital linearization is typically limited to the RF signals with up to 20 MHz bandwidth. Based on the current technologies of signal processing hardware, linearization for 1 GHz RF signals can be done, but the complexity and cost are beyond the practical applications. In order to explore broadband RoF transmission systems that support broadband front-haul, simple, low cost, and broadband linearization is pivotal.

In this thesis, two linearization technologies for RoF transmission systems are investigated comprehensively, i.e., analog predistortion circuit (PDC) and dual wavelength optical linearization. Two novel PDCs are designed and investigated to suppress 3rd order IMD (IMD3) of RoF transmission systems. The PDCs have the advantages of broad bandwidth, compact size, and low cost. The first PDC is designed to have a bandwidth from 7 to 18 GHz, using two zero-bias Gallium Arsenide (GaAs) Schottky diodes as predistorter. The linearization using this PDC is verified in externally modulated RoF transmission systems. When a Mach-Zehnder modulator (MZM) is used for the optical subcarrier modulation, the input power at 1 dB compression point (P_{1dB}) of the RoF transmission system is improved by 0.4 and up to 2.2 dB from 7 to 18 GHz. The spurious-free dynamic range (SFDR) is improved by more than ~10 dB from 7 to 14 GHz and ~6 dB from 15 to 18 GHz. When an electro-absorption modulator (EAM) is used, the input P_{1dB} is improved by 0.8 and up to 3.8 dB from 8 to 17 GHz. The SFDR is improved by more than ~9 dB from 7 to 14 GHz and ~4 dB from 15 to 18 GHz.

The second PDC is designed to have an ultra broad bandwidth from 10 MHz to 30 GHz, using a dual Schottky diode as the predistorter. The linearization using this PDC is investigated in both directly and externally modulated RoF transmission systems. The SFDR at 8 GHz is improved by 11.9 dB for a directly modulated RoF transmission. The SFDR is improved by more than 10 dB from 1 to 5 GHz and more than 5 dB from 1 to 30 GHz for an externally EAM modulated RoF transmission. Similarly, the SFDR is improved by more than 12 dB from 2 to 5 GHz and more than 5 dB from 2 to 30 GHz for an externally MZM modulated RoF transmission. When WiFi signals are transmitted over the externally modulated RoF systems for back-to-back (BTB) and 20 km single mode fiber (SMF), the error vector magnitudes (EVMs) are improved by 0.4 and up to 5.1 dB by using the PDC.

Dual wavelength linearization (DWL) technique is investigated compressively to suppress 2^{nd} and 3^{rd} order nonlinearities of externally modulated RoF transmission systems simultaneously, including HDs and IMDs. The linearization is verified in both EAM and MZM modulated RoF transmission systems. Theoretical analysis is given for the first time to understand DWL technique. The experimental results agree with the theoretical analyses. In the externally EAM modulated RoF transmission systems, when the 2^{nd} order nonlinearity is maximally suppressed, 11.5 and 1.8 dB improvements of the SFDRs with respect to HD2 and HD3 respectively are achieved by using DWL simultaneously. 8.5 and 1.3 dB improvements of the SFDRs with respect to IMD2 and IMD3 respectively are also achieved. Correspondingly, 3 and 4 dB improvements of the input and output P_{1dB}s respectively are obtained. When the 3^{rd} order nonlinearity is maximally suppressed, the SFDRs with respect to HD3 and IMD3 are improved by 8.1 and 20.4 dB, respectively, and corresponding 7.7 and 11.7 dB improvements of the input and output P_{1dB}s respectively are achieved. Furthermore, IMD5 is also suppressed, and the $SFDR_5$ with respect to IMD5 is improved by 7.1 dB. Moreover, the RoF transmission of WiFi signals at 2.4 and 5 GHz are also linearized by using DWL technique. 3.5 dB at 2.4 GHz and 2.8 dB at 5 GHz improvements of the EVMs are obtained.

For an externally MZM modulated RoF transmission system, DWL is also investigated theoretically and experimentally. In the system, it is found that the SFDRs with respect

to HD2 and HD3 are both improved at the same time when the even order nonlinearities are suppressed, in which the power of the RF signal and 3rd order nonlinearity is increased by the same level. Thus, the $SFDR_3$ is still improved even the 3rd order nonlinearity is increased. Compared to using a single 1553 nm laser, the SFDRs with respect to HD2 and HD3 are improved by 38.4 and 12.1 dB.

ACKNOWLEDGEMENTS

I would like to express my sincere thanks to my supervisor Prof. John Xiupu Zhang for his advice, help, and support for me to finish this thesis.

I am grateful to my wife Dr. Ye Zhang for her love and encouragement.

I would like to thank my parents for their love, understanding, and support.

I would like to express my thanks to Prof. Glenn Cowan for his help.

I would also like to express my thanks to my colleagues and friends for their help in my life and study, especially to Dr. Hakim Mellah and Dr. Zouhair Briqech.

Table of Contents

List of Figures

List of Tables

List of Abbreviations

ACP	Adjacent Channel Power
ADC	Analog-to-Digital Converter
AM-AM	Amplitude-to-Amplitude
ASE	Amplified Spontaneous Emission
ATT	Attenuator
AWG	Arbitrary Waveform Generator
BTB	Back-to-Back
CD	Chromatic Dispersion
CDP	Carrier Density Pulsation
CPRI	Central Public Radio Interface
CPU	Central Process Unit
CW	Continuous Wave
C-Ran	Cloud Radio Access Network
DAC	Digital-to-Analog Converter
DCF	Dispersion Compensated Fiber
DPD	Digital Predistortion
DPP	Digital Post Processing
DSB	Double Sideband
DSB-SC	Double-Sideband Suppressed-Carrier
DSO	Digital Storage Oscilloscope
DSP	Digital Signal Processing

DWL	Dual Wavelength Linearization
EAM	Electro-Absorption Modulator
EDFA	Erbium Doped Fiber Amplifier
EML	Electro-Absorption Modulated Laser
EVM	Error Vector Magnitude
FWM	Four-Wave Mixing
GaAs	Gallium Arsenide
HD	Harmonic Distortion
HD2	2^{nd} Order Harmonic Distortion
HD3	3^{rd} Order Harmonic Distortion
IC	Integrated Circuit
IMD	Intermodulation Distortion
IMD2	2^{nd} Order Intermodulation Distortion
IMD3	3^{rd} Order Intermodulation Distortion
IMD5	5^{th} Order Intermodulation Distortion
IMD7	7^{th} Order Intermodulation Distortion
IP	Intercept Point
$LiNbO_3$	Lithium Niobate
LNA	Low Noise Amplifier
LP	Linear Polarizer
MIMO	Multiple-Input and Multiple-Output
MMF	Multi Mode Fiber

MP	Mixed-Polarization
MZI	Mach-Zehnder Interferometer
MZM	Mach-Zehnder Modulator
NF	Noise Figure
OC	Optical Coupler
OFDM	Orthogonal Frequency-Division Multiplexing
ORx	Optical Receiver
OTN	Optical Transport Network
OTx	Optical Transmitter
P_{1dB}	Input power at 1-dB compression point
PA	Power Amplifier
PC	Polarization Controller
PCB	Printed Circuit Board
PD	Photodetector
PDC	Predistortion Circuit
QAM	Quadrature Amplitude Modulation
RF	Radio Frequency
RoF	Radio-over-Fiber
RRU	Remote Radio Unit
SA	Spectrum Analyzer
SFDR	Spurious Free Dynamic Range
SMF	Single Mode Fiber

SOA	Semiconductor Optical Amplifier
SSB	Single Sideband
TE	Transverse Electric
TIA	Transimpedance Amplifier
TM	Transverse Magnetic
UWB	Ultra Wideband
VNA	Vector Network Analyzer
WPD	Wilkinson Power Divider

List of Symbols

a_n	n^{th} order coefficient of the PDC
b_n	n^{th} order coefficient of the RoF system
c	Speed of the light in the vacuum
C_k	k^{th} order coefficient of the polynomial
d	Thickness of the active layer
D	Dispersion coefficient
e	Electron charge
E_{FWM_DC}	Electric field of the FWM light for the DC modulation
E_{in}	Input electric field
E_{out}	Output electric field
E_{out_DSB}	Output electric field for the optical DSB modulation
$E_{out\_DSB\text{-}SC}$	Output electric field for the optical DSB-SC modulation
E_{out_SSB}	Output electric field for the optical SSB modulation
E_p	Amplitude of the optical field of the pump light
f	Frequency
g	Gain coefficient
G_A	Gain/loss induced by the photon-electron conversion
G_{A0}	Transmission of the EAM without the pulsation
I	Photocurrent
J	Current density
$J_n(\,)$	n^{th} order Bessel function of the first kind

L	Length or loss
N	Carrier density
P	Photon density per unit time
P_0	Photon density per unit time without the pulsation
P_i	Optical input power
P_{in}	Optical input power
P_{out}	Optical output power
R	Responsivity
t	Time
T	Transmission
T_k	k^{th} order coefficient of the exponential polynomial
V	Applied voltage
V_{bias}	Bias voltage
V_{DC}	DC bias voltage
V_{eff}	Effective RF voltage
V_{in}	Input voltage
V_{out}	Output voltage
V_{RF}	RF signal voltage
V_π	Half-wave voltage
α_c	Linewidth enhancement factor
$\Delta\omega$	Difference of the angular frequencies
η	Refractive index

θ	Phase of the applied voltage
λ	Wavelength
τ	Carrier recombination time
ω	Angular frequency
ω_p	Angular frequency of the pump light
ω_{RF}	Angular frequency of the RF signal
$\hbar$	Reduced Planck constant

Chapter 1 Introduction

1.1 Radio-over-Fiber Transmission Systems

More and more customers are attracted by the diverse services and entertainments based on wireless mobile devices. The dramatic increase in the use of smart phones, tablets, and other mobile data consuming devices, combined with the advanced applications, is requiring high capacity heterogeneous wireless networks. Because of the increasing density of remote radio units (RRUs) and the enhanced diversity of wireless communication technologies, back-haul and front-haul networks are developed to support the wireless access network as shown in Figure 1-1.

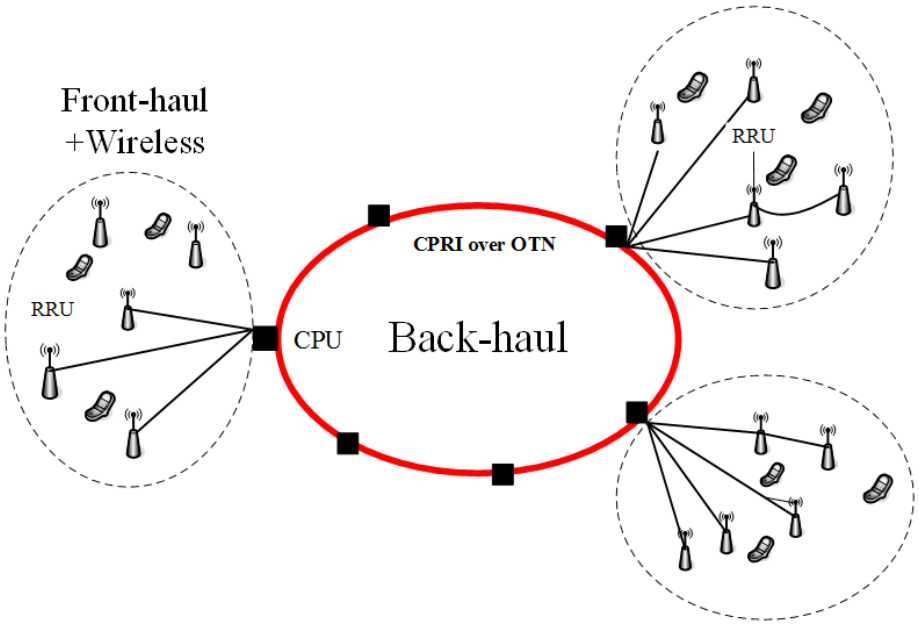

Figure 1-1 Schematic of wireless access networks including back-haul and front-haul as well as wireless networks. CPRI: Common Public Radio Interface, OTN: Optical transport network, RRU: remote radio unit, CPU: central process unit.

High capacity digital fiber systems can be used in the back-haul networks to transmit baseband signals. For the front-haul networks, traditional techniques for wireless signals distributed to antenna towers are based on narrow band analog radio frequency (RF) transmission over coaxial cable, digital fiber transmission, narrow band analog point to

point microwave transmission, and narrow band analog radio-over-fiber (RoF) transmission, etc. Microwave coaxial cable is too costly, and high frequency signals suffer from high loss in the cable. Compared to the microwave coaxial cable, the optical fiber has the features of extremely broad bandwidth, low cost, low loss, light weight, safety, and immunity to electromagnetic interference. Digital fiber transmission studied for decades is a matured technology [1]-[9]. It has been used widely for digital signal transmission. But the digital fiber transmission has a serious drawback for wireless signal distribution: The antenna tower site, i.e., the RRU, is very complicated since digital to/from analog signal processing is required. The microwave point-to-point transmission is more suitable for buildings in dense cities, and doesn't support long distance and high capacity wireless signal transmission. And the quality of the transmitted signal through microwave transmission is extremely susceptible to the environmental conditions, especially the rainfall.

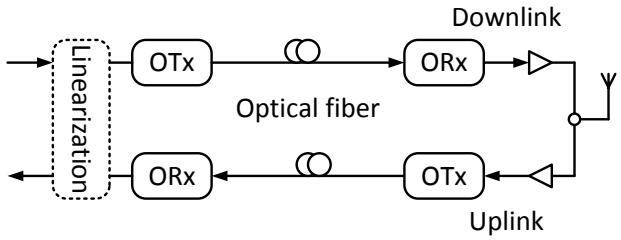

Figure 1-2 Schematic of an RoF transmission system. OTx: optical transmitter. ORx: optical receiver.

RoF transmission system is an appropriate solution for the front-haul networks in broadband wireless access [10]-[19]. The RoF based front-haul systems are shown in Figure 1-2. The RoF system is to directly transmit analog RF signals over fiber from central process unit (CPU) to RRUs, and vice versa, which has been used since 1990s for narrow band wireless signal distribution. Due to the upcoming broadband applications, such as LTE and LTE advanced with the application of multiple-input and multiple-output (MIMO), RoF transmission system has become a hot technology for the future cloud radio access networks (C-RANs).

RoF transmission systems combine the advantages of the optical fiber and wireless access. In the downlink, RF signals are generated and up-converted to specific subcarrier frequencies in the CPU. The optical transmitter (OTx) is used to modulate optical carrier

with the RF signals. Thus, the RF signals are carried by the optical carrier and then transported by the optical carrier through optical fiber from CPU to RRUs. Usually single mode fiber (SMF) is used because it is cheap and provides better performance in bandwidth and transmission distance. Moreover, compared to the SMF, multi-mode fiber (MMF) induces severer mode dispersion. An optical receiver (ORx) at the RRU is used to demodulate optical signals to RF signals. The demodulated RF signals are distributed by RF amplifiers and antennas. In the uplink, the received RF signals from the antennas are amplified and then used to modulate an optical carrier by an OTx at the RRU. After the transmission in the optical fiber, an ORx demodulates the light. The demodulated RF signals are down-converted and processed at the CPU. The up/down-conversions, analog-to-digital/digital-to-analog converters (ADCs/DACs), and signal processing are moved to the CPU. The ORx is usually a photodiode (PD), and the OTx could be a laser or a laser plus an external modulator. The modulation using a laser is called direct modulation and the modulation using a laser plus an external modulator is called external modulation. Direct modulation is simpler than external modulation, but external modulation has lower chirp and higher bandwidth compared to the direct modulation. Chirp could induce phase distortion and signal spectrum broadening, and also makes chromatic dispersion (CD) more severe. The CD is a phenomenon that lights with different wavelengths in an optical pulse in the optical fiber move with different velocities so that the pulse is broadened. To reduce CD, optical single sideband (SSB) modulation [20]-[22] and dispersion compensating fiber (DCF) [23], [24] are studied. Optical SSB modulation can be achieved by accurately adjusting DC bias and phase difference between the two RF inputs of a Mach-Zehnder modulator (MZM). Compared to optical double sideband (DSB) modulation, SSB modulation generates only one optical sideband so that lower bandwidth is occupied, thus the CD is reduced. It also can be used to compensate for the power fading caused by the CD. DCF is dispersive fiber with negative dispersion coefficient. The dispersion induced by DCF can be used to compensate for that induced by SMF. Since the signal processing, ADC/DAC, and up/down-conversions are located at the CPUs in RoF systems, and thus the RRUs are simplified. More importantly, the RoF transmission systems are transparent to wireless bit rates, wireless carrier frequencies, and also wireless protocols. The transparent infrastructure and centralization make not

only the replacement and maintenance easier, but also the dynamic cloud access achievable. This is the main reason why the RoF has been revisited by academia and industries recently.

Nowadays, many companies offer a variety of RoF solutions and products. After acquisitions of Avaya Connectivity Solutions, Andrew Inc., and TE Connectivity, Commscope provides wired and wireless networks solutions including fiber-to-the-antenna connectivity. Photonic Systems Inc. and RF Optic Ltd. design RoF transmitters, receivers, and links up to 20 GHz. Microwave Photonic Systems Inc. designs RoF modules up to 18 GHz. ViaLite Communications provides RoF link up to 100 km transmission and up to 4.2 GHz. Moreover, Emcore, Fiber-Span, Pharad, Foxcom, and Finisar also have RoF module designs up to 3 GHz.

1.2 Motivations and Contributions

RoF transmission systems are based on optical subcarrier modulation and analog optical transmission and therefore are susceptible to nonlinear distortions. So the suppression of nonlinear distortions, i.e., linearization, is the key technique for successful application of RoF transmission systems for broadband front-haul networks. Nonlinear distortions are caused by nonlinear characteristics of the microwave and optical components in RoF transmission systems. Two main sources of the nonlinearities in RoF transmission systems are optical subcarrier modulation and RF power amplification. Nonlinearities can generate spurious signals that may overlap with the desired RF signals, so that the transmission performance is degraded and the transmission system cannot conform to the standards of the applications.

3^{rd} order intermodulation distortion (IMD3) has been considered in most cases. This is because the IMD3 certainly falls in the passband of the RF signals. However, when broadband and/or multi-band wireless signals, which have been suggested by LTE-advanced, are transmitted, 2^{nd} order nonlinearities and harmonic distortions (HDs) may also generate spurious components that overlap with the RF signals. Consequently, the

suppressions of both the 2nd and 3rd order nonlinearities should be considered in RoF transmissions systems.

For the RoF downlink in Figure 1-2, the main sources of the nonlinearities stem from the optical subcarrier modulation at the CPU and the RF power amplifiers (PAs) at the RRU. While for the RoF uplinks in Figure 1-2, the nonlinearities originate from the optical subcarrier modulation at the RRU. If the RF PAs work in almost the saturation, the nonlinearities from the PAs are comparable to the optical subcarrier modulation. Otherwise the nonlinearities from the optical subcarrier modulation are dominant. The rest of the components also introduce nonlinearities, but typically very small compared to the above.

In this thesis, the research focuses on the linearization technologies of RoF transmission systems, includes the analog predistortion circuit (PDC) and optical linearization technologies are studied and proposed. The main contributions include:

(1) A broadband analog PDC based on zero bias Schottky diodes is designed and proposed to linearize the externally modulated RoF transmission systems. Broadband linearization from 7 to 18 GHz and low power consumption is obtained. The dimension of the PDC is 3.5×1.6 cm^2.
(2) A novel ultra broadband analog PDC based on monolithic dual Schottky diode is designed and proposed to linearize the directly and externally modulated RoF transmission systems. Ultra broadband linearization from 10 MHz to 30 GHz is obtained. The dimension is further reduced to 2.4×1 cm^2.
(3) Dual wavelength linearization (DWL) technique is studied to suppress 2nd and 3rd order nonlinearities generated by electro-absorption modulator (EAM) simultaneously in an RoF transmission system. Theoretical model and experiment are presented.
(4) DWL technique is studied to improve the spurious-free dynamic ranges (SFDRs) with respect to 2nd and 3rd order nonlinearities simultaneously in an RoF transmission system using an MZM. Theoretical model and experiment are presented.

1.3 Organization of the Thesis

In this chapter, the basic concepts of RoF transmission systems have been introduced. The nonlinearities from RoF transmission systems are also introduced briefly. The motivations and contributions of the research are given.

Chapter 2 introduces the background of RoF transmission systems. The literature review about the linearization technologies for RoF transmission systems is presented and discussed.

In Chapter 3, a broadband analog PDC using zero bias Schottky diodes is designed and experimentally verified to linearize externally modulated RoF transmission systems. The experiments are given.

In Chapter 4, an ultra broadband analog PDC based on monolithic dual Schottky diode is designed and experimentally verified to linearize directly and externally modulated RoF transmission systems. And the experiments are given.

In Chapter 5, DWL technique is proposed to linearize the externally modulated RoF transmission systems. Theoretical models are given, and the simulation based on the model is presented to predict the performance of the technique. The experiments are presented to verify the model.

In Chapter 6, the research is summarized. And the future works on the linearization technologies for the RoF transmission systems are suggested.

Chapter 2 Background and Literature Review

2.1 Introduction

In recent two decades, RoF technologies have been attracting attention because they provide a solution for the delivery and distribution of broadband RF signals. Based on the analog optical transmission and optical subcarrier modulation, RoF transmission systems distribute RF signals directly through the optical fibers. RoF transmission systems are different from the conventional digital optical transmission systems. In this chapter, the key technologies employed in RoF transmission systems are introduced briefly. The nonlinearities in RoF transmission systems are also introduced. A review about the linearization technologies for RoF systems is presented and discussed.

2.2 RoF Technologies

2.1.1 Optical Subcarrier Modulation

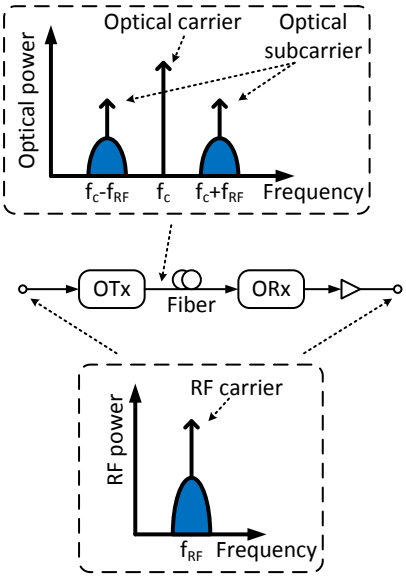

Figure 2-1 Schematic of optical subcarrier modulation.

The principle schematic of the optical subcarrier modulation is given in Figure 2-1. In Figure 2-1, the optical carrier is double sideband modulated with a RF signal in an OTx.

Then the RF signal is carried by the optical carrier, i.e., the RF carrier in RF domain is transferred to the subcarrier in optical domain. This process is called optical subcarrier modulation. It can be seen that the optical spectrum occupies double bandwidth of that the RF signal occupied in the RF spectrum. Compared to the digital optical modulation in digital optical fiber systems, optical subcarrier modulation leads to broad bandwidth occupation. Thus the system is more susceptible to CD and nonlinear distortions.

2.2.1 Direct Modulation of Laser

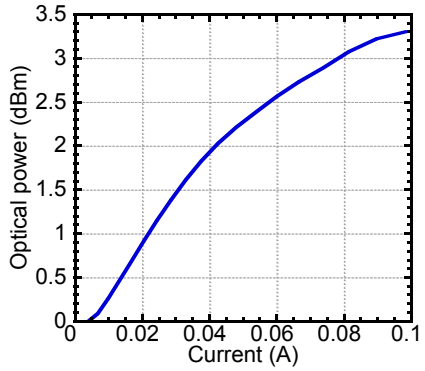

Figure 2-2 Transmission characteristic of a directly modulated laser.

Optical modulation includes direct and external modulation. Direct modulation is the technique that the intensity of a laser is modulated directly by the electrical current. Despite of the simple implementation, the direct modulation is limited by the bandwidth and chirp of the laser. The chirp could induce frequency and phase distortions. The measured transmission characteristic of a directly modulated laser is shown in Figure 2-2. When the bias current is higher than the threshold of the laser, the optical output power is almost proportional to the bias current. Nevertheless, it is obvious that the transmission characteristic is nonlinear. In the direct modulation, only the magnitude of the optical carrier can be modulated.

2.2.2 External Modulation of EAM

EAM and MZM are the two modulators used for the external modulation. The EAM is designed in the method of semiconductor waveguide with an electrode for electric field application. Compared to MZM, EAM has the advantages of small size, lower bias

voltage, and integration with laser diode on one chip. Laser integrated with EAM is called electro-absorption modulated laser (EML) and it has higher bandwidth and lower chirp than the directly modulated laser. The absorption recovery time of EAM can be reduced to less than 10 ps for high reverse bias voltage [25]. The characteristics of EAM have been already analyzed in [26], [27]. The optical transmission characteristic of an EAM versus DC bias is shown in Figure 2-3. The bias voltage of the EAM is negative.

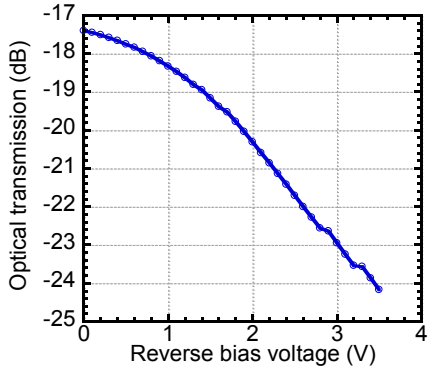

Figure 2-3 Measured transmission of an EAM.

Generally speaking, the insertion loss of EAM is higher than MZM's. When the reverse bias voltage is increased, the absorption is increased, which means that the transmission is reduced. The reverse bias voltage applied to EAM is generally lower than 3 V because high reverse bias voltage induces too much loss. The modulation efficiency is low when the reverse bias voltage is lower than 1 V. Figure 2-3 shows some drifts at reverse bias voltage of 1.7, 2.8, and 3.2 V. These are caused by the deviation of the temperature. EAM is susceptible to the temperature so the temperature control is required. The nonlinearity of EAM is induced by the intrinsic nonlinear absorption. Some other nonlinearities in optical domain also can be generated in EAM, such as four-wave mixing (FWM) [28]-[30], cross-absorption modulation [31]-[33], and cross-polarization rotation [34]-[36]. These optical nonlinearities can be changed by adjusting the DC bias.

2.2.3 External Modulation of MZM

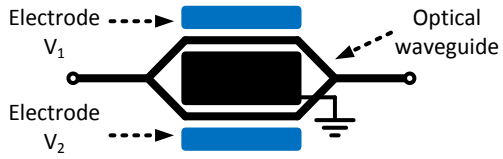

Figure 2-4 Structure of MZM.

Compared to EAMs, MZMs are commonly used because of their multi modulation schemes and zero chirp. The structure of an MZM is given in Figure 2-4. The light from optical fiber is injected to the optical waveguide and divided into two paths in exact the same lengths. In each path, an electrode is added to apply the electric field. When a voltage is applied to the electrode, the generated electric field will change the refractive index of the optical waveguide, i.e., transmission speed of the light in the optical waveguide. Each path is actually an optical phase modulator. The interferometric structure converts the phase modulation to intensity modulation. The output electric field of an MZM can be described as

$$E_{out}(t) = \frac{1}{2} E_{in}(t) \left[e^{j\frac{\pi}{V_\pi} V_1(t)} + e^{j\frac{\pi}{V_\pi} V_2(t)} \right] \tag{2.1}$$

where $E_{out}(t)$ is the output electric field of the MZM, $E_{in}(t)$ is the input electric field of the MZM, V_π is the half-wave voltage, $V_1(t)$ and $V_2(t)$ are the two applied voltages. It can be seen that the output electric field is the sum of the output electric fields of the two optical phase modulators. The two applied voltages are given as follows:

$$V_1(t) = V_{RF} \cos(\omega_{RF} t) + V_{bias} \tag{2.2}$$

$$V_2(t) = V_{RF} \cos(\omega_{RF} t + \theta) \tag{2.3}$$

where V_{RF} and θ are the magnitude and phase of the applied RF signal respectively, and V_{bias} is the bias voltage applied to the MZM. By adjusting V_{bias} and θ, several different modulation schemes can be achieved.

Table 2-1 shows three frequently used modulation schemes of an MZM and their required modulation conditions. The k and n in Table 2-1 are integer constants. Besides, some other modulation schemes such as the odd orders suppression also can be achieved.

The spectra of the three modulation schemes are shown in Figure 2-5. DSB modulation is the most frequently used because the chirp can be eliminated by push-pull modulation. The push-pull modulation can be achieved by setting

$$\theta = (2n+1)\pi \tag{2.4}$$

Table 2-1 Modulation schemes of MZM and required conditions.

Modulation schemes	Conditions
DSB modulation	$V_{bias}/V_\pi = (2k+1)/2$ and $\theta = (2n+1)\pi$
SSB modulation	$V_{bias}/V_\pi = (2k+1)/2$ and $\theta = (2n \pm 1/2)\pi$
DSB-SC	$V_{bias}/V_\pi = 2k+1$ and $\theta = (2n+1)\pi$

Substituting (2.2), (2.3), and (2.4) into (2.1), the output electric field for DSB modulation can be expressed as

$$E_{out\_DSB}(t) = E_{in}(t)\cos\left[\frac{\pi V_{bias}}{2V_\pi} + \frac{\pi V_{RF}}{V_\pi}\cos(\omega_{RF}t)\right] e^{j\frac{\pi V_{bias}}{2V_\pi}} \tag{2.5}$$

Because V_{bias} is a constant voltage, the phase of the output electric field is not modulated by the RF signal, i.e., the chirp of MZM is eliminated. Similarly, double-sideband suppressed-carrier modulation (DSB-SC) modulation also can cancel the chirp of MZM. Figure 2-5 shows that the optical carrier is suppressed by DSB-SC modulation. This is caused by setting

$$V_{bias} = (2k+1)V_\pi \tag{2.6}$$

Using Jacobi-Anger expansion, (2.5) can be expanded as

$$E_{out\_DSB-SC}(t) = 2E_{in}(t)\sum_{n=1}^{\infty} J_{2n-1}\left(\frac{\pi V_{RF}}{V_\pi}\right)\cos[(2n-1)\omega_{RF}t]\, e^{j\frac{\pi V_{bias}}{2V_\pi}} \tag{2.7}$$

where $J_{2n-1}(\ )$ is the 2n-1th order Bessel function of the first kind. It can be seen that only the odd order subcarriers are kept in (2.7). The optical carrier is also suppressed. Without the optical carrier, the frequency of the RF signal will be doubled after photodetection. This effect is also useful in RoF transmission systems.

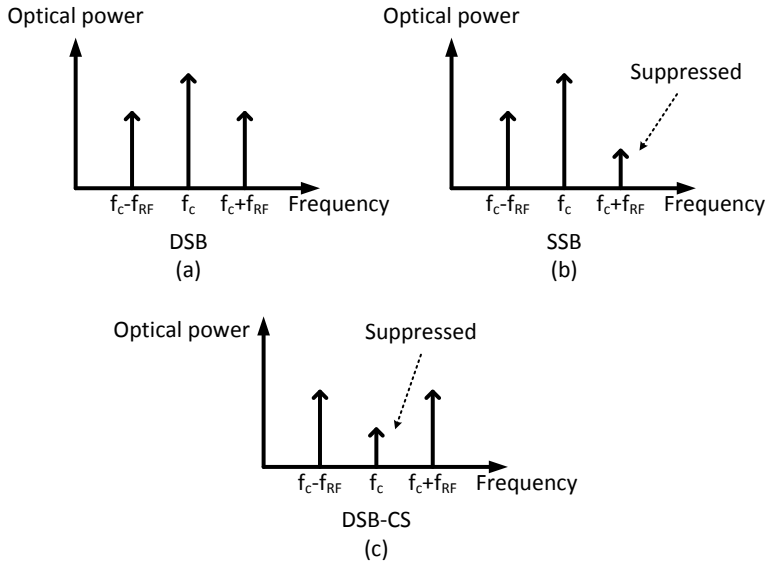

Figure 2-5 Spectra of (a) DSB, (b) SSB, and (c) DSB-SC modulation schemes.

Optical SSB modulation is used to reduce CD and nonlinearity, because it occupies narrower bandwidth and some specific nonlinear components are suppressed compared to DSB modulation. Referring to the condition for the optical SSB modulation in Table 2-1, the output electric field of the MZM for SSB modulation can be described as

$$E_{out\_SSB}(t) = \frac{1}{2}E_{in}(t)\left[je^{j\frac{\pi}{V_\pi}V_{RF}\cos(\omega_{RF}t)} + e^{-j\frac{\pi}{V_\pi}V_{RF}\sin(\omega_{RF}t)}\right] \tag{2.8}$$

Using Jacobi-Anger expansion, (2.8) can be expanded as

$$E_{out\_SSB}(t) = \frac{1}{2}E_{in}(t)\sum_{n=-\infty}^{\infty}\left\{[(-1)^n + j^{n+1}]J_n\left(\frac{\pi}{V_\pi}V_{RF}\right)e^{jn\omega_{RF}t}\right\} \tag{2.9}$$

(2.9) shows that one subcarrier is suppressed for each pair of the odd order components. On the other hand, the even order components are always nonzero. Table 2-2 shows the components for different orders.

Table 2-2 Output electric field components for different order for optical SSB modulation.

Order	Output electric field component
0	$\frac{1}{2}E_{in}(t)(1+j)J_0\left(\frac{\pi}{V_\pi}V_{RF}\right)$
1	$-E_{in}(t)J_1\left(\frac{\pi}{V_\pi}V_{RF}\right)e^{j\omega_{RF}t}$
-1	0
2	$\frac{1}{2}E_{in}(t)(1-j)J_2\left(\frac{\pi}{V_\pi}V_{RF}\right)e^{j2\omega_{RF}t}$
-2	$\frac{1}{2}E_{in}(t)(1-j)J_{-2}\left(\frac{\pi}{V_\pi}V_{RF}\right)e^{-j2\omega_{RF}t}$
3	0
-3	$-E_{in}(t)J_{-3}\left(\frac{\pi}{V_\pi}V_{RF}\right)e^{-j3\omega_{RF}t}$

2.2.4 Photodiode

PD is used in ORx to convert light to current. When a light is injected to a PD, the light is absorbed in the PD and a current is produced. The mechanism is similar to the envelope detection. The frequency of the optical carrier is much higher than the frequency of the carried electrical signal, so the electrical signal is recovered. PD also produces weak current when no light is injected. This current is called dark current which needs to be reduced. PD is reverse biased to reduce the junction capacitance so that its response time is decreased. The relationship between the photocurrent and light is presented as follows:

$$I = RP_{opt} \tag{2.10}$$

where I is the photocurrent, P_{opt} is the received optical power, and R is the responsivity of the PD. Usually the responsivity is ~0.6 A/W.

2.3 Nonlinearities in RoF Transmission Systems

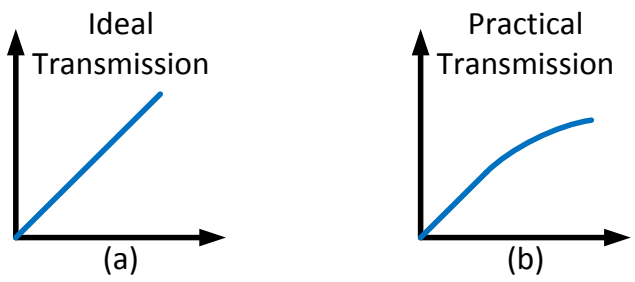

Figure 2-6 Schematic diagram of (a) the ideal and (b) practical transmissions of an RoF transmission system.

When an RoF transmission system is designed, it should be linear in principle, i.e., the ratio of the RF output power and RF input power should be a constant as shown in Figure 2-6 (a). But in reality, it is impossible to obtain an ideal linear system, especially when the RF input power is high. The schematic diagram of the ideal and practical transmissions of an RoF transmission system is given in Figure 2-6. When the RF input power is very low, the practical system is almost a linear system. The nonlinearities are too low to be measured. However, when the RF input power is increased for higher output, the transmission of the system begins to be suppressed, i.e., the system is nonlinear. If a system is nonlinear, nonlinear components are generated and transmitted with the RF signal so that nonlinear distortions are induced. So the nonlinearities must be suppressed. Nonlinearities include harmonics and intermodulations. Harmonics are the components whose frequencies are integer multiples of the signal. Intermodulations are the components which contain two or more signal frequencies. In an RoF transmission system, the nonlinearities could be generated in RF domain such as from PA and optical modulator, or in optical domain such as FWM in the EAM or semiconductor optical amplifier (SOA). They are called the RF nonlinearities and optical nonlinearities respectively. The details are introduced as follows.

2.3.1 RF Nonlinearities

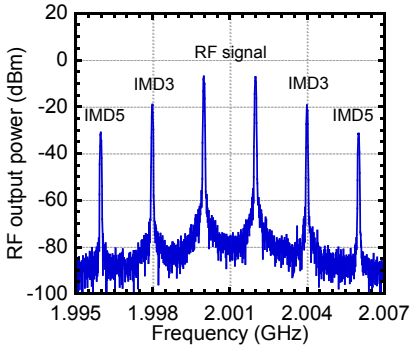

Figure 2-7 RF nonlinearities in the two-tone test in an externally modulated RoF transmission system.

In an RoF transmission system, the RF nonlinearities are generated mainly by RF amplification and optical subcarrier modulation. When the RF input power is high, the nonlinearities are induced obviously. A two-tone test in an externally modulated RoF transmission system is given as an example in Figure 2-7. The two-tone signals are at 2 GHz and 2.002 GHz and the RF input power is -5 dBm per channel. It can be seen that the power of the 3rd order IMDs and 5th order IMDs (IMD5) is comparable to the RF signal power. Because the frequency spacing between the two RF signals is 2 MHz, the frequency spacing between the RF signal and IMD3 is also 2 MHz and it is 4 MHz for IMD5. So it is obvious that the IMDs cannot be eliminated by RF filtering.

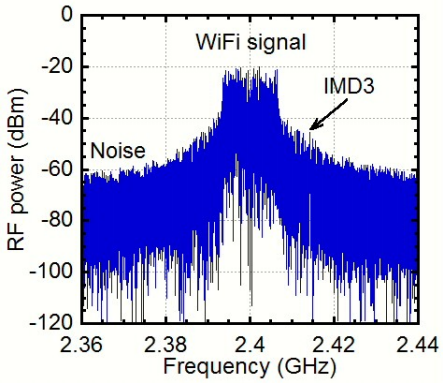

Figure 2-8 Spectrum of a transmitted WiFi signal through a directly modulated RoF system.

Except for the two-tone test, a WiFi signal transmitted through a directly modulated RoF transmission system is also given in Figure 2-8. The WiFi signal occupies 20 MHz bandwidth. It can be seen that the generated IMD3 is ~20 dB higher than the noise. The

bandwidth of the IMD3 is about 3 times of the bandwidth of the WiFi signal. Since they have the same center frequency, the IMD3 overlaps with the WiFi signal. When the signal power is increased, the power of the IMD3 is increased by 3 times so that the error vector magnitude (EVM) is decreased dramatically.

2.3.2 Optical Nonlinearities

In RoF transmission systems, SOA and EAM can generate nonlinearities in optical domain such as FWM, cross-absorption modulation, and cross-polarization rotation [28]-[36]. Among the optical nonlinearities, the FWM is an important effect in RoF transmission systems. The FWM effect is similar to the IMD3 generated in a two-tone test. When two lights at frequencies of f_1 and f_2 are injected into an SOA or an EAM, two more lights are generated at the frequencies of $2f_1$-f_2 and $2f_2$-f_1. The FWM effect is shown in Figure 2-9. The magnitudes and phases of the two FWM lights depend on the intrinsic characteristic of the EAM or SOA and also the bias voltage [37]. So the magnitudes of the FWM lights are tunable. This illustrates that the FWM effect is predictable and adjustable.

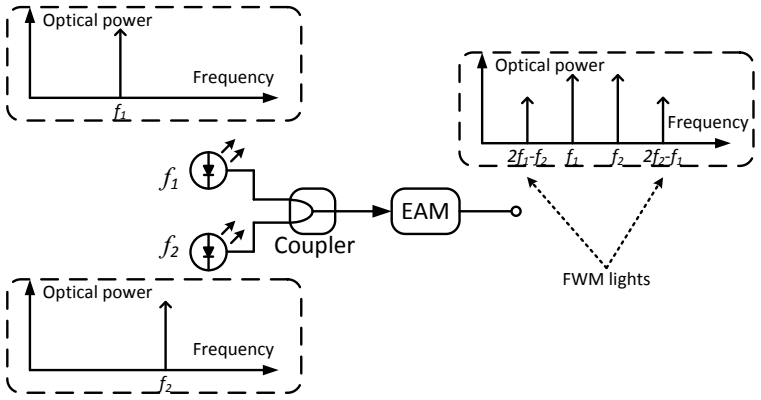

Figure 2-9 Effects of the FWM in an EAM.

To calculate the FWM efficiency, a model of FWM in EAM is established [37]. EAM and SOA are both semiconductor devices but they have reverse carrier transfer behaviors. EAM converts photons to electrons, but SOA absorbs electrons to generate photons. So the model can be also used for SOA. The FWM in EAM is mainly caused by the carrier

density pulsation (CDP) [28]. A classic rate equation is used to derive the FWM efficiency in an EAM. The rate equation can be described as follows:

$$\frac{dN}{dt} = \frac{J}{ed} - G_A P - \frac{N}{\tau} \tag{2.11}$$

where J is the current density, d is the thickness of the active layer, P is the photon density per unit time, N is the carrier density, e is the electron charge, G_A denotes the gain/loss induced by the photon-electron conversion in the EAM, and τ is the carrier recombination time. It is assumed that the photon density is not so high that the nonlinear absorption induced saturation effect can be ignored. A pulsation is induced by the beating of the two pump lights. The transmission characteristic of the EAM and its fitting curve are given in Figure 2-10. It shows that the 15th order polynomial and 5th order exponential polynomial can fit the transmission curve properly. The polynomials are as follows:

$$G_A = \frac{P_{out}}{P_{in}} = \sum_{k=0}^{15} C_k V^k = e^{\sum_{k=0}^{5} T_k V^k} \tag{2.12}$$

where P_{in} (P_{out}) is the input (output) power to (from) the EAM, C_k and T_k are the coefficients of the polynomials, and V is the input voltage.

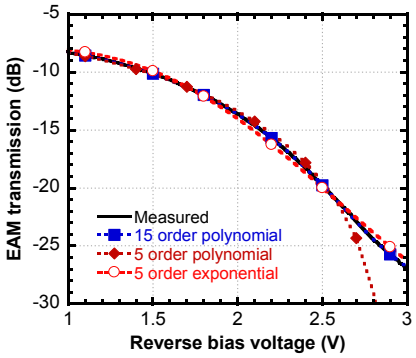

Figure 2-10 Measured transmission of the EAM and fitting curves.

From (2.11), (2.12), and some common equations, the FWM efficiency for DC modulation can be derived as

$$E_{FWM\_DC} = \frac{1}{LG_A\left(i\frac{\omega}{c}\eta + \frac{g}{2}\right)}\left[\frac{\hbar\left(i\Delta\omega + \frac{1}{\tau}\right)}{\left(\frac{E_{p1}^2}{\omega_{p1}} + \frac{E_{p2}^2}{\omega_{p2}}\right)C_1} - \frac{C_V}{C_1}\right]\frac{dG_A}{dV} \times \frac{i(\alpha_c + i)G_{A0}\frac{E_{p1}^2 E_{p2}^*}{\hbar\omega}}{\left\{\frac{1}{\tau} + \left[-\frac{\left(i\Delta\omega + \frac{1}{\tau}\right)}{C_1} + \left(\frac{E_{p1}^2}{\omega_{p1}} + \frac{E_{p2}^2}{\omega_{p2}}\right)\frac{C_V}{\hbar C_1}\right]\frac{dG_A}{dV} + i\Delta\omega\right\}} \quad (2.13)$$

where c is the speed of light in vacuum, ω_{p1} and ω_{p2} are the angular frequencies of the two pump lights, $\Delta\omega = \omega_{p1} - \omega_{p2}$, η is the refractive index, g is the gain coefficient given by $g = ln(G_A)/L$, L is the length of the active waveguide, α_c is the linewidth enhancement factor which is defined as $\alpha_c = -2\frac{\omega}{c}\frac{d\eta}{dn}/\frac{dg}{dn}$, $\omega = 2\omega_{p1} - \omega_{p2}$, E_{p1} and E_{p2} are the amplitudes of the optical fields of the two injected pump lights, $\hbar$ is the reduced Planck constant and C_V is introduced by the 1st order coefficient of Taylor series of $ln(n)$, and it is given by $C_V = 1.85G_{A0}\frac{E_{p1}E_{p2}^*}{\hbar\omega P_0 n_{max}}$. n_{max} is a constant, G_{A0} is the EAM transmission without the pulsation, and P_0 is the photon density per unit time without the pulsation. Using (2.13), the electric field of the FWM light can be calculated. The measured and calculated FWM efficiencies are given in Figure 2-11. It can be seen that the calculation matches the measured results. The highest FWM power is achieved at reverse bias voltages of 2.2 and 2.3 V.

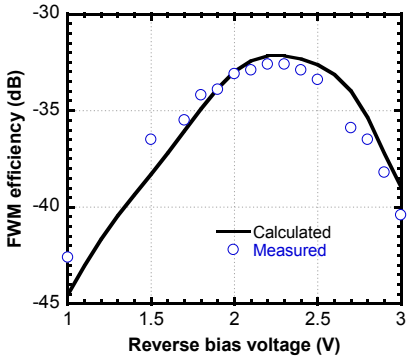

Figure 2-11 Measured and calculated FWM efficiencies.

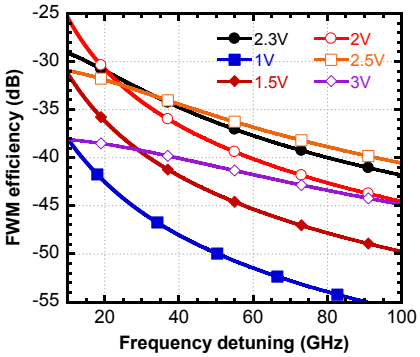

Figure 2-12 Calculated detuning characteristics.

By using this model, the detuning characteristics also can be calculated. The results of calculation are given in Figure 2-12 and they agree with the common frequency detuning phenomenon of EAM, i.e., the FWM efficiency decreases when the frequency detuning is increased. Figure 2-12 shows that the detuning characteristics depend on the bias voltage of EAM.

By using similar approach, the electric field of the FWM light with RF modulation can be derived as

$$E_{FWM\_RF} = \frac{i(\alpha_c + i)}{2L\left(i\frac{\omega}{c}\eta + \frac{g}{2}\right)}\left[\frac{\hbar\left(i\Delta\omega + \frac{1}{\tau}\right)}{\left(\frac{E_{p1}^2}{\omega_{p1}} + \frac{E_{p2}^2}{\omega_{p2}}\right)C_1} - \frac{C_V}{C_1}\right] nE_{p1} \times \left(T_1 + 2T_2V_{DC} + 3T_3V_{DC}^2 + \frac{3}{2}T_3V_{RF}^2 + 4T_4V_{DC}^3 + 6T_4V_{DC}V_{RF}^2 + 5T_5V_{DC}^4 + 15T_5V_{DC}^2V_{RF}^2 + \frac{15}{8}T_5V_{RF}^4\right) \quad (2.14)$$

where $n = -\frac{2G_{A0}\frac{E_{p1}E_{p2}^*}{\hbar\omega}}{\frac{1}{\tau}+\frac{dG_A}{dn}P_0+i\Delta\omega}$.

To show the impact of the effective RF voltage V_{eff} on FWM efficiency, the calculated FWM efficiencies versus V_{eff} are given in Figure 2-13. The reverse DC bias voltage is set to 1, 1.5, 2, 2.3, 2.5 and 3 V. V_{eff} is the root mean square of the applied RF voltage. It can be seen that the FWM efficiency is the highest for V_{eff} from 0 to 0.7 V at the bias voltage of 2.3 V. The dependences of the FWM efficiency on V_{eff} at different DC bias voltages are shown in Figure 2-13. It is seen that the FWM efficiency increases at bias voltages of

1 and 1.5 V, and decreases at bias voltages of 2, 2.3, 2.5 and 3 V, with the increase of V_{eff}. More importantly, it is seen that, for some bias voltages such as 1.5 V and 2 V, the FWM efficiency has less dependence on V_{eff}. When V_{eff} is 0 V, the calculated results in Figure 2-13 agree with the results in Figure 2-12. When V_{eff} is increased from 0 V, the FWM efficiencies begin to deviate from the FWM efficiency for DC. So it can be seen that this is a tradeoff to balance the modulation efficiency and FWM in an EAM. The bias voltage of the EAM has to be chosen for enough modulation efficiency and FWM efficiency as low as possible. As mentioned before, these equations are also applicable for SOA, but the G_A is the gain of SOA.

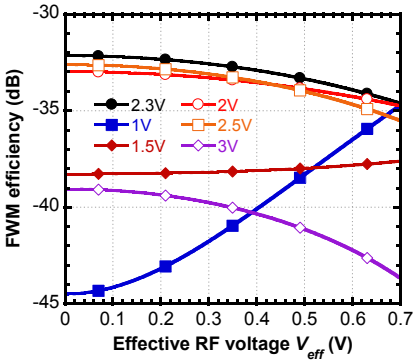

Figure 2-13 Calculated FWM efficiencies versus V_{eff} for the reverse DC bias voltages of 1, 1.5, 2, 2.3, 2.5 and 3 V.

2.3.3 Spurious-Free Dynamic Range

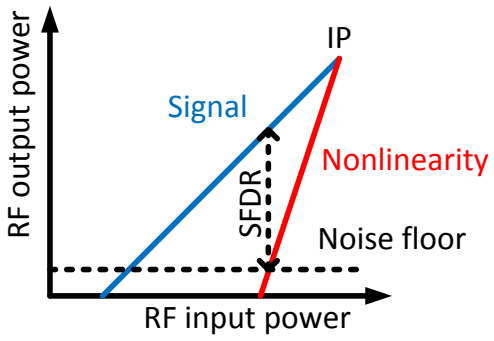

Figure 2-14 Schematic diagram of SFDR. IP: Intercept point.

SFDR is commonly used to evaluate the linearity of an RF system. It is defined as the RF power range where the dominant nonlinearity is lower than the noise level. The schematic diagram is given in Figure 2-14.

2.3.4 Error Vector Magnitude

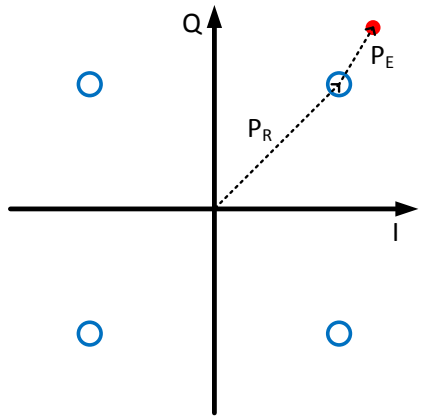

Figure 2-15 Schematic diagram of EVM.

Because EVM is independent of modulation scheme, it is a good measurement to evaluate the quality of a modulated signal. The principle of EVM is shown in Figure 2-15. In an ideal system, the constellation points of the output signal should be located at the ideal positions. However, in a practical system, the deviations from the ideal positions of the constellation points are caused by imperfections such as noise and distortion. EVM is employed to measure the deviation. It is defined as follow:

$$EVM(dB) = 10\log_{10}\left(\frac{P_E}{P_R}\right) \tag{2.15}$$

where P_E and P_R are the root mean square average power of the error vector and reference vector, respectively. EVM is the reciprocal of signal-to-noise ratio [38].

2.4 Literature Review of Linearization Technologies for RoF Transmission Systems

To suppress the nonlinear distortions induced mainly by an optical modulator in RoF transmission systems, several linearization techniques have been proposed. These techniques mainly focus on 2nd order nonlinearities, IMD3, and IMD5. The 2nd order nonlinearities have the highest power among the nonlinearities, but it falls out of the passband of RF signals. However, 2nd order nonlinearities may overlap with other signals in multiband RoF transmission systems, such as a WiFi signal at 2.4 GHz and a

multiband orthogonal frequency-division multiplexing (OFDM) ultra wideband (UWB) signal at 3.96 GHz. 2nd order nonlinearities include 2nd order harmonic distortion (HD2) and 2nd order IMD (IMD2). IMD3 also has high power among nonlinearities, and it is in the passband of RF signal. So IMD3 must be considered as the most important nonlinear distortion. IMD5 also falls in the passband of RF signal, but its power is much lower than 2nd order nonlinearities and IMD3. In an RoF transmission system, electrical and optical methods can be employed for linearization.

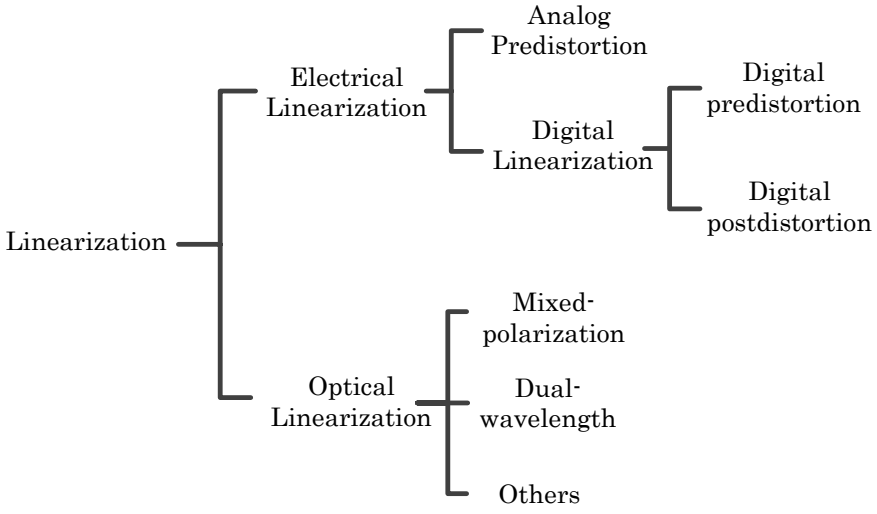

Figure 2-16 Linearization technologies for RoF transmission systems.

Figure 2-16 summarizes the linearization technologies that have been developed. The electrical and optical linearization technologies mean implementations completed in electrical and optical domain, respectively. The predistortion means that a spurious distortion is firstly generated and then is used to suppress the transmission generated distortion. The postdistortion is opposite to the predistortion in the process sequence. Optical linearization is the technology that two or more nonlinear optical components are combined and adjusted to suppress the total system nonlinearities. Electrical methods include analog PDC and digital linearization. Analog PDC is low-cost because ICs are cheap and all components are integrated in one circuit and its size is very compact. PDC can provide ~10 dB improvement of SFDR. Although the analog PDC can suppress IMD3 in an RoF transmission system, it cannot deal with memory effect. Memory effects are the circuit behaviors which cannot be modeled by the standard steady-state

characterization techniques. Digital linearization is more precise but more complicated compared to the analog PDC, in which an ADC must be employed to sample analog signals, and then an algorithm is used to calculate and analyze the sampled signals. Finally a predistortion signal is added to the signal generator. The disadvantages of the digital linearization are high cost and low sample rate of ADC. Most of the ADCs are designed for 1 GSample/s and less. A few ADCs can work for higher than 10 GSample/s, but they cost more than $10,000 for each typically. Speaking, the bandwidth of RF signals in digital linearization is lower than 100 MHz. Synchronization is also difficult for RoF transmissions, so most of broadband digital linearizations use off-line signal processing with computer. Compared to the electrical methods, the optical methods have higher bandwidth because the bandwidth is only limited by the optical subcarrier modulation. But the linearization may be complex. The comparison of the linearization methods is presented in Table 2-3.

Table 2-3 Comparison of linearization technologies.

Linearization method	PDC	Digital	Optical
Bandwidth	High	Low	High
Loss	Medium	Low	Low/Gain
Complexity	Low	High	High
Cost	Low	High	Medium
Even order nonlinearity	No	Difficult	Yes
Improvement	Good	Best	Good

2.4.1 Analog PDC

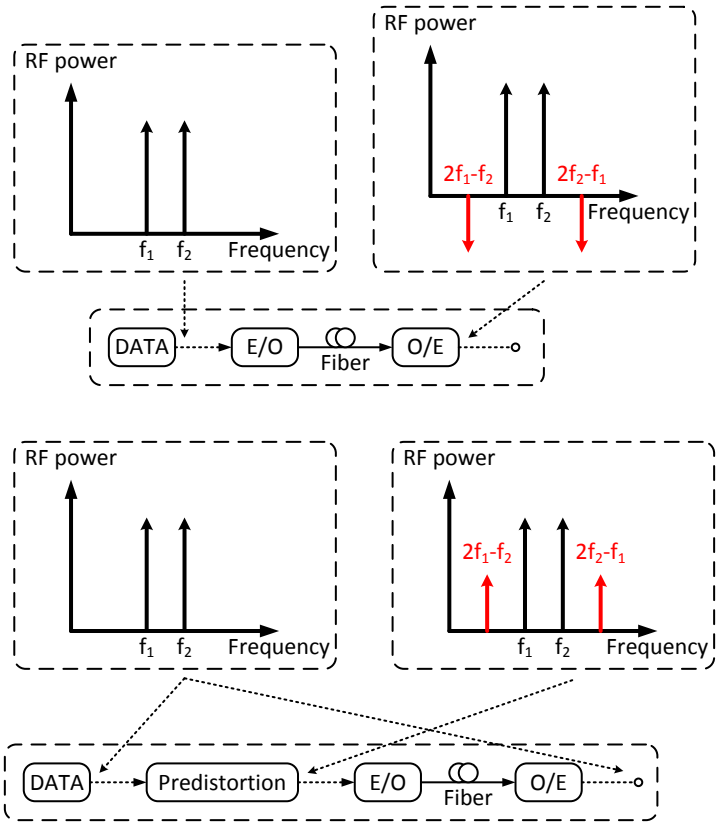

Figure 2-17 Linearization principle of analog PDC.

Figure 2-17 shows the linearization principle of an analog PDC [39]-[48]. Among the nonlinearities, only the IMD3 is considered in the principle. The analog PDC for an RoF transmission system is similar to that for a PA. The upper part of Figure 2-17 shows the nonlinearity caused by the optical subcarrier modulation in an RoF transmission system. The PD also induces nonlinearities but it is so small that it can be neglected. The IMD3 induced by the optical subcarrier modulation is antiphase with the RF signal in Figure 2-17. For the most cases in RoF transmission systems, the IMD3 induced by the optical subcarrier modulation is antiphase with the RF signal, but sometimes they are inphase with each other, such as modulation using an EAM at some specific bias voltages. But these bias voltages are rarely used because of high loss or low RF modulation efficiency at these bias voltages. The lower part of Figure 2-17 shows the linearization principle of the analog PDC. The PDC generates the IMD3 that is inphase with RF signal due to its intrinsic characteristic. So the IMD3 generated by the optical subcarrier modulation and

the IMD3 generated by the PDC will cancel each other. The RF signal can be kept but some loss is induced.

For broadband analog PDC, the phase and magnitude must be maintained precisely for the whole band. The phase difference between the RF signal and IMD3 should be no more than 10º. The capacitor, inductor, and parasitics can induce phase shift. The magnitudes of the RF signal and IMD3 should be constant for the whole passband. This depends on the S_{21} of all the components, connectors, and design of the circuit. The most important component is the predistorter, i.e., one or two diodes. Diode is the smallest nonlinear component and it can generate IMD3 that is inphase with RF signal due to its intrinsic characteristic. Usually analog PDC can provide ~10 dB improvement of SFDR.

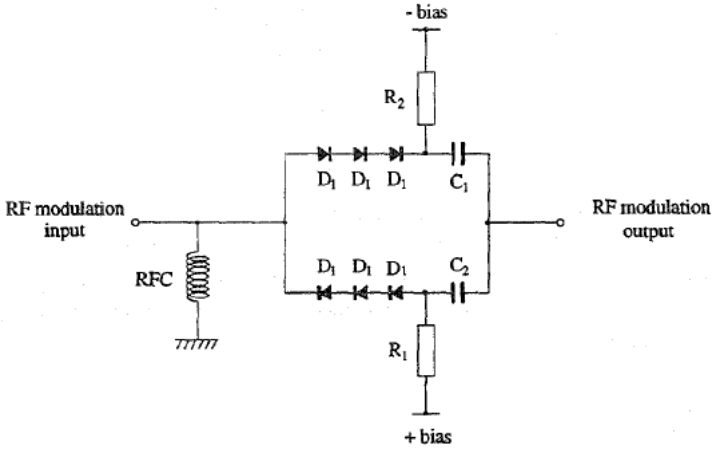

(a)

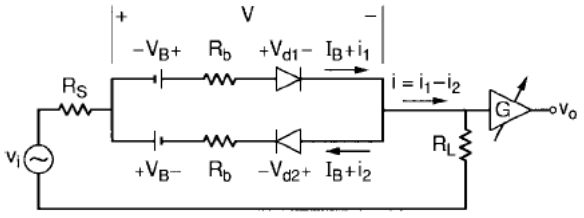

(b)

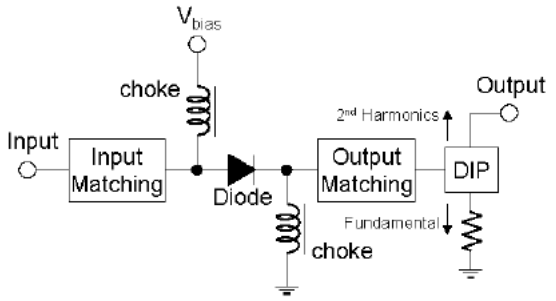

(c)

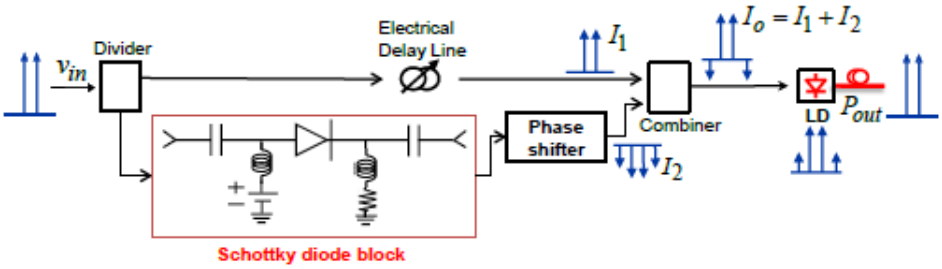

(d)

Figure 2-18 Schematics of the analog PDCs [39]-[42].

Figure 2-18 shows the schematics of the previously reported analog PDCs using diodes [39]-[42]. Several setups are used to form predistortion, such as serial diode, anti-parallel diodes, and multiple diodes. However, they can only offer limited bandwidth up to hundreds of MHz. The broadest bandwidth of previously reported PDCs is from 3.1 to 4.8 GHz [43]. The predistorter also can be designed using integrated circuit (IC) techniques [46]-[48]. This is similar to the PDC using diodes, but the design is moved from board-level to chip-level. However, despite the bandwidth of the predistorter based on IC techniques is extended to several GHz for PAs [47], [48], the bandwidth for RoF transmission is still limited to be lower than 100 MHz.

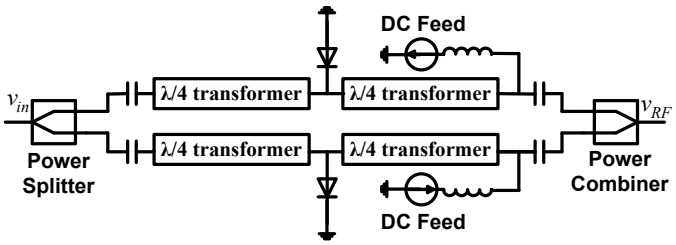

Figure 2-19 Schematic of the analog PDC reported in [43].

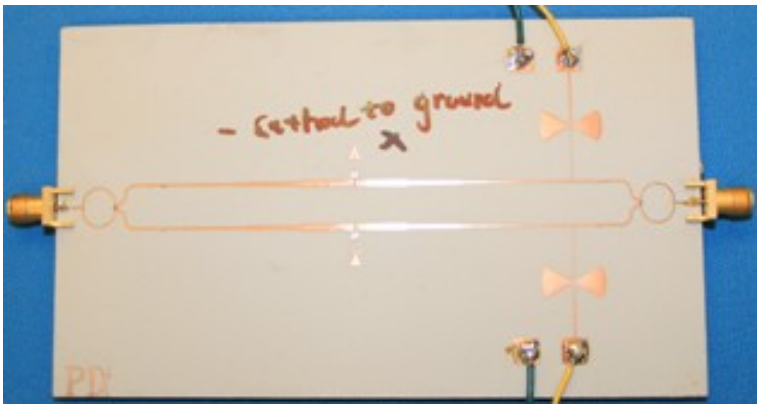

Figure 2-20 Prototype of the analog PDC reported in [43].

The schematic of the analog PDC reported in [43] is shown in Figure 2-19. The RF input signal is equally split into two paths by a Wilkinson power divider (WPD), and goes through a pair of anti-parallel diodes. The even-order nonlinear products are cancelled due to the anti-parallel connection, and only odd-order nonlinear products are remained. Four three-section quarter-wave impedance transformers are used for broadband impedance matching. Another WPD is used as power combiner. Figure 2-20 presents the prototype of the PDC. It can be seen that the three-section quarter-wave impedance transformers occupy most of the space on the circuit. The dimension of the PDC is 13.2 × 7.7 cm^2.

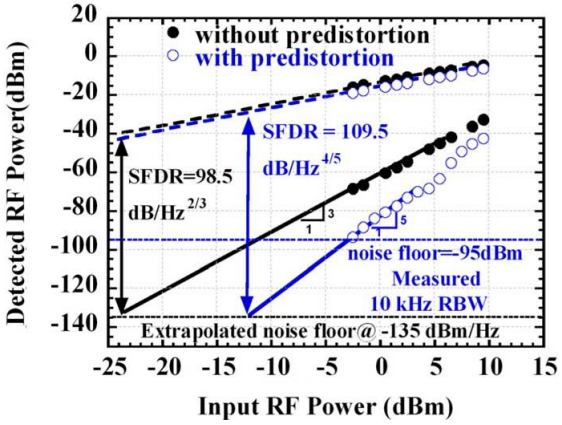

Figure 2-21 Experimental results in a two-tone test [43].

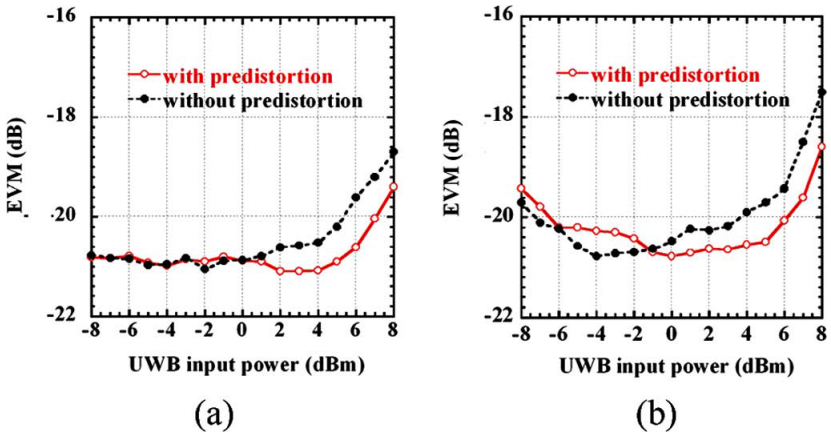

Figure 2-22 Measured EVM versus UWB input power for (a) BTB and (b) 20 km SMF transmission.

Figure 2-21 shows the measured SFDRs of 109.5 dB $Hz^{4/5}$ and 98.5 dB $Hz^{2/3}$ for the EAM with and without the PDC. It is shown that the IMD is 5^{th} order limited (the slope of IMD3 power) for the RoF system using the predistorted EAM. Without the PDC, it is third-order limited. This shows that the IMD3 is suppressed from the predistorted EAM. Figure 2-21 shows that the PDC leads to an SFDR improvement of 11 dB. The broadband linearization from 3.1 to 4.8 GHz is also verified. Moreover, the PDC is evaluated in an RoF transmission of multiband-OFDM UWB from 3.168 to 4.752 GHz. The experimental results in Figure 2-22 show that the EVM can be improved by ~1 dB for back-to-back (BTB) and 20 km SMF transmission.

Despite the broadband linearization over GHz was achieved by using analog PDC, the bandwidth of PDC is still needed to be improved to satisfy the bandwidth requirement of RoF transmission systems and the dimension of PDC has to be reduced for simple implementation.

2.4.2 Digital Linearization

Digital linearization includes digital predistortion (DPD) [49]-[60] and digital post processing (DPP) distortion [61]-[67]. The DPD has been developed for decades, to suppress the IMD3 generated by RF PAs [68]. Digital linearization uses ADC to sample the analog signal and linearize the transmission by digital signal processing (DSP). Generally speaking, current digital linearization is limited to 20 MHz bandwidth [60]. Technically, it is now possible to achieve wideband, greater than 1 GHz bandwidth.

However, the required DSP is complicated and the power consumption is huge, beyond the practical applications. To reduce the DSP requirements, multi-band DPD techniques have been developed recently, in which only RF signals occupied bandwidth is processed [59], [65].

In order to use the DPD for broadband RoF downlinks and DPP for broadband RoF uplinks, both located in CPU, it is required to simplify the currently developed digital techniques that are being used for RF PAs and also improve the linearization bandwidth.

The principle of the digital linearization technique is that a predistorter is used to generate opposite nonlinear characteristic digitally to compensate for the nonlinearity of the RoF transmission. When the broadband signals are transmitted over the RoF system, memory effect in the RoF transmission has to be considered. So, memoryless polynomial is not sufficient to model RoF transmissions. More than 10 dB of additional accuracy can be obtained when using a memory polynomial to estimate the nonlinear behaviors than using memoryless polynomial in an RoF transmission [51]. Volterra series is commonly considered to be an appropriate memory polynomial. Memory length and nonlinearity order of the memory polynomial are related to the performance and complexity of the digital linearization. Up to 5^{th} order nonlinearity may be sufficient for the model. Even order nonlinearities also need to be considered because even order nonlinearities contribute to the generation of odd order IMDs. The memory length of two may be adequate to model memory effect of RoF transmission systems. When higher nonlinearity order and memory length are used, the accuracy is improved slightly but more coefficients need to be extracted. This dramatically increases the complexity and calculation time of digital linearization. Moreover, when the nonlinearity is increased, the accuracy of the model is decreased.

The DPD technique uses the feedback of the nonlinearity information of the RoF transmission to generate a distorter. By sampling the input and output data of an RoF transmission without the DPD, a predistorter with inversed nonlinearity characteristic can be generated. A memory polynomial can be used to approximate the predistorter. To obtain the coefficients of the memory polynomial, the input and output data of the RoF

transmission system is used for training the output and input data of the predistorter. Gain of the RoF transmission system needs to be removed before the training input data is injected to the predistorter. Then, using the least-square error minimization method or other algorithms, the coefficients of the distorter model can be extracted and the predistorter is established. When up to 5^{th} order nonlinearity is used in digital linearization, ~15 dB suppression of the adjacent channel power (ACP) and ~9 dB improvement of the EVM can be achieved [59]. But at least five times of the signal bandwidth for sampling is required. DPD includes baseband predistortion and RF predistortion. For the baseband predistortion, signals are sampled and processed in baseband before up-conversion. The RF predistortion is applied for RF signal, i.e., the up-converted signal is sampled and processed. Compared to the RF predistortion, the baseband predistortion needs lower sampling frequency but double complexity of the algorithm. ~10 dB suppression of the ACP and 8 dB improvement of EVM can be obtained when the RF predistortion is used.

Unlike the DPD, because the nonlinearity information of an RoF transmission system is blind at receiver side, DPP has to use recursive sweep and monitor the ACP to find the optimum coefficients of memory polynomial. This drawback degrades the linearization performance of DPP by ~3 dB [65].

Generally speaking, digital linearization is adaptive and provides the best performance than other linearization methods in specified limited bandwidth. And linearization efficiency is higher, and in particular several nonlinearities can be linearized simultaneously. But, higher digitizer bandwidth is required to sample higher order nonlinearities. The bandwidth and cost limit the application of digital linearization substantially.

2.4.3 Optical Linearization Methods

The principles of optical linearization methods are similar to electrical linearization. The nonlinear components generated by an RoF transmission system at two operation points can cancel each other, but the RF signal remains. Most optical components have higher bandwidth than RF components. This advantage can be employed for broadband

linearization in RoF transmission systems but the complexity of the linearized system is increased. Several linearization methods using optical components have been proposed such as mixed-polarization (MP) linearization [69]-[78], linearization by saturated SOA [79]-[81], cascaded MZMs [82]-[93], DWL [94]-[96], and other techniques [97]-[106].

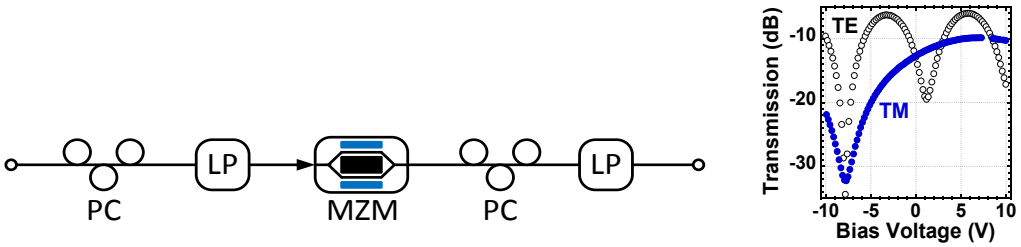

Figure 2-23 Schematic of the MP linearized optical modulator and the transmissions of TE mode and TM mode of an MZM [75]

MP linearization means that, to use transverse electric (TE) and transverse magnetic (TM) transmission characteristics of an RoF transmission system, the nonlinear components generated by TE and TM transmissions are cancelled by each other, if the nonlinear components from the TE and TM transmissions are in antiphase ($n\pi$ phase difference, n=1,3,5…). Therefore, the TE and TM characteristics must be different, which means that the RoF transmission must be polarization dependent, such as the RoF transmission system using polarization dependent MZM or EAM. Using the MP linearization, both 2nd and 3rd order nonlinear distortions can be significantly suppressed by appropriately adjusting polarization angles. However, the RF signal may be also suppressed to some extent, and the suppression is strongly dependent on the TE and TM characteristics of the MZM or EAM. For example, using Lithium Niobate ($LiNbO_3$) MZM, an additional loss of 13 dB may be introduced by the MP [72]. When using Gallium Arsenide (GaAs) MZM, the TE and TM transmission characteristics that have opposite phase modulation indices are quite different from $LiNbO_3$ MZM, and thus additional loss may not be introduced for RF signals [77], [78]. However, the MP linearization may not be used to suppress both 2nd and 3rd order nonlinearities at the same time. The schematic of the MP linearization is shown in Figure 2-23. An MZM is used as an example in Figure 2-23. Two polarization controllers (PCs) and linear polarizers (LPs) are used in front of and behind the optical modulator. LP allows only the light with specific polarization state to

pass through. All of the MZMs and some of the EAMs are polarization dependent. TE mode and TM mode experience different modulation characteristics as shown in Figure 2-23. So TE mode and TM mode will generate different IMD3s. By carefully adjusting the two PCs, the maximum RF signal and minimum IMD3 can be achieved. This method also can be used for phase modulator. When an MZM is used for optical subcarrier modulation, the MP linearization can improve the SFDR by more than 12 dB [72] and improve the EVM of an OFDM UWB signal by ~9 dB [76]. The MP linearization technique also can be applied to EAM. If an EAM is used for optical subcarrier modulation, the MP linearization can improve the SFDR by ~10 dB and improve the EVM of the OFDM UWB signal by ~3 dB [73], [74].

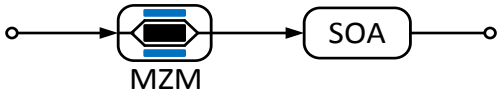

Figure 2-24 Schematic of the linearization by saturated SOA.

The schematic of the linearization by saturated SOA is given in Figure 2-24. The SOA is placed behind the MZM to compensate for the nonlinearities of the MZM. SOA is also a nonlinear device and its gain decreases when it is saturated. When the bias voltage of the MZM is set to $V_{bias} = \frac{3\pi}{2} V_{\pi}$, its IMD3 is antiphase with the RF signal and its IMD2 is minimized. By tuning the bias current of the SOA, the IMD3 generated by the SOA is antiphase with that generated by the MZM so that the total IMD3 is suppressed. By using this linearization technique, the IMD3 is suppressed by 9 dB and thus the SFDR is improved by 4.5 dB [79]. However, because the SOA is saturated, its gain is low and the power of the RF signal is reduced. The SOA will also induce amplified spontaneous emission (ASE) noise.

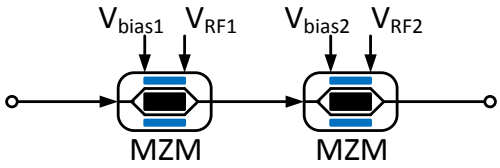

Figure 2-25 Schematic diagram of the linearization by cascaded MZMs.

The linearization method using cascaded MZMs is shown in Figure 2-25. Two MZMs are cascaded and they are biased and modulated with different biases and RF signal power separately. The two biases need to be adjusted and the magnitudes and phases of the two RF signals also need to be adjusted to achieve suppression of nonlinearity. The second MZM generates an IMD3 which is used to compensate for that generated by the first MZM. More than 30 dB suppression of the IMD3 can be achieved by using this method [82]. However, it is too complicated to adjust two bias voltages and two RF signals. Further, it has high cost. Two broadband MZMs increase the cost of the RoF transmission system dramatically.

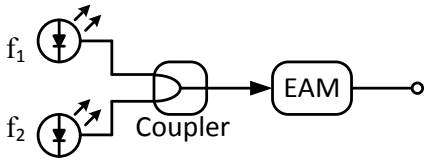

Figure 2-26 Schematic of the DWL technique.

Figure 2-26 shows the schematic of DWL technique. DWL technique is proposed to eliminate the 3rd order nonlinearities generated by an EAM [94]. The principle of DWL is given as follows: Nonlinear distortion components generated at two wavelengths λ_1 and λ_2 can be cancelled by each other. Therefore, it is required that the transmission characteristics of the RoF transmission are different for λ_1 and λ_2, i.e., wavelength dependent transmission. The nonlinear components generated at λ_1 and λ_2 can be suppressed if they are antiphase with each other, while the RF signals can be improved if they are inphase. Fortunately, both MZM and EAM have wavelength dependent transmission characteristics. In other words, when an RoF system uses one of those two external modulators, the RoF transmission characteristic becomes wavelength dependent. For example, we consider an RoF transmission using an EAM. Lights emitted from two lasers at wavelengths λ_1 and λ_2 are coupled and transmitted to an EAM which is used for optical subcarrier modulation. The two lights experience different modulation characteristics in the EAM so that the RF signals and nonlinear components for the two lights are generated. The two lights are incoherent and carry their own RF signals and nonlinear components, respectively. After photodetection, the two groups of the RF signals and nonlinear components at the same frequencies are obtained. If the two RF

signals and nonlinear components are inphase and antiphase, respectively, the RF signals and nonlinear components will be improved and suppressed in power, respectively. By adjusting the power ratio of the two lasers, improvements of the RF signals and suppressions of the nonlinear components can be optimized. In [94], 30 dB suppression of 3^{rd} order nonlinearity and 8 dB improvement of SFDR are achieved in an RoF transmission system. It was also proved that the IMD3 generated by an MZM can be suppressed by more than 26 dB by DWL technique in [96].

Chapter 3 Broadband Predistortion Circuit Using Zero Bias Schottky Diodes

3.1 Introduction

Analog PDC is a practical solution for the linearization of RoF transmission systems due to the advantages of low cost, high bandwidth, and compact size. In [43], a broadband PDC using Schottky diode was proposed to linearize the RoF transmission system from 3.1 GHz to 4.8 GHz. The schematic is presented in Figure 2-19. However, this bandwidth is not sufficient because broadband RoF transmission system is a transparent infrastructure for wireless protocols. Therefore the bandwidth of the PDC needs to cover multi-band. Moreover, PDCs are installed in both the CPU and RRU, thus it has to be efficient in size and power consumption to meet the requirement of RRU.

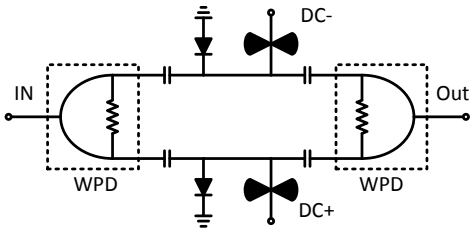

Figure 3-1 Schematic of the proposed PDC.

In this chapter, a novel low-cost PDC with compact size and low power consumption, using zero bias Schottky diodes, is proposed to linearize broadband RoF transmission systems [107], [108]. This design is based on the previous work [43]. The schematic of the proposed PDC is presented in Figure 3-1. Two zero bias GaAs beam lead detector diodes in anti-parallel are used as the predistorter. The nonlinearity of the PDC can be adjusted through the bias currents of the diodes. Two DC current sources are required to bias the two diodes. Compared to [43], no broadband matching network is required due to the high series resistance of the zero bias diodes so that the dimension of the circuit is reduced and the bias current of the PDC is further reduced. The bias currents can be set to lower than 3 mA due to the zero bias diode. The proposed PDC is verified in the RoF transmission systems using MZM and EAM, respectively. The S-parameters, input 1-dB compression power (P_{1dB}), and SFDRs are measured with and without using the PDC in

the experiments. The bandwidth from 7 GHz to 18 GHz is achieved and the IMD3 is suppressed by the PDC.

3.2 Input/Output Relation of RoF System with PDC

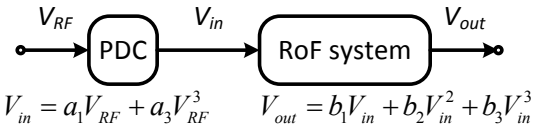

Figure 3-2 Principle of linearization using the PDC.

The principle of using an analog PDC to linearize an RoF system is depicted in Figure 3-2. The relationships of the input and output of the PDC and the RoF transmission system are also given. The PDC is symmetrical and the two arms are driven with push-pull biases as shown in Figure 3-1. Thus, all even order nonlinear distortion components generated by the PDC are eliminated. In other words, only the 1st and 3rd order components, as well as other higher odd order components, remain. When the PDC is designed appropriately, the IMD3 generated by the RoF transmission system can be suppressed by that generated by the PDC. The output voltage after the PDC and RoF transmission system can be described as

$$V_{out} = a_1 b_1 V_{RF} + a_1^2 b_2 V_{RF}^2 + (a_3 b_1 + a_1^3 b_3) V_{RF}^3 \tag{3.1}$$

It can be seen that the total IMD3 is removed if the condition $\frac{a_1^3}{a_3} = -\frac{b_1}{b_3}$ is met. Generally speaking, for an RoF transmission system, it has $b_1/b_3 < 0$, so the generated IMD3 and RF signal from the PDC must be inphase with each other.

3.3 Prototype

Figure 3-1 shows the schematic of the proposed PDC. It can be seen that no matching network is used. A WPD following the input port is used to split the RF input signal to the two branches. WPD is lossless and provides isolation between the two outputs. Two broadband capacitors ATC 550Z are used in each branch as DC blocks. Two zero bias GaAs beam lead Schottky detector diodes whose model number is MZBD-9161 are attached to the microstrip lines in anti-parallel. They generate nonlinear signals while the

RF signal passes through. The diode presents low zero bias junction capacitance which is 0.03 pF and low transit time. Its beam lead allows low parasitics. The junction capacitance, transit time, and parasitics induce phase distortion and resonance. Positive and negative DC bias currents feed through two butterfly stubs and quarter wavelength transmission lines which block broadband RF signals. The two diodes are both forward biased at the same DC currents. Another WPD works as a power combiner. The diodes generate IMD3 which is inphase with the RF signal due to its intrinsic UI-characteristic. The anti-parallel structure in the circuit eliminates even order nonlinearities of the diodes. If an RoF transmission system generates IMD3 antiphase with RF signal and the proposed PDC is added in the system, the generated IMD3 can be cancelled by properly tuning the bias currents of the PDC. The phase distortion between the RF signal and IMD3 of the circuit degrades the linearization. So in the design of the circuit, the phase distortion should be suppressed by reducing capacitance and transit time of diodes and parasitic inductance in the layout.

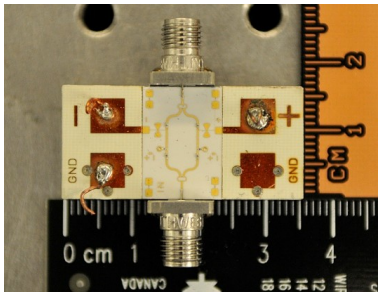

Figure 3-3 Fabricated prototype of the proposed PDC.

The fabricated prototype of the proposed PDC is presented in Figure 3-3. It is obvious that the size of the proposed PDC is significantly reduced compared to the reported PDC shown in Figure 2-20. Its dimension without connectors is 3.5 × 1.6 cm^2. The circuit consists of three parts. The top and bottom are two printed circuit boards (PCBs) which provide connections of DC power supplies. The PCBs are designed in large size for test and soldering, so their sizes can be further reduced. The prototype with 50 Ohms characteristic impedance is placed between the two PCBs. The substrate of the prototype is alumina with 9.9 dielectric constant and 10 mils thickness. The three circuits are connected by bonding wires and fixed on a metal base connected to the ground. 100

Ohms thin film resistors are used for WPD and four test thin film resistors are placed near the four corners of the prototype. Two 2.92 mm connectors are used.

3.4 Experimental Evaluation of the Proposed PDC

3.4.1 Characteristics of the Proposed PDC

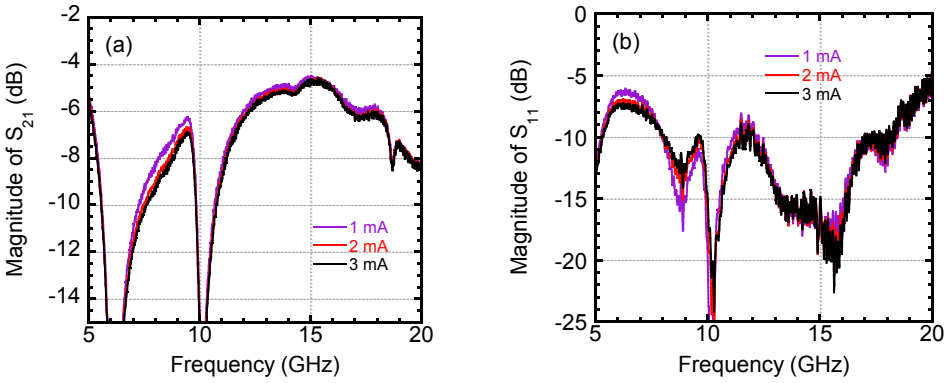

Figure 3-4 S-parameters of the proposed PDC.

The magnitudes of S_{21} and S_{11} of the PDC are given in Figure 3-4. The fabrication defects generate high loss around 10 GHz. The S-parameters change little when the bias current is changed. The magnitude of S_{21} from 7 to 8 GHz is ~4 dB lower than the peak. The magnitude of S_{11} is -7 dB at 7 GHz and around -10 dB or lower than -10 dB for other frequencies. The measured S-parameters show high power loss at 10 GHz. Both transmission and reflection are lower than -10 dB. So it is illustrated that the power passes to the ground at 10 GHz by a short circuit. This should be caused by the fabrication defects of soldering and glue. The soldering and glue induce inductor with high inductivities which resonate with the parasitic capacitors. Then a short circuit to the ground is generated by the resonance so that the power flows to the ground.

Matching networks are important components to improve power transmission. However for broadband design, multi-section quarter-wave impedance transformer is required. Four impedance transformers are required in [43]. Each impedance transformer is several centimeters long. The transformer increases the circuit size and parasitic inductance. Schottky diode has lower series resistance to reduce power loss, but zero bias diode usually has higher series resistance. This may induce some loss but it makes the

impedance of the diode close to the characteristic impedance of the transmission line. MZBD-9161 has a series resistance of 50 ohms which leads to ~50 Ohms device impedance. So the matching network can be removed in the proposed PDC.

Schottky diodes must be biased at a voltage higher than its threshold for proper working. Zero bias diodes are specially designed to eliminate the threshold. So it can work at lower bias or zero bias. This advantage reduces the power consumption of the proposed PDC. The proposed PDC works at bias current lower than 3mA. The PDC is biased at 2.6 mA from 7 to 11 GHz and 1.1 mA from 12 to 18 GHz. The current is adjusted due to more loss induced by the PDC from 7 to 11 GHz.

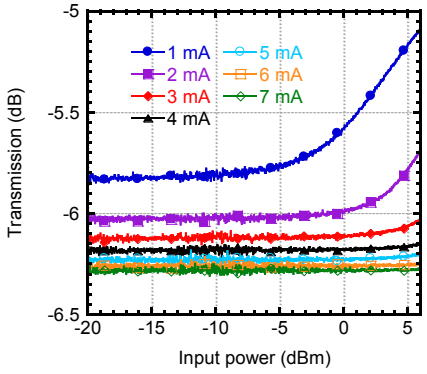

Figure 3-5 AM-AM characteristics for different bias currents.

The amplitude-to-amplitude (AM-AM) characteristics of the circuit for different bias currents are given in Figure 3-5. The power transmission drops a little when the bias current is increased. Moreover, it can be seen that the transmission and its slope show increasing trends for all biases. It also shows that higher nonlinearity appears at lower bias current and its nonlinearity decreases with the increase of the bias current. So the bias current can be tuned to adjust nonlinearity of the PDC to match the nonlinearity of the RoF transmission system.

3.4.2 PDC Linearization for an RoF Transmission System Using an MZM

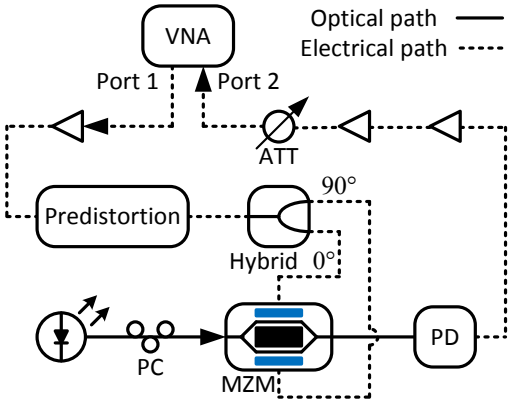

Figure 3-6 Experimental setup for the input P_{1dB}. VNA: Vector network analyzer. MZM: Mach-Zehnder modulator. PD: Photodetector.

To evaluate the linearization of the PDC, the proposed PDC is verified in an RoF transmission system where an MZM is used for optical subcarrier modulation. The input P_{1dB} without and with the PDC is measured. Figure 3-6 shows the experimental setup. A vector network analyzer (VNA) is used to generate RF signal and measure the power transmission. The output power of the VNA is swept from -27 to 0 dBm for the linearized RoF system and from -27 to -5 dBm for the unlinearized RoF system. A 100 kHz to 50 GHz broadband RF PA TA0L50VA is used to boost the RF output power of the VNA. It has the gain of 30 dB, return loss of -10 dB, saturation output power of 22 dBm, and noise figure (NF) of 5 dB. The PDC is connected between the PA and a 3-dB 90° hybrid. Anritsu MG9541A tunable laser source emits a continuous wave (CW) light with the optical power of 8.48 dBm and wavelength of 1550 nm to the MZM. A PC is used to adjust the polarization state for the maximum output power of the MZM. Sumitomo Osaka Cement 40 Gbit/s dual electrode MZM is employed and its transmission characteristic and bias point are shown in Figure 3-7. The MZM is biased at quadrature of 4.1 V to achieve optical SSB. At the quadrature bias, the IMD3 generated from the MZM is out of phase with the RF signal. A Discovery 40 GHz PD with responsivity of 0.6 A/W is used for photodetection. Two SHF 810 30 kHz to 40 GHz broadband RF PAs are used to amplify the photocurrent. The PAs have the gain of 30 dB, return loss of -15 dB, NF of 6 dB, and output P_{1dB} of 17 dBm. To limit the input power to the VNA, a variable

attenuator (ATT) is connected in front of the port 2 of the VNA. Three amplifiers and MZM are nonlinear devices in the RoF transmission system.

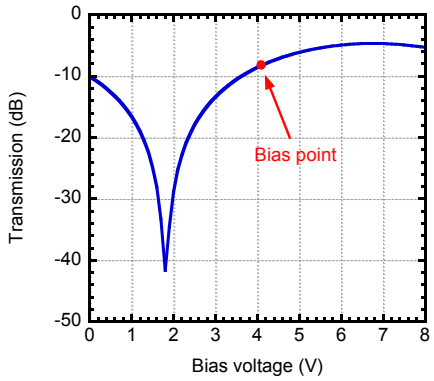

Figure 3-7 Transmission characteristic of the MZM and the bias point.

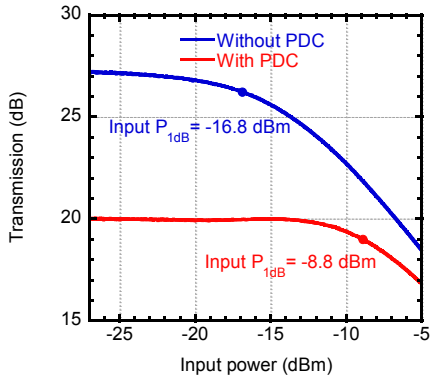

Figure 3-8 AM-AM characteristics without and with the PDC at 12 GHz.

The AM-AM characteristics without and with the PDC at 12 GHz is presented in Figure 3-8. It can be seen that the power transmission of the RoF transmission system without the PDC and its slope show decreasing trends. The AM-AM characteristics of the RoF transmission system without the PDC are reverse to the AM-AM characteristics of the PDC as shown in Figure 3-5. So working with the PDC, the transmission compression of the RoF system is compensated by the transmission expansion of the PDC. Figure 3-8 also shows that the input P_{1dB} is improved from -16.8 to -8.8 dBm at 12 GHz. The effective improvement of 1.8 dB is achieved at 12 GHz considering the insertion loss of the circuit.

The input P_{1dB}s without and with the PDC are given in Figure 3-9 (a). Without the PDC, the RoF system has the input P_{1dB} from -18 to -13 dBm. The input P_{1dB} is enhanced to be

more than -9 dBm with the PDC. However, the PDC induces loss to the system. Considering the insertion loss, the input power of the MZM is measured, and the effective improvement of the input P_{1dB} is given in Figure 3-9 (b). As it is shown in Figure 3-4, the circuit has high insertion loss at 10 GHz because of the fabrication defects. So the power of the IMD3 generated in the circuit is reduced. This leads to the magnitude mismatch and the RoF system cannot be linearized at 10 GHz. Figure 3-4 shows that the S_{21} from 7 to 8 GHz is lower. However Figure 3-9 (b) shows that the input P_{1dB} is improved by more than 1.2 dB from 7 to 8 GHz. The reason is that the phase mismatch is more severe for higher frequency, and the phase mismatch degrades the linearization. The decrease of the effective improvement of input P_{1dB} from 16 to 17 GHz is also caused by the phase mismatch.

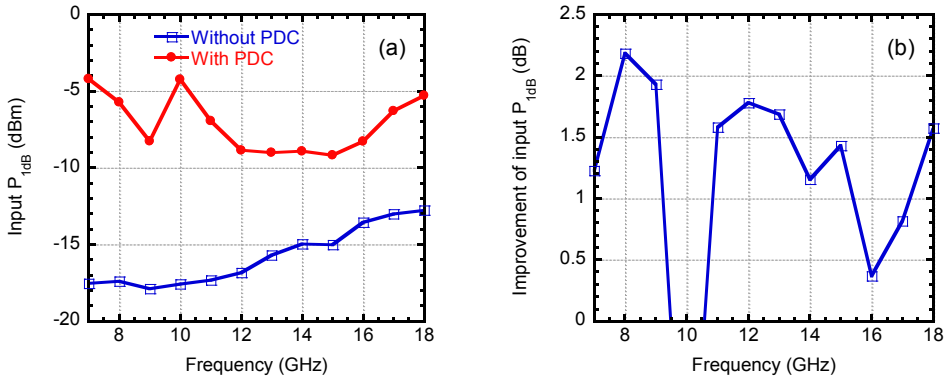

Figure 3-9 (a) Input P_{1dB}s without and with the PDC. (b) Effective improvement of the input P_{1dB}.

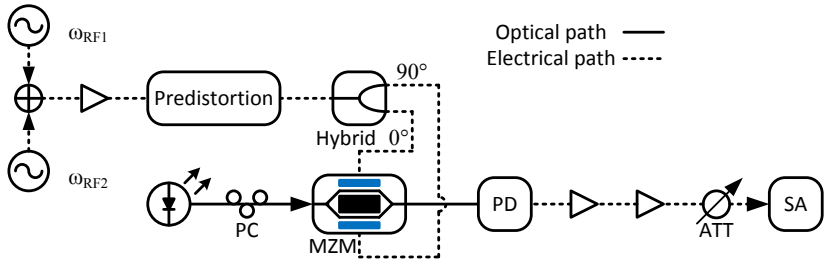

Figure 3-10 Experimental setup of the two-tone test.

A two-tone test is also employed. The experimental setup is given in Figure 3-10. Two RF signal generators are used to generate two-tone signals whose frequency spacing is 4 MHz. All the components are the same to the experimental setup of the input P_{1dB} except the fact that the VNA is replaced with a spectrum analyzer (SA). The SA is used to

measure the RF power of the RF signals and IMD3s. In this measurement, all the PAs work in their linear regions. The MZM is still biased at quadrature and optical SSB modulation is used.

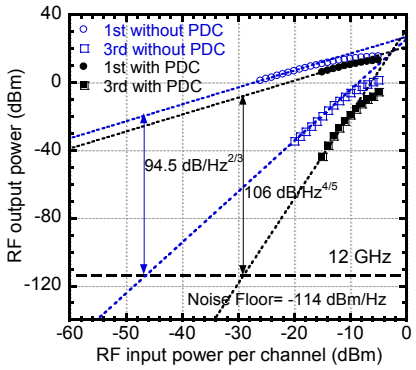

Figure 3-11 Measured SFDRs of the RoF transmission systems without and with the PDC at 12 GHz.

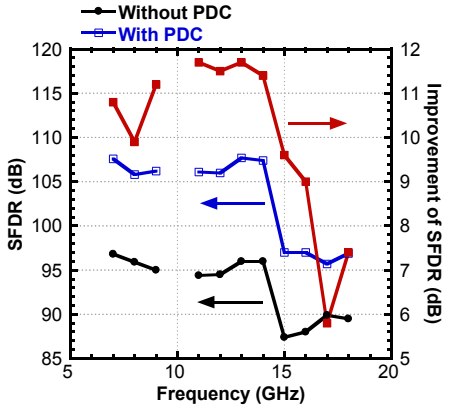

Figure 3-12 SFDRs of the RoF transmission systems without and with PDC and the improvements of SFDRs.

The measured SFDRs without and with the PDC at 12 GHz are given in Figure 3-11. It can be seen that the slope of the IMD is 3 without the PDC, which means the IMD is 3rd order limited. By applying the PDC, the nonlinearity is 5th order limited. It illustrates that the IMD3 is suppressed by the PDC and the dominant nonlinearity is IMD5. The SFDRs without and with the PDC and the improvements of the SFDRs are given in Figure 3-12. It can be seen that the improvement is high from 7 to 14 GHz and it decreases from 15 to 18 GHz. The SFDRs without and with the PDC both decrease from 15 GHz to 18 GHz. This is induced mainly by the loss from the microwave cables and adapters. Moreover, the PAs generate ~10 dB more noise from 15 to 18 GHz. From 7 to 14 GHz, the PDC

improves the SFDR by more than 9.9 dB and from 15 to 18 GHz, it improves the SFDR by more than 5.8 dB.

3.4.3 PDC Linearization for an RoF Transmission System Using an EAM

The PDC is also verified in an RoF transmission system using an EAM and erbium doped fiber amplifier (EDFA). The measurement is similar to the experiments for the MZM. Input P_{1dB} and SFDRs are measured. The experimental setup is given in Figure 3-13. A bias tee is used to combine the DC bias and RF signal. An OKI 40 Gbit/s EAM is used. An Amonics EDFA is used to compensate for the high insertion loss of the EAM, and its pump power is set to 40 mA. Two 800 MHz to 21 GHz wideband PAs ZVA-213+ are used to amplify the photocurrent. The PAs have the gain of 26 dB, NF of 3 dB, and output P_{1dB} of 24 dBm. All other components are the same as in Figure 3-6.

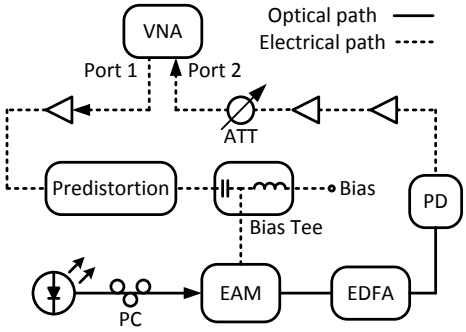

Figure 3-13 Experimental setup for the input P_{1dB}.

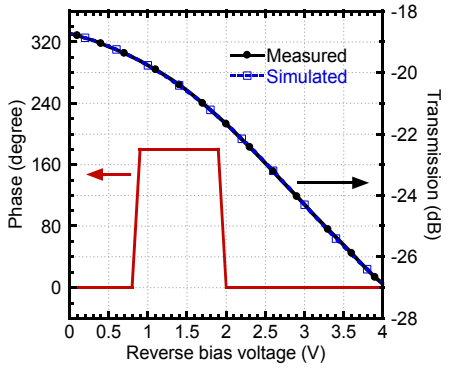

Figure 3-14 Transmission of the EAM, its simulated fitting curve, and phase difference between the generated RF signal and IMD3 from the EAM.

The transmission of the EAM, its fitting curve, and phase difference between the generated RF signal and IMD3 from the EAM are given in Figure 3-14. A 5th order polynomial is used to approximate the transmission. It can be seen that 5th order polynomial is enough to approximate the transfer function of the EAM. The generated RF signal and IMD3 from the MZM are always antiphase because of the Mach-Zehnder interferometer (MZI) structure. Unlike MZM, the phases of the generated RF signal and IMD3 from EAM depend on its bias voltage. The phase difference between the generated RF signal and IMD3 from the EAM is calculated through the fitting curve by Matlab. Figure 3-14 shows that the phase difference is 180° for the bias voltages from -0.9 to -1.9 V and it is 0° for other bias voltages. The PDC generates only inphase IMD3 no matter its bias current, so the EAM can be linearized for the bias voltages from -0.9 to -1.9 V. However, this range of bias voltage is sufficient for the EAM because low bias voltage induces low modulation efficiency and high bias voltage generates high insertion loss in the EAM. In the experiment, the bias voltage is set to -1.5 V.

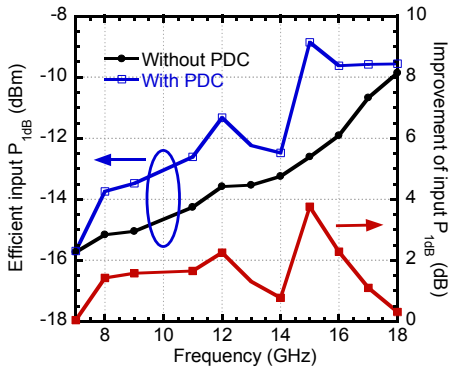

Figure 3-15 Input P_{1dB}s without and with the PDC and the improvements of the input P_{1dB}.

The measured input P_{1dB}s and improvements are shown in Figure 3-15. By using the PDC, the transmission compression of the RoF transmission system can be compensated by the PDC. The effective input power to the EAM is measured considering the insertion loss of the PDC. The input P_{1dB}s without and with using the PDC for the whole band are given. Without using the PDC, the RoF system has the input P_{1dB} from -16 to -10 dBm. Figure 3-15 shows ~1 dB and above improvements of the input P_{1dB} by the PDC from 8 to 17 GHz. The reasons of low improvement at 7 and 18 GHz are high power of the even order IMD generated in the RoF system and high power of the IMD5 generated by the PDC.

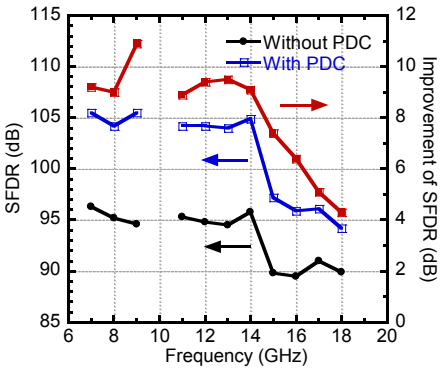

Figure 3-16 Measured SFDRs and improvement using the PDC.

The SFDR of the RoF transmission system using the EAM is also measured without and with using the PDC. The experimental setup is the same to Figure 3-13 except the fact that the VNA is replaced by the SA. The experimental results are given in Figure 3-16. The IMD3 generated by the RoF system is cancelled by the PDC and the nonlinearity is 5^{th} order limited. It can be seen that the improvement is ~9 dB and higher from 7 to 14 GHz and decreases from 15 to 18 GHz. The SFDRs without and with using the PDC both are decreased from 15 to 18 GHz. This is induced mainly by the loss from the microwave cables and adapters. Thus, the PDC improves the SFDR by more than ~9 dB from 7 to 14 GHz and more than ~4 dB from 15 to 18 GHz. Note that the PAs generate ~6 dB more noise from 15 to 18 GHz. If this additional noise is removed, higher improvement of SFDR could be obtained.

3.5 Summary

In this chapter, a low-cost analog broadband PDC is designed and experimentally verified. Two zero bias beam lead GaAs Schottky diodes are used as the predistorter. Zero bias leads to lower bias current which is lower than 3 mA so that lower power consumption is achieved. Because of the high series resistance of the zero bias diode, no broadband multi-section matching network is required. Therefore the size and parasitics of the circuit are significantly reduced. Without the bandwidth limitation of the matching network, the bandwidth of the PDC from 7 GHz to 18 GHz is obtained. Using the designed PDC, the input P_{1dB} of an RoF transmission system using an MZM is improved

by 0.4 and up to 2.2 dB for the frequencies from 7 to 18 GHz. The measured SFDRs are improved by more than ~10 dB from 7 to 14 GHz and ~6 dB from 15 to 18 GHz.

Moreover, the proposed PDC is also verified in an RoF transmission system using an EAM. The phase difference between the generated RF signal and IMD3 from the EAM is simulated. The simulation result shows that the EAM can be linearized by the PDC for the bias voltages from -0.9 to -1.9 V. So the EAM is biased at -1.5 V. The measured input P_{1dB} of the system is also improved by 0.8 and up to 3.8 dB for the frequencies from 8 to 17 GHz. And the measured SFDR is improved by more than ~9 dB from 7 to 14 GHz and ~4 dB from 15 to 18 GHz by the PDC.

Compared to the previous PDC [43], this PDC has many advantages: lower bias currents used and thus low power consumption, no matching network required and thus further smaller size and lower parasitics, and higher bandwidth. The comparison is shown in Table 3-1.

Table 3-1 Comparison of the proposed PDC and the previous work [43].

Parameters	Proposed PDC	Previous Work [43]
Bandwidth	7 to 18 GHz	3.1 to 4.8 GHz
Bias Current	< 3 mA	13.3 mA
Dimension	3.5×1.6 cm^2	13.2×7.7 cm^2

Chapter 4 Ultra Broadband Predistortion Circuit Using Dual Schottky Diode

4.1 Introduction

The broadband PDC using zero bias Schottky diodes proposed in Chapter 3 offers the advantages of high bandwidth, compact size, and low power consumption. However, the bandwidth is still limited because two WPDs are used. WPD has quarter wavelength transmission lines and the bandwidth to center frequency ratio is limited. It means that the center frequency has to be increased if the bandwidth needs to be broadened. Usually the bandwidth of WPD cannot exceed its center frequency. So the WPD cannot cover a band from low frequency to high frequency. If the WPD is replaced by another power divider, the bandwidth can be further improved.

In this chapter, a novel ultra broadband analog PDC is proposed and verified experimentally [109]. The predistorter is a dual Schottky diode where two Schottky diodes are integrated in anti-parallel design in a single chip. By using the dual diode, no power divider is required in the proposed PDC. So the bandwidth of the PDC is further increased. Also only one DC current source is required to bias the dual diode compared to the PDC using zero bias diodes proposed in Chapter 3. The bandwidth range from 10 MHz to 30 GHz is achieved in the experiments. Furthermore, the dimension of the PDC is further reduced to 2.4×1 cm^2. The PDC is evaluated using two-tone test in the RoF transmission systems, where the direct modulation, EAM, and MZM are used for optical subcarrier modulation. The improvements of the SFDRs by using the PDC are measured. Moreover, to verify the linearization of wideband signal, EVM of WiFi signals transmitted in the RoF transmission systems without and with the PDC are also measured and compared. The mechanism of the proposed PDC in this chapter is the same as that in Chapter 3. If a PDC has reverse gain characteristic of an RoF transmission system, the system is linearized by connecting it with the PDC.

4.2 Schematic and Prototype

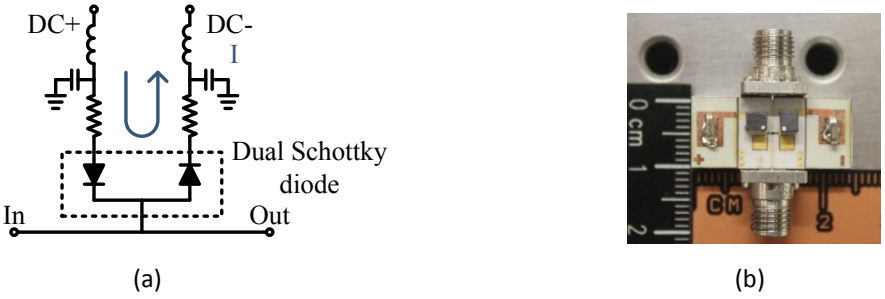

Figure 4-1 (a) Schematic of the proposed PDC. (b) The photo of the prototype.

The schematic of the proposed PDC is given in Figure 4-1 (a). The input and output ports of the PDC are connected by a microstrip transmission line whose characteristic impedance is 50 Ohms. A flip-chip dual Schottky diode is connected to the center. Inside the three-port chip, two diodes are connected in anti-parallel. There are two identical broadband resistors, and each of them is connected to the diode in series. The broadband capacitors and inductors work as bias tees. One DC current source is used to bias the dual diode as shown in Figure 4-1 (a). Both diodes are forward biased. It can be seen that push-pull structure is formed so that even order nonlinear components generated by the two diodes are eliminated. Even order nonlinear components from the PDC also contribute to the generation of the IMD3 in RoF transmission systems. In the PDC proposed in Chapter 3, two WPDs are employed because of their high isolation between two outputs, reciprocal, and matching to all ports. However, WPD is bandwidth limited because quarter-wave transformers are required. Furthermore, the dimension of WPD is further increased when the bandwidth to center frequency ratio is high. In addition, two DC bias current sources are required for the two divided branches. In this proposed PDC, no power divider is required because the anti-parallel diodes are integrated in one chip. So, the dimension of the circuit is further reduced and also broadband operation from low to high frequency can be easily obtained. In addition, only one bias current source is used.

Schottky diodes have ultra high bandwidth up to several THz, so the bandwidth of the PDC is mainly limited by the junction capacitance, parasitic capacitance, parasitic inductance, and phase distortion induced by the transit time of the diode. For the prototype of the proposed PDC, the series resistance of the diode is 4.4 Ohms which is

very low. Most of the input power will flow to the dual diode so that the transmission of the PDC will be degraded. Also, the PDC generated nonlinearities could be too high to compensate for the IMD3 of an RoF transmission system. Therefore, the two identical resistors are required to be tuned carefully for improving the S_{21} of the PDC. If the resistances of the resistors are too high, the predistortion will be too weak to compensate for the nonlinearity of the system. Simulation by Agilent ADS momentum shows that 150 Ohms thin film resistor will balance the transmission and the predistortion generation of the PDC. Broadband single layer ceramic capacitors are used for DC block and they can provide good connection to the ground for RF signals. The dimension of the PDC without connectors is 2.4×1 cm^2. The photo of the PDC is given in Figure 4-1 (b).

4.3 Measurement Results

4.3.1 Characteristics of the Proposed PDC

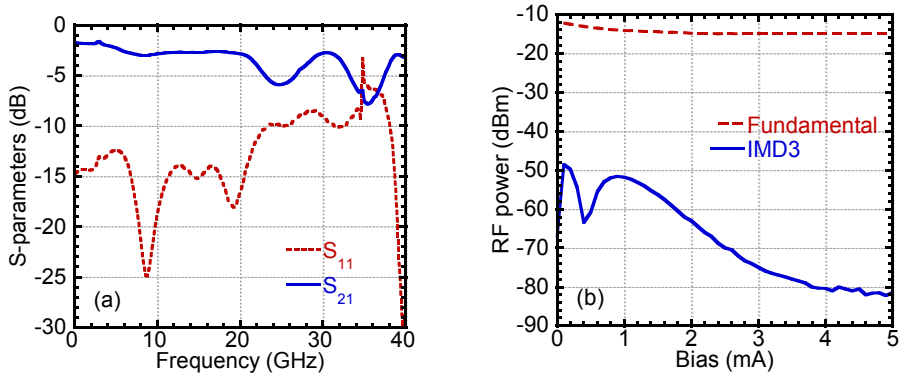

Figure 4-2 (a) Measured S-parameters of the proposed PDC. (b) Two-tone test of the proposed PDC.

The measured S-parameters of the PDC are given in Figure 4-2 (a). Flat S_{21} is achieved from 10 MHz to 33 GHz except a drop to -5.9 dB at 25 GHz. The S_{11} is lower than -10 dB from 10 MHz to 26 GHz. Then it increases to -8.5 dB at 28 GHz and decreases to -10 dB when the frequency is increased to 32 GHz. At around 35 GHz, a peak up to -3 dB of the S_{11} appears and the S_{21} drops to -8 dB. When the frequency is increased to be higher than 35 GHz, the S_{21} increases to -3 dB and the S_{11} decreases to -30 dB. The measured S-parameters show that the PDC can effectively work for more than 30 GHz. Even from 30 to 40 GHz, the S_{21} and S_{11} show that the PDC may be functional.

A two-tone test is conducted for the PDC to measure the RF power of the RF signal and IMD3 generated by the PDC. The bias current of the PDC is tuned from 0 to 5 mA. The frequencies of the two tones are 10 and 10.2 GHz. Figure 4-2 (b) shows that the RF signal is reduced by 3.2 dB as the bias current increases from 0 to 5 mA. The IMD3 achieves the highest power of 48.6 dBm at 0.1 mA and decreases to -82 dBm at 5 mA. Figure 4-2 (b) shows the IMD3 to RF signal ratio can be adjusted by tuning the bias current of the PDC. But the ratio range is limited so the PDC needs to be designed for the specific nonlinearity of the RoF transmission, i.e., choice of the resistance of the resistors is important.

4.3.2 PDC Linearization for a Directly Modulated RoF Transmission System

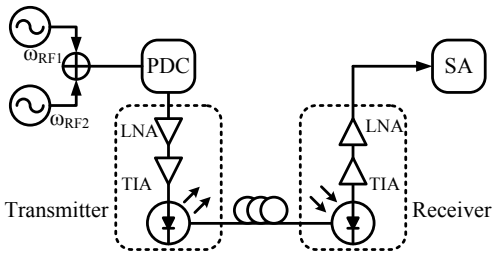

Figure 4-3 Experimental setup of the PDC linearization for a directly modulated RoF transmission system.

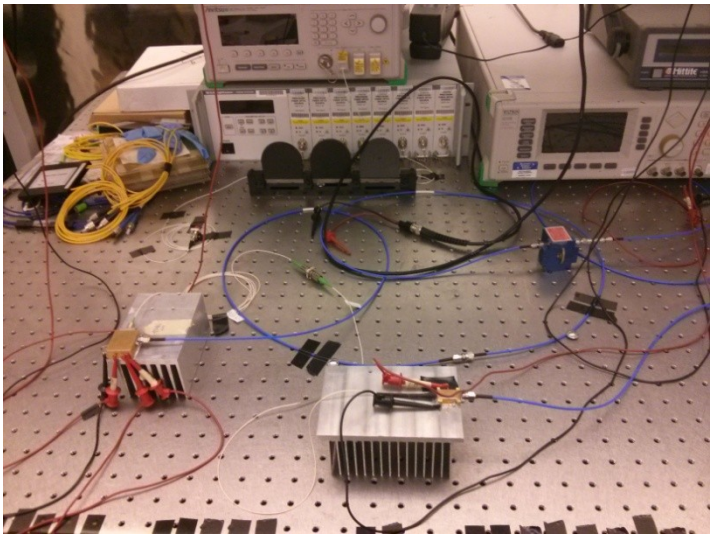

Figure 4-4 Photo of the experimental setup.

Firstly, the PDC is tested in a directly modulated RoF transmission system. Direct modulation is low-cost and the implementation is simple. Nonlinearities in directly modulated RoF transmission systems are mainly from the optical subcarrier modulation of the laser. The laser has a bandwidth of about 10 GHz. The experimental setup of the PDC linearized directly modulated RoF transmission system is given in Figure 4-3. Two RF signal generators are used for two-tone test. The frequencies are 8 and 8.002 GHz. The OTx is a laser integrated with a low noise amplifier (LNA) and a transimpedance amplifier (TIA), and the ORx is a PD with a TIA followed by an LNA. They are connected in BTB. The SA is used to measure the RF output power. The photo of the experimental setup is given in Figure 4-4.

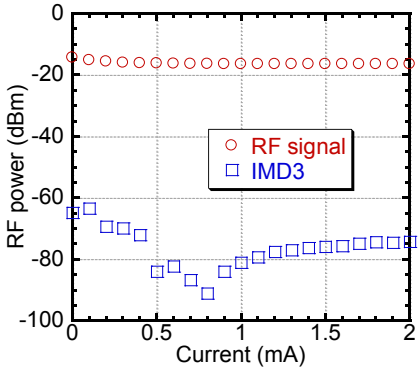

Figure 4-5 Measured RF output power of the RF signal and IMD3.

The RF input power is set to -10 dBm for each RF signal generator. The bias current of the PDC is tuned to find the maximal suppression of the IMD3. Figure 4-5 shows the measured RF output power of the RF signal and IMD3. It can be seen that the maximal suppression of the IMD3 is achieved at 0.8 mA. The IMD3 is suppressed from -63.3 to -91 dBm for the bias current from 0 to 0.8 mA and increased from -91 to -74.3 dBm for the bias current from 0.8 to 2 mA.

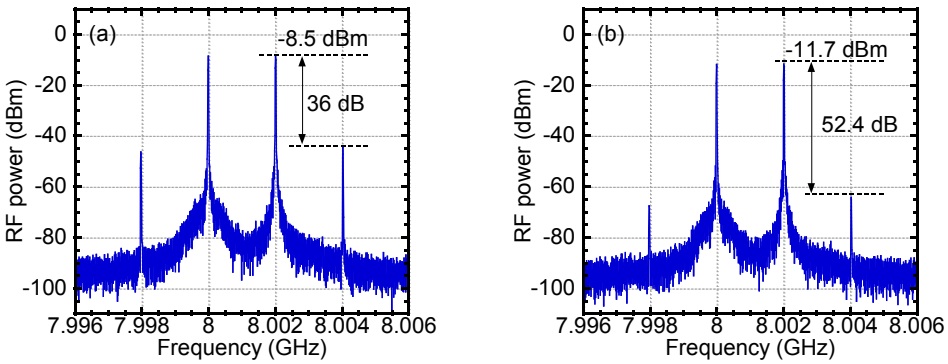

Figure 4-6 Measured RF spectra (a) without and (b) with the PDC.

The bias current is set to 0.8 mA for the maximal suppression of the IMD3 and the RF input power is -5 dBm per channel. Figure 4-6 shows the measured RF spectra without and with the PDC. It depicts that the RF signal is reduced by 3.2 dB due to the insertion loss of the PDC and the IMD3 is suppressed by 19.6 dB. Considering the 3.2 dB insertion loss to the RF signal, the effective suppression of the IMD3 is 10 dB.

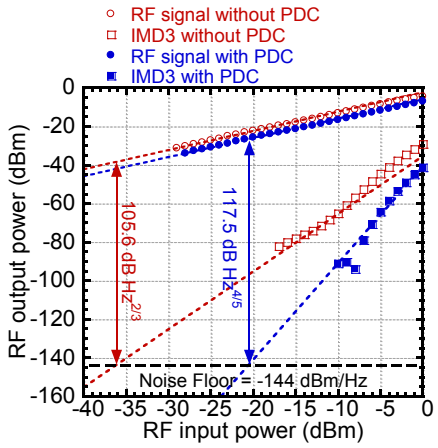

Figure 4-7 Measured SFDRs without and with the PDC of the directly modulated RoF transmission system.

The SFDR of the directly modulated RoF transmission system is also measured. The measured SFDRs without and with the PDC are given in Figure 4-7. It shows that the power of the IMD3 using the PDC is 5th order limited. This means that the IMD3 is suppressed and the IMD5 is dominant. In Figure 4-7, the SFDR is improved from 105.6 dB Hz$^{2/3}$ to 117.5 dB Hz$^{4/5}$. 11.9 dB improvement is obtained. So the directly modulated RoF transmission system is linearized by the PDC, with the SFDR improvement of ~12 dB.

4.3.3 PDC Linearization for an RoF Transmission System Using an EAM

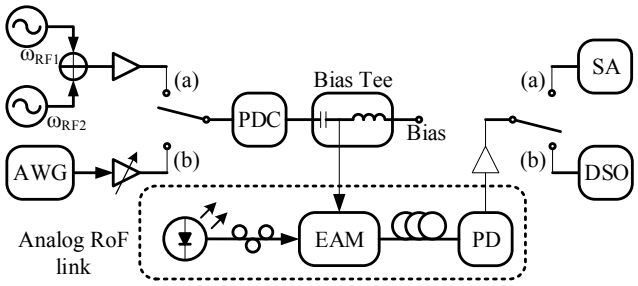

Figure 4-8 Experimental setup for (a) two-tone test and (b) WiFi signals.

The PDC is then evaluated in an RoF transmission system using an EAM. The experimental setup is given in Figure 4-8. Two-tone test and WiFi signals are used to verify the linearization by the PDC. The experimental setup for the two-tone test is given in Figure 4-8 (a). Two RF signal generators and a broadband power combiner are used to generate two-tone signal and the frequency spacing is 2 MHz. A PA TA0L50VA is used to boost the two-tone signal. The PDC is connected between the PA and a broadband bias tee which is used for combination of the RF signals and DC bias of the EAM. A laser source emits CW light with optical power of 8.48 dBm at wavelength of 1550 nm. A PC is used to adjust the polarization state for the maximum output power from the EAM. A 40 Gbit/s EAM OM5653C-30B from OKI is employed for the optical subcarrier modulation. The 40 GHz PD with responsivity of 0.6 A/W is used. The recovered RF signal is amplified by a 40 GHz PA SHF810. Finally, the RF power is measured in an SA U3772 from ADVANTEST. The photo of the experimental setup is presented in Figure 4-9.

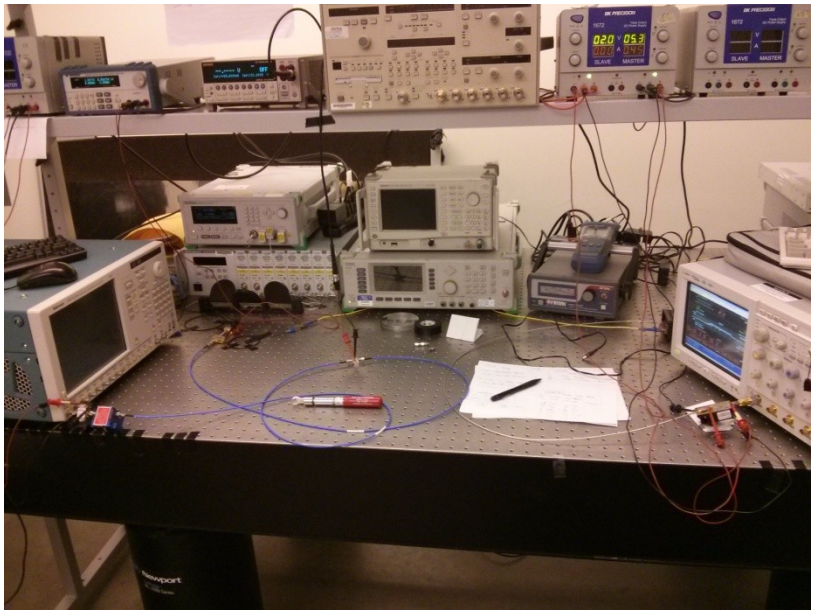

Figure 4-9 Photo of the experimental setup.

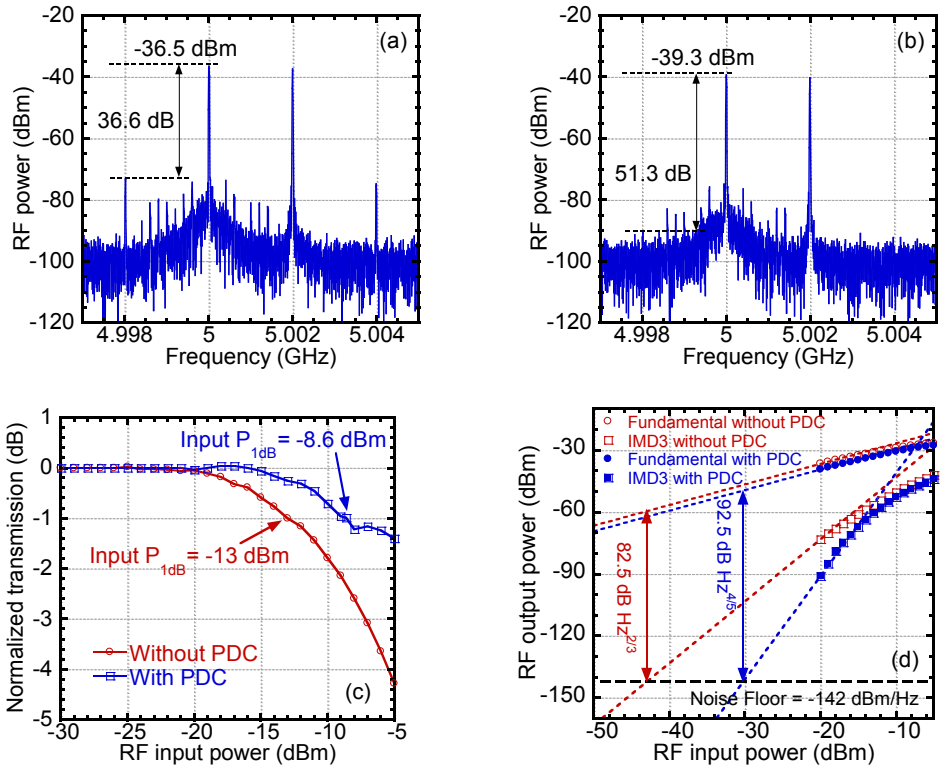

Figure 4-10 Measured RF spectra (a) without the PDC and (b) with the PDC at 5 GHz. (c) Normalized gain compression. (d) SFDRs without and with the PDC at 5 GHz.

The measured RF spectra at 5 GHz of the system output without and with the PDC respectively are given in Figure 4-10 (a) and (b). Considering the insertion loss induced

by the PDC, the IMD3 is suppressed effectively by 9.1 dB by the PDC. Figure 4-10 (c) shows the measured normalized transmission at 5 GHz. It can be seen that the input P_{1dB} is improved from -13 to -8.6 dBm and the effective improvement is 1.6 dB. The output P_{1dB} is improved from -31.4 to -29.8 dBm and 1.6 dB improvement is obtained. Figure 4-10 (d) shows the measured SFDRs without and with the PDC. It shows that the IMD3 is suppressed and thus 5^{th} order limitation is obtained when the PDC is used. The SFDR is improved by 10 dB at 5 GHz.

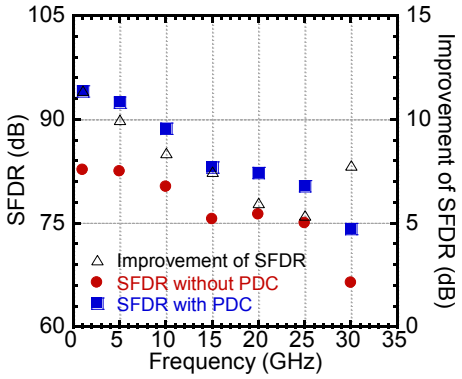

Figure 4-11 Measured SFDRs without and with the PDC respectively and the improvement of the SFDR versus the frequency.

Then the frequency is swept from 1 to 30 GHz and the SFDRs are measured. The measured SFDRs and the improvements of the SFDRs are given in Figure 4-11. It can be seen that the SFDR is improved by more than 10 dB from 1 to 5 GHz and by more than 5 dB from 1 to 30 GHz. The SFDRs drops by ~20 dB when the frequency is increased from 1 to 30 GHz. The reason is attributed to the accumulated loss in the system and increased noise for higher frequency.

WiFi signals are also transmitted in the RoF transmission system to test the PDC. The experimental setup is given in Figure 4-8 (b). An arbitrary waveform generator (AWG) 7122B from Tektronix generates WiFi signals at 2.4 GHz and 5 GHz compliant with 802.11a. The generated OFDM signal consists of 64 subcarriers with 16 quadrature amplitude modulation (QAM) occupying 20 MHz bandwidth. The signal rate is 36 Mb/s. A PA ZVA-213+ and a broadband variable attenuator constitute a variable PA. The gain is adjusted so that the RF input power to the EAM is always the same. After transmission

in the RoF system, a digital storage oscilloscope (DSO) 81204B from Keysight is used to receive and demodulate the WiFi signals. The constellation diagrams and EVMs are measured and given in Figure 4-12. It shows that the EVM is reduced from -21.15 to -22.15 dB at 2.4 GHz and from -20.5 to -21.5 dB at 5 GHz. Thus, 1 dB improvement is achieved.

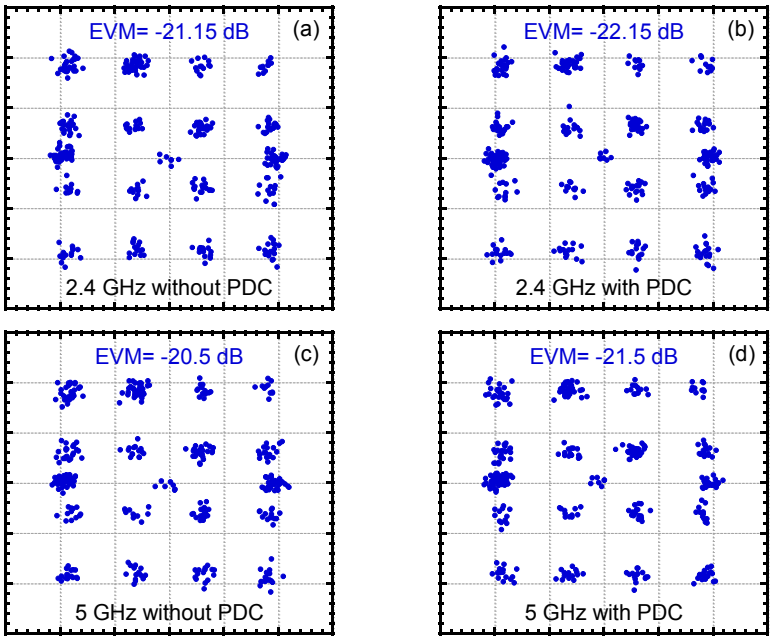

Figure 4-12 Measured constellation diagrams and EVMs at 2.4 GHz (a) without, and (b) with the PDC, and at 5 GHz (c) without and (d) with the PDC.

4.3.4 PDC Linearization for an RoF Transmission System Using an MZM

Like the experiments in Chapter 3, this proposed PDC is also evaluated in an RoF transmission system using an MZM. The experimental setup is given in Figure 4-13. A 40 Gbit/s MZM is used as the external modulator. Two tests are conducted to verify the PDC in the system. One is two-tone test from 2 to 30 GHz. The other is WiFi signal transmission test at 2.4 GHz. For two-tone test, the frequency spacing is 2 MHz. Two RF signals are combined by the broadband RF combiner and boosted by a PA TA0L50VA. The amplified RF signals are injected into the PDC, and then divided by a 90° hybrid to feed the MZM. A laser emits 8 dBm CW at 1550 nm. A PC is used because the MZM is polarization dependent. The half-wave voltage of the MZM is 5 V and the minimum transmission point is at 2.3 V as shown in Figure 4-14. The MZM is biased at its

quadrature point of 4.8 V so that the optical SSB modulation is achieved. After the photodetection by a 40 GHz PD, the signals are amplified by a broadband PA SHF810 and measured by an SA. The photo of the experimental setup is shown in Figure 4-15.

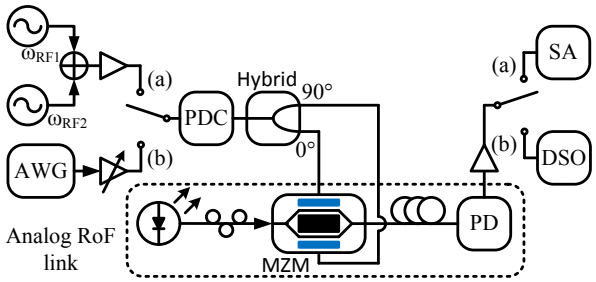

Figure 4-13 Experimental setup of the linearized RoF transmission system using the MZM. (a) Two-tone test. (b) WiFi signal transmission test.

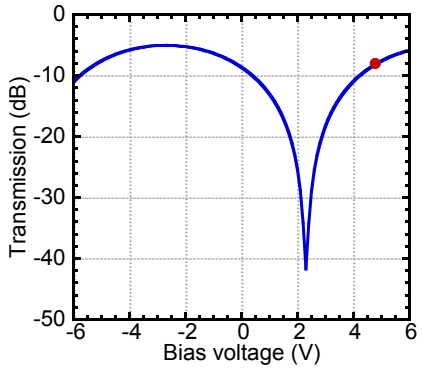

Figure 4-14 Measured transmission of the MZM.

The measured RF spectra without and with the PDC at 10 GHz are given in Figure 4-16. The bias current of the PDC is adjusted for the maximal suppression of the IMD3. Figure 4-16 shows that the IMD3 is suppressed effectively by 1.3 dB. Figure 4-17 shows the measured SFDRs without and with the PDC. It shows that the IMD3 is suppressed and the IMD5 is dominant. The SFDR is improved by 8.8 dB. Moreover, the SFDRs from 2 to 30 GHz are measured and given in Figure 4-18. It can be seen that the SFDRs are improved by more than 12 dB from 2 to 5 GHz and more than 5 dB from 2 to 30 GHz. Because of the accumulated loss in the system, the improvements of the SFDRs for higher frequencies are decreased. Figure 4-18 illustrates that the PDC linearizes the broadband RoF system from low frequency to 30 GHz.

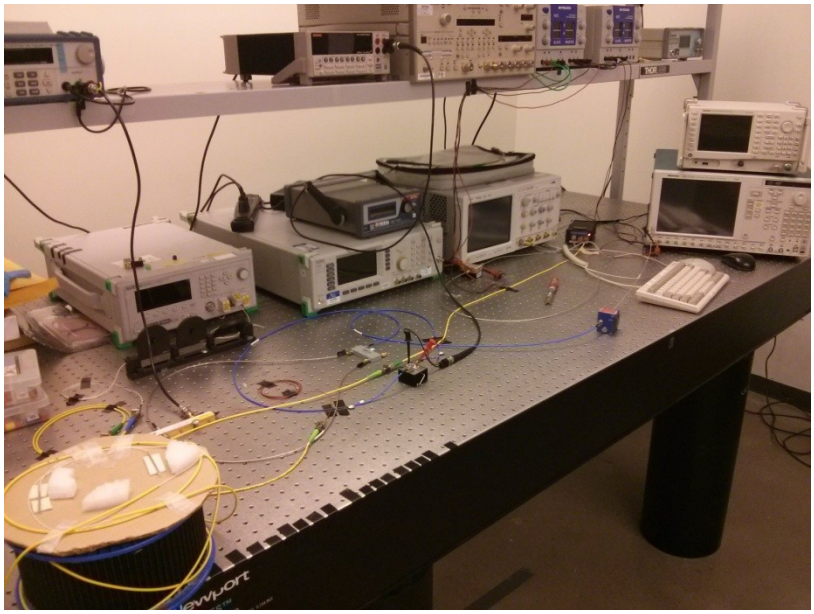

Figure 4-15 Photo of the experimental setup.

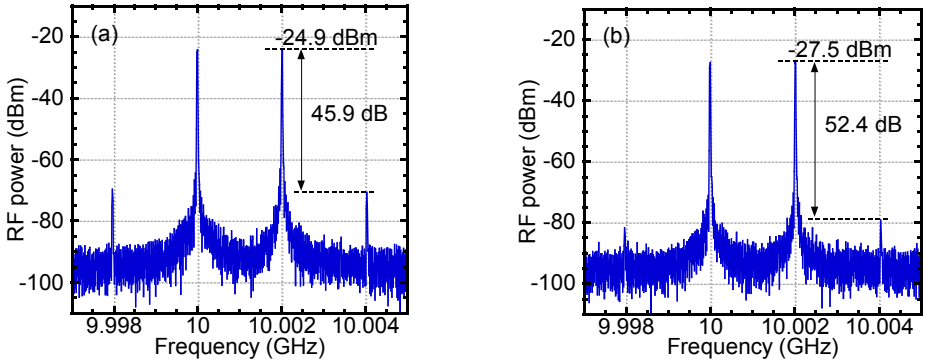

Figure 4-16 Measured RF spectra (a) without and (b) with the PDC.

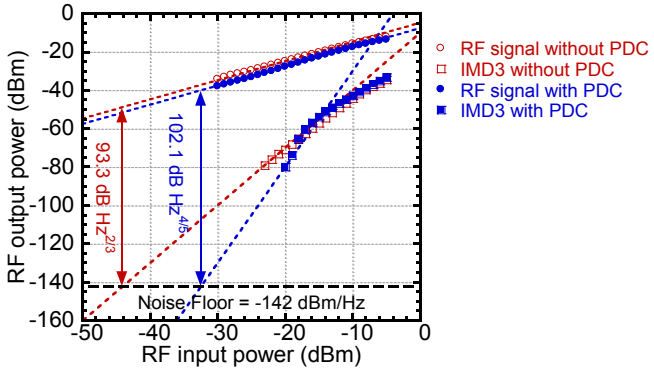

Figure 4-17 Measured SFDRs (a) without and (b) with the PDC for the RoF transmission system using an MZM.

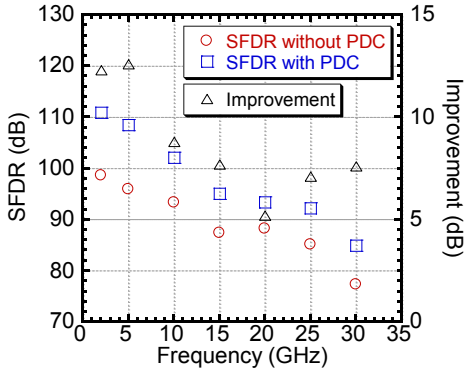

Figure 4-18 Measured SFDRs from 2 to 30 GHz and the improvements.

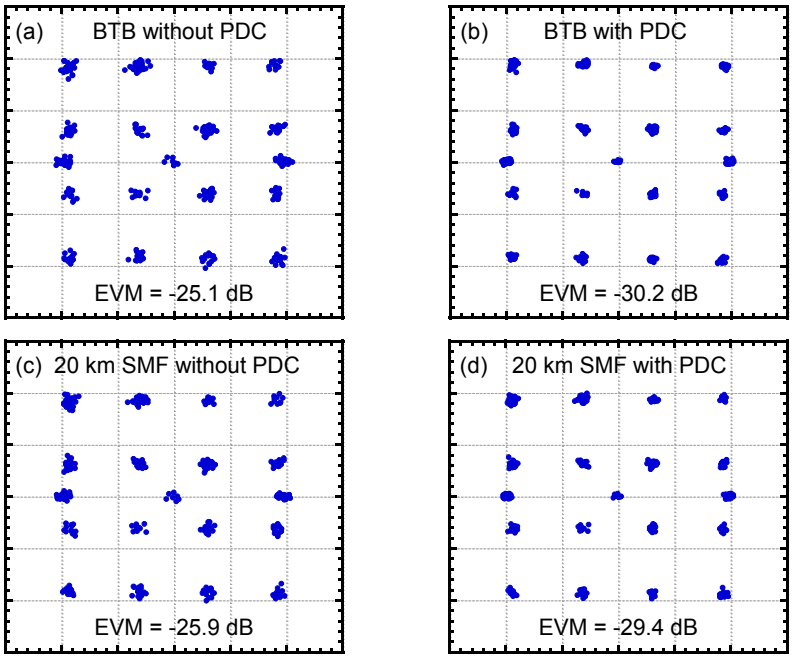

Figure 4-19 Measured constellation diagrams and EVMs for (a) BTB without the PDC, (b) BTB with the PDC, (c) 20 km SMF transmission without the PDC, and (d) 20 km SMF transmission with the PDC.

Additional to the two-tone test, a WiFi signal transmission is also used to verify the linearization performance of the PDC for wideband signals. The experimental setup is shown in Figure 4-13 (b). The AWG 7122B generates a WiFi signal at 2.4 GHz compliant with 802.11a. A PA ZVA-213+ and a broadband variable attenuator constitute a variable amplifier. A DSO 81204B is used to demodulate the WiFi signals. The variable amplifier is adjusted so that the RF input power to the MZM is the same for both RoF transmission systems without and with the PDC. The WiFi signals are verified for BTB and 20 km SMF transmission.

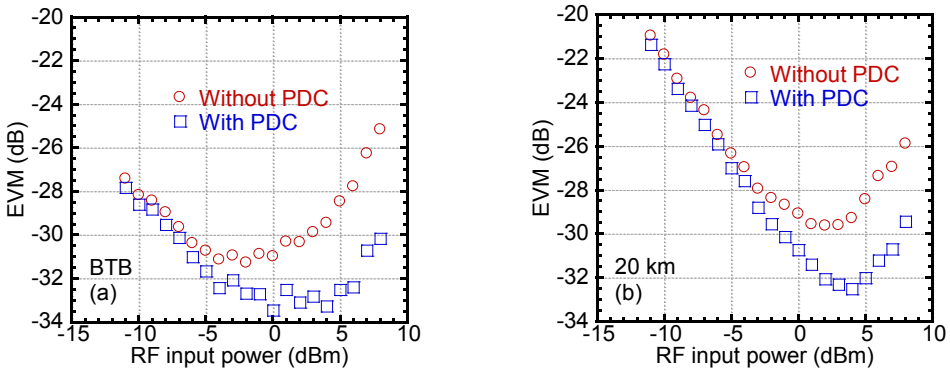

Figure 4-20 Measured EVMs without and with the PDC for (a) BTB and (b) 20 km SMF transmission.

Figure 4-19 presents the measured constellation diagrams and EVMs without and with the PDC respectively. The RF input power to the MZM is set to 8 dBm. For BTB, the EVM is improved from -25.1 to -30.2 dB. And for 20 km SMF transmission, the EVM is improved from -25.9 to -29.4 dB. The measured constellation diagrams also show improvements by the PDC. Figure 4-20 shows the measured EVMs without and with the PDC for BTB and 20 km SMF transmission versus the RF input power to the MZM. The gain of the variable amplifier in front of the PDC is adjusted by 1 dB step to change the RF input power to the MZM. The RF input power to the MZM is from -11 to 8 dBm. In Figure 4-20, it is obvious that the EVMs without the PDC are higher for low and high RF input power. The reason is that the noise is dominant for low RF power and the nonlinearities are dominant for high RF power. It can be seen that the EVM is improved by the PDC independent of the RF power level. The PDC improves the EVM by more than 0.4 dB for the RF input power from -11 to 8 dBm. This shows that the PDC can linearize an RoF system for broad RF input power range. When the RF input power is increased, the improvements of the EVMs are also enhanced for both BTB and 20 km SMF transmission. For BTB, the improvements of the EVMs are higher than 1 dB for the RF input power from -4 to 8 dBm, and the maximal improvement of 5.1 dB is achieved at 8 dBm RF input power. For 20 km SMF transmission, the improvements are higher than 1 dB for the RF input power from -2 to 8 dBm. The maximal improvement is achieved at 6 dBm RF input power. Here the maximal improvement of the EVM is 3.5 dB which is 1.6 dB lower than that for BTB. This is due to the deteriorated signal-to-noise ratio induced by the optical fiber loss. The WiFi test shows that the PDC can effectively linearize the 20 km SMF RoF transmission for the wideband RF signals.

4.4 Summary

In this chapter, a novel ultra broadband analog PDC is proposed and designed to linearize RoF transmission systems. A dual anti-parallel Schottky diode is used as the predistorter. Push-pull operation using only one DC bias is obtained; in addition there is no need for quarter-wavelength transmission line and power divider. The PDC is adjusted by tuning the bias current. The experimental results show that the replacement of the WPD by the dual diode does not degrade the linearization. The bandwidth from 10 MHz to 30 GHz is achieved. The dimension of the PDC is 2.4×1 cm^2. Both RoF transmission systems with direct modulation and external modulation are tested in the experiments. In two-tone test, a directly modulated RoF transmission is linearized and the SFDR at 8 GHz is improved by 11.9 dB. The PDC is also evaluated in an RoF transmission system using an EAM. In two-tone test, it is found that the IMD3 is suppressed by the PDC and the nonlinearity is 5th order limited. The input and output P_{1dB} are both improved. The measurements show that the SFDR is improved by more than 10 dB from 1 to 5 GHz and more than 5 dB from 1 to 30 GHz by the PDC. The low SFDR improvement at higher frequency is limited by the increased noise and accumulated loss. Moreover, WiFi signals at 2.4 and 5 GHz are transmitted in the RoF transmission systems to test the PDC. The measurements show that the EVM is reduced by 1 dB at both 2.4 GHz and 5 GHz by the PDC. For an externally modulated RoF transmission system using an MZM, the SFDR is improved by more than 12 dB from 2 to 5 GHz and more than 5 dB from 2 to 30 GHz. The IMD3 is suppressed and the IMD5 is dominant. Moreover, WiFi signal at 2.4 GHz is verified in the RoF transmission system with external modulation using the MZM for BTB and 20 km SMF transmission. For the RF input power to the MZM from -11 to 8 dBm, the EVM is improved by more than 0.4 dB. The maximal improvements of the EVMs are 5.1 dB for BTB and 3.5 dB for 20 km SMF transmission. It is proved that the low-cost ultra broadband PDC can linearize the RoF transmission systems with direct modulation and external modulation. To our knowledge, this is the reported PDC with the broadest bandwidth.

Comparison of the previous work, the PDC in this chapter and the PDC in Chapter 3 is presented in Table 4-1. It can be seen that the proposed PDC in this chapter has several

advantages, such as wider bandwidth, smaller dimension, and requiring only one bias current source, but its power consumption is higher than that of the PDC using zero bias diode proposed in Chapter 3.

Table 4-1 Comparison of the PDCs.

Parameters	PDC in Chapter 4	PDC in Chapter 3	Previous Work [43]
Bandwidth	10 MHz to 30 GHz	7 to 18 GHz	3.1 to 4.8 GHz
Bias Current	< 6 mA	< 3 mA	13.3 mA
Dimension	2.4×1 cm^2	3.5×1.6 cm^2	13.2×7.7 cm^2
Bias	1	2	2

Chapter 5 Dual Wavelength Linearization for RoF Transmission Systems

5.1 Introduction

In Chapters 3 and 4, the analog PDCs are used to suppress the IMD3 of RoF transmission systems. Although the PDCs provide several advantages, they induce more loss to the systems. Moreover, the PDCs cannot deal with HDs and even order IMDs. In multiband RoF transmission systems, it is possible for HDs and even order IMDs to drop in the passband of signals. So the HDs and even order IMDs have to be suppressed in RoF transmission systems. Because the digital linearization cannot be applied for a system with high bandwidth such as 10 GHz by now, the optical linearization method is the only way to suppress HDs and even order IMDs. In this chapter, the DWL is used and investigated to linearize the externally modulated RoF transmission systems. The DWL technique was proposed to suppress the 3^{rd} order nonlinearities of an EAM [94], the IMD3 of a phase modulator [95], and the IMD3 of an MZM [96]. The bandwidth of the DWL technique is only limited by the RF bandwidth of the employed external modulator. In this chapter, the DWL technique is investigated to suppress both the 2^{nd} and 3^{rd} order nonlinearities of an EAM simultaneously [110]. It is also used to suppress the 2^{nd} order nonlinearities of an MZM in this chapter. Single-tone test and two-tone test are used to measure the SFDRs of RoF transmission systems. Comprehensive theoretical and experimental studies of DWL technique are presented in this chapter.

5.2 Principle

DWL technique can be applied if an externally modulated RoF transmission has wavelength dependent transmission characteristics [94]. Two lasers with different wavelengths are injected to an externally modulated RoF transmission system that introduces wavelength dependent transmission characteristics. The RF signal drives the RoF transmission system for optical subcarrier modulation. Each of the two optical carriers carries its own RF signal and nonlinear components. The nonlinear components can be suppressed if the nonlinear components from the two optical carriers are in

antiphase with each other and the RF signal power can be improved if the two RF signals are inphase. By adjusting the optical power ratio of the two lasers, the optimal suppression of the nonlinearity can be achieved. The EAM and MZM both can be linearized by DWL technique because the two modulators are wavelength dependent.

5.3 DWL for an RoF Transmission System Using an EAM

The EAM provides several advantages as presented in Chapter 2, so it is a good solution for optical subcarrier modulation in RoF transmission systems. However, EAM generates strong odd and even order nonlinearities which have to be suppressed. Also EAM has higher insertion loss. Analog PDC can linearize EAMs, but more loss is induced to the system. DWL technique can suppress the nonlinearities and improve the signal power in an RoF system using an EAM. Therefore DWL technique applied to an RoF transmission system using an EAM will be studied theoretically and experimentally.

5.3.1 Theory

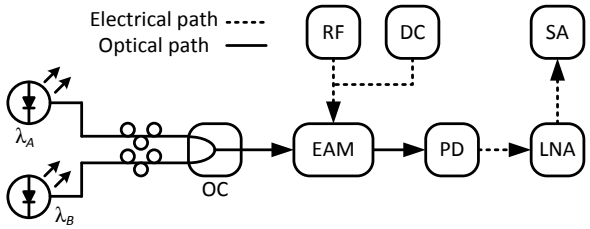

Figure 5-1 Schematic diagram and experimental setup of DWL for an RoF transmission system using an EAM.

Figure 5-1 shows the schematic diagram. Two lights emitted from two lasers with different wavelengths are coupled through an optical coupler (OC) and transmitted to an EAM. The two lights are modulated by the same RF signal. Due to the different modulation characteristics of the EAM for the two wavelengths, each light transports its own components of the RF signal and nonlinearities to the optical receiver. Because the two lights are emitted from two different lasers, they are incoherent with each other. In a PD, the two lights are detected separately and thus the sums of the RF signals and nonlinear components are obtained. The total detected RF signal and nonlinear components can be changed by tuning the optical power ratio.

Single-tone is considered in the theory. Two lights A and B are assumed to be emitted to an EAM. The 2nd and 3rd order nonlinearities are the main concerns in an RoF transmission system, so a 5th order polynomial is employed to approximate the transmission characteristics of the EAM [37], i.e.,

$$\frac{P_{o\_A}}{P_{i\_A}} = T_A = \sum_{n=0}^{5} a_n V^n \tag{5.1}$$

where P_{i_A} is the optical input power of the EAM for light A, P_{o_A} is the optical output power for light A, T_A is the optical transmission of the EAM for light A, a_n is the n^{th} order coefficient of the polynomial, and V is the reverse voltage applied to the EAM. The transmission of the EAM for light B can be also described as follows:

$$\frac{P_{o\_B}}{P_{i\_B}} = T_B = \sum_{n=0}^{5} b_n V^n \tag{5.2}$$

The applied reverse voltage of the EAM is expressed as

$$V = V_{DC} + V_{RF} \cos \omega_{RF} t \tag{5.3}$$

where V_{DC} is the DC reverse bias voltage of the EAM, V_{RF} is the magnitude of the RF signal voltage, and ω_{RF} is the angular frequency of the RF signal. Substituting (5.3) into (5.1), the optical output power of the EAM for light A is given as follows:

$$P_{o\_A} = P_{i\_A} \sum_{n=0}^{5} m_{n\_A} \cos(n\omega_{RF} t) \tag{5.4a}$$

where

$$\begin{aligned} m_{0\_A} = {} & a_0 + a_1 V_{DC} + a_2 \left(V_{DC}^2 + \frac{1}{2} V_{RF}^2 \right) + a_3 \left(V_{DC}^3 + \frac{3}{2} V_{DC} V_{RF}^2 \right) \\ & + a_4 \left(V_{DC}^4 + 3 V_{DC}^2 V_{RF}^2 + \frac{3}{8} V_{RF}^4 \right) \\ & + a_5 \left(V_{DC}^5 + 5 V_{DC}^3 V_{RF}^2 + \frac{15}{8} V_{DC} V_{RF}^4 \right) \end{aligned} \tag{5.4b}$$

$$m_{1\_A} = a_1 V_{RF} + a_2 2V_{DC}V_{RF} + a_3\left(3V_{DC}^2 V_{RF} + \frac{3}{4}V_{RF}^3\right) + a_4(4V_{DC}^3 V_{RF} + 3V_{DC}V_{RF}^3) + a_5\left(5V_{DC}^4 V_{RF} + \frac{15}{2}V_{DC}^2 V_{RF}^3 + \frac{5}{8}V_{RF}^5\right) \quad (5.4c)$$

$$m_{2\_A} = a_2\frac{1}{2}V_{RF}^2 + a_3\frac{3}{2}V_{DC}V_{RF}^2 + a_4\left(3V_{DC}^2 V_{RF}^2 + \frac{1}{2}V_{RF}^4\right) + a_5\left(5V_{DC}^3 V_{RF}^2 + \frac{5}{2}V_{DC}V_{RF}^4\right) \quad (5.4d)$$

$$m_{3\_A} = a_3\frac{1}{4}V_{RF}^3 + a_4 V_{DC}V_{RF}^3 + a_5\left(\frac{5}{2}V_{DC}^2 V_{RF}^3 + \frac{5}{16}V_{RF}^5\right) \quad (5.4e)$$

$$m_{4\_A} = a_4\frac{1}{8}V_{RF}^4 + a_5\frac{5}{8}V_{DC}V_{RF}^4 \quad (5.4f)$$

$$m_{5\_A} = a_5\frac{1}{16}V_{RF}^5 \quad (5.4g)$$

The RF signal and nonlinear components carried by light *A* are expressed by (5.4). The optical output power for light *B* is also obtained by expanding (5.2) with (5.3). m_{n_B} can be derived in the same way. The two lights are transmitted to a PD and detected. Photocurrent is given by

$$I = R\left(P_{o\_A} + P_{o\_B}\right) \quad (5.5)$$

where *R* is the responsivity of the PD. The components generated by the beating of the two lights in the PD are not involved because the frequency spacing of the two lights is too high to be detected by the PD. It can be seen that each of the two lights carries its own components of the RF signal and nonlinearities, and the sums of the two RF signals and different order nonlinear components are obtained after photodetection. The n^{th} order nonlinear component of the photocurrent is expressed as

$$I_n = RP_{i\_A}m_{n\_A}\cos(n\omega_{RF}t) + RP_{i\_B}m_{n\_B}\cos[n\omega_{RF}(t + DL\Delta\lambda + \Delta t)] \tag{5.6}$$

where D is the fiber CD coefficient, L is the fiber length, $\Delta\lambda$ is the wavelength difference, and Δt is the delay induced by the chirp of the EAM. The CD induces delay, and the higher order nonlinearity is more susceptible to the delay. Combining the components with cosine in (5.6), the n^{th} order nonlinear component of the photocurrent is given in (5.7).

$$\begin{aligned} I_n &= R\sqrt{\left(P_{i\_A}m_{n\_A}\right)^2 + \left(P_{i\_B}m_{n\_B}\right)^2 + 2P_{i\_A}m_{n\_A}P_{i\_B}m_{n\_B}\cos[n\omega_{RF}(DL\Delta\lambda + \Delta t)]}\cos \\ &\quad + \tan^{-1}\frac{P_{i\_B}m_{n\_B}\sin[n\omega_{RF}(DL\Delta\lambda + \Delta t)]}{P_{i\_A}m_{n\_A} + P_{i\_B}m_{n\_B}\cos[n\omega_{RF}(DL\Delta\lambda + \Delta t)]}\Bigg] \\ &= R\sqrt{\left[P_{i\_A}m_{n\_A} + P_{i\_B}m_{n\_B}\cos[n\omega_{RF}(DL\Delta\lambda + \Delta t)]\right]^2 + \left[P_{i\_B}m_{n\_B}\sin[n\omega_{RF}(DL\Delta\lambda\right.}} \\ &\quad + \tan^{-1}\frac{P_{i\_B}m_{n\_B}\sin[n\omega_{RF}(DL\Delta\lambda + \Delta t)]}{P_{i\_A}m_{n\_A} + P_{i\_B}m_{n\_B}\cos[n\omega_{RF}(DL\Delta\lambda + \Delta t)]}\Bigg] \end{aligned} \tag{5.7}$$

Required condition for the maximal suppression of the n^{th} order nonlinear component is given by

$$\frac{P_{i\_A}m_{n\_A}}{P_{i\_B}m_{n\_B}} = -\cos[n\omega_{RF}(DL\Delta\lambda + \Delta t)] \tag{5.8}$$

It can be seen that the nonlinear components carried by the two lights can be suppressed by each other by adjusting the optical power ratio if the nonlinear components from the two transmissions are antiphase with each other. However, (5.7) and (5.8) show that the nonlinearities cannot be eliminated completely because the fiber dispersion and transmitter's chirp degrade the suppression.

Here the suppressions of both the 2nd and 3rd order nonlinearities are considered. Two SFDR definitions are used: SFDR with respect to the 2nd order nonlinearity in which the 2nd order nonlinearity is considered as the major nonlinear distortion contribution, named as $SFDR_2$. SFDR with respect to the 3rd order nonlinearity in which the 3rd order nonlinearity is considered as the major nonlinear distortion contribution, called $SFDR_3$. Moreover, both the 2nd and 3rd order nonlinearities can be suppressed simultaneously by DWL technique, but the maximal suppressions cannot occur simultaneously. Thus, to

comprehensively study DWL technique, two cases are considered: Case I—maximal suppression of the 2nd order and Case II—maximal suppression of the 3rd order. In addition, both the single RF tone and two RF tones are considered. Thus, the suppressions of both the HDs and IMDs can be analyzed.

5.3.2 Theoretical Analysis

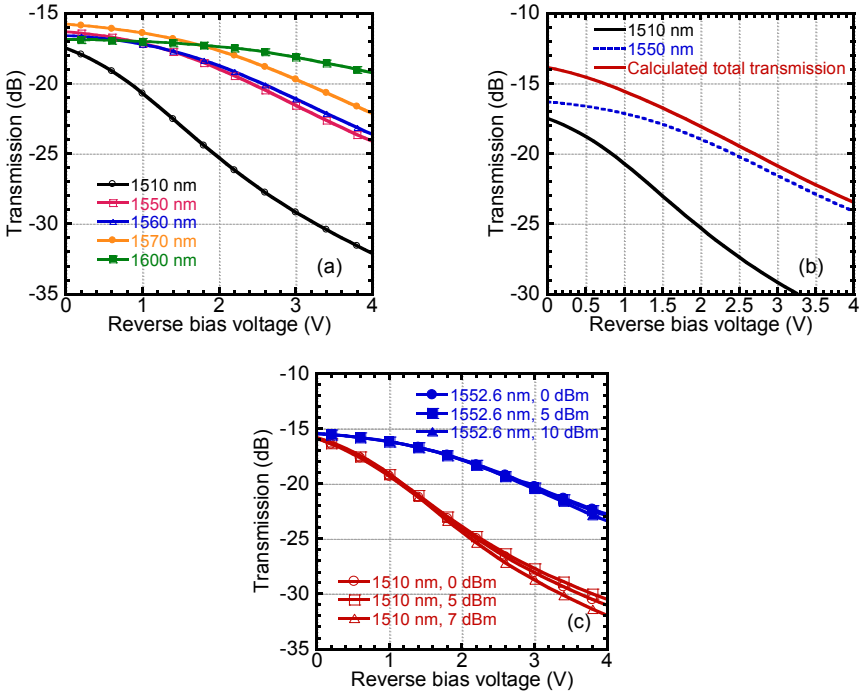

Figure 5-2 Measured transmissions of the EAM.

To verify DWL technique, the RF signals and nonlinearities in an RoF transmission system using DWL technique are calculated and analyzed using the theory provided above. The schematic used for the calculation is given in Figure 5-1. Transmissions of the EAM for different wavelengths are measured and given in Figure 5-2 (a). It shows that the transmission of the EAM depends on the light wavelength and the absorption of the EAM is higher for lower wavelength. Figure 5-2 (b) shows that the calculated total transmission of the EAM when two injected wavelengths are 1510 nm and 1550 nm. Optical input power for the two wavelengths is the same. It can be seen that the total transmission is more linear than the two individual transmissions. This EAM is designed for C-band. The 1510 nm wavelength cannot be used individually for this EAM because the insertion loss is too high. Usually the EAM is biased from -1 to -3 V for low insertion

loss and high modulation efficiency. In the calculation, 1510 nm and 1552.6 nm are used. The measured transmissions for 1510 nm and 1552.6 nm of the EAM with different optical input power are given in Figure 5-2 (c). The absorption for 1510 nm is higher than that for 1552.6 nm. Figure 5-2 (c) presents the optical input power dependence of the EAM. The transmission characteristics shift little, especially for the reverse bias voltages from 0 to 2 V, when the optical input power is swept from 0 to 10 dBm at 1552.6 nm and from 0 to 7 dBm at 1510 nm. This denotes that the transmission characteristic of the EAM is independent of the optical input power. The fitting polynomials as shown in (5.1) and (5.2) are used to approximate the two transmissions of the EAM for 1510 nm and 1552.6 nm. The coefficients of the fitting polynomial are extracted as $a_0 = 0.0179$, $a_1 = -0.0077$, $a_2 = -0.0049$, $a_3 = 0.0044$, $a_4 = -0.0011$, $a_5 = 0.0001$, $b_0 = 0.0242$, $b_1 = -0.0034$, $b_2 = 0.0012$, $b_3 = -0.0021$, $b_4 = 0.0007$, $b_5 = -0.0001$.

Case I: Maximal suppression of 2nd order

By using the theories provided above, the RF output power of the RF signal, HD2, and 3rd order harmonic distortion (HD3) in the RoF transmission system using DWL, 1552.6 nm laser, and 1510 nm laser is calculated and given in Figure 5-3. Here the single-tone test is used. The EAM is biased at -1.5 V. The frequency and power of the RF input signal is 3.96 GHz (single tone) and 10 dBm, respectively. Responsivity of 0.6 A/W for the PD and 50 Ohm of characteristic impedance are assumed. The optical power of the 1552.6 nm laser is 10 dBm and the optical power of the 1510 nm laser is adjusted. In Figure 5-3 (a), the RF output signal is improved by using DWL. The 2nd order component HD2 is suppressed by using DWL in Figure 5-3 (b). These calculated results illustrate that the RF signals and HD2s carried by the two optical carriers are inphase and antiphase, respectively. The total HD2 is suppressed by 20 dB by the 1510 nm laser when its optical power is 2.7 dBm. In Figure 5-3 (c), the total 3rd order component HD3 is also suppressed by 17 dB when the optical power of the 1510 nm laser is 11.5 dBm. It is illustrated that the HD3s are also in antiphase. However, the maximal suppressions of both the HD2 and HD3 cannot be achieved simultaneously. Figure 5-3 also shows that the total HD2 and HD3 can be increased if the power of the 1510 nm laser is too high.

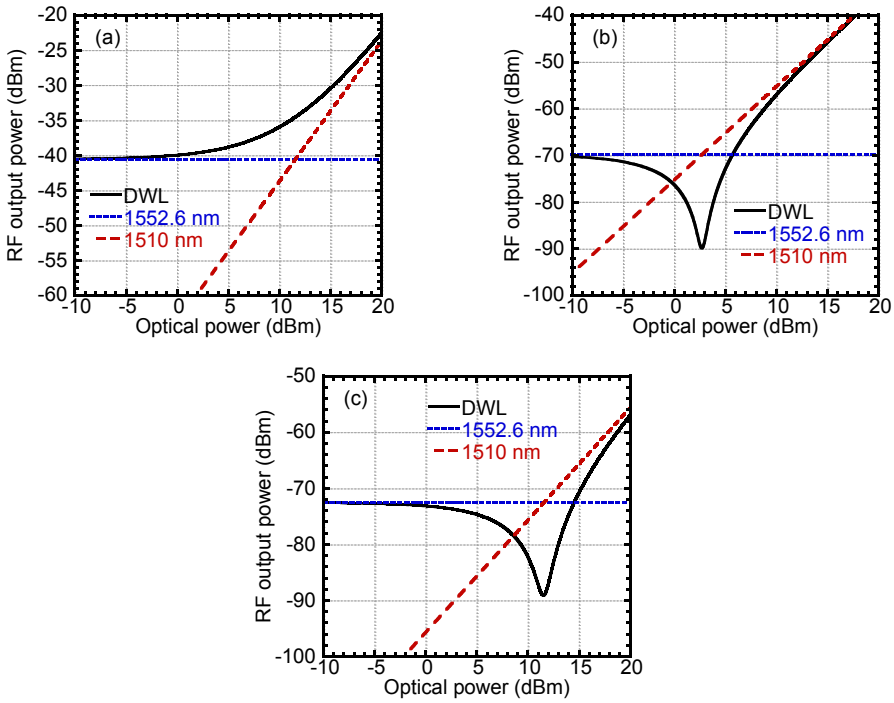

Figure 5-3 Calculated RF output power of (a) the RF signal, (b) HD2, and (c) HD3 using DWL, 1552.6 nm laser, and 1510 nm laser versus the optical power of the 1510 nm laser. V_{DC} = -1.5 V.

The $SFDR_2$ (with respect to HD2) and $SFDR_3$ (with respect to HD3) of the RoF system are calculated and given in Figure 5-4. The optical power of the two lasers is set to 10 dBm at 1552.6 nm and 2.7 dBm at 1510 nm to achieve the maximal suppression of the HD2. Measured noise floor of the RoF system is -143 dBm/Hz. Figure 5-4 (a) shows that the $SFDR_2$ is 75.9 dB $Hz^{1/2}$ for DWL. Figure 5-4 (b) and (c) show that the $SFDR_2$ at 1552.6 nm is 65.4 dB $Hz^{1/2}$ and the $SFDR_2$ at 1510 nm is 47 dB $Hz^{1/2}$. It can be seen that the HD2 is suppressed and the RF output signal is improved in power. More than 10.5 dB improvement of $SFDR_2$ is obtained. Figure 5-4 (a) also shows that the HD2 cannot be eliminated completely. It should be noted that the maximal suppression of the HD3 is not achieved for this case but the HD3 is still suppressed by 1 dB. Therefore, the $SFDR_3$ is still improved by 1.2 dB.

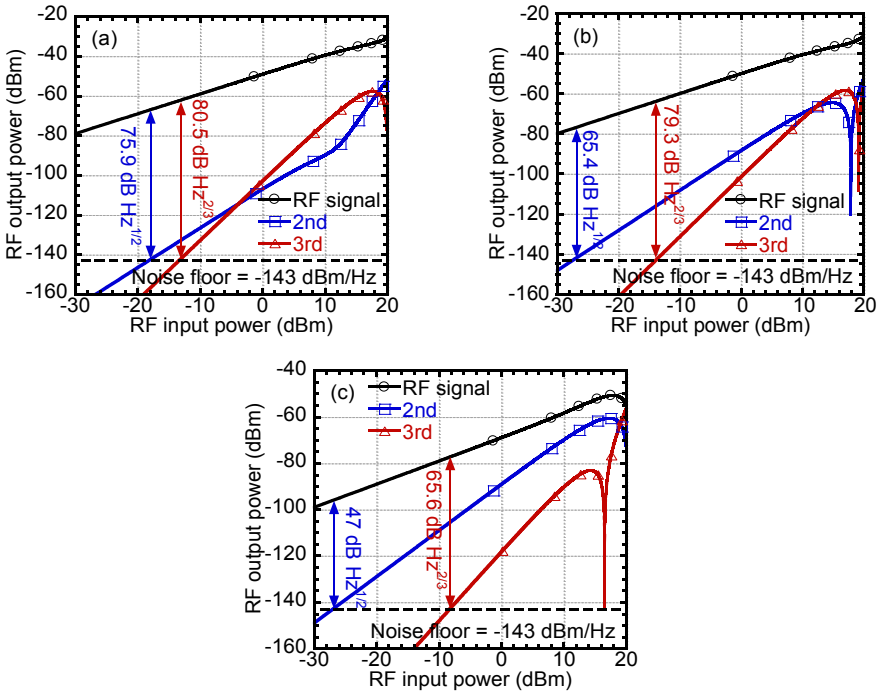

Figure 5-4 Calculated SFDRs of the RoF transmission system using (a) DWL, (b) 1552.6 nm laser, and (c) 1510 nm laser. V_{DC} = -1.5 V.

Case II: Maximal suppression of 3rd order

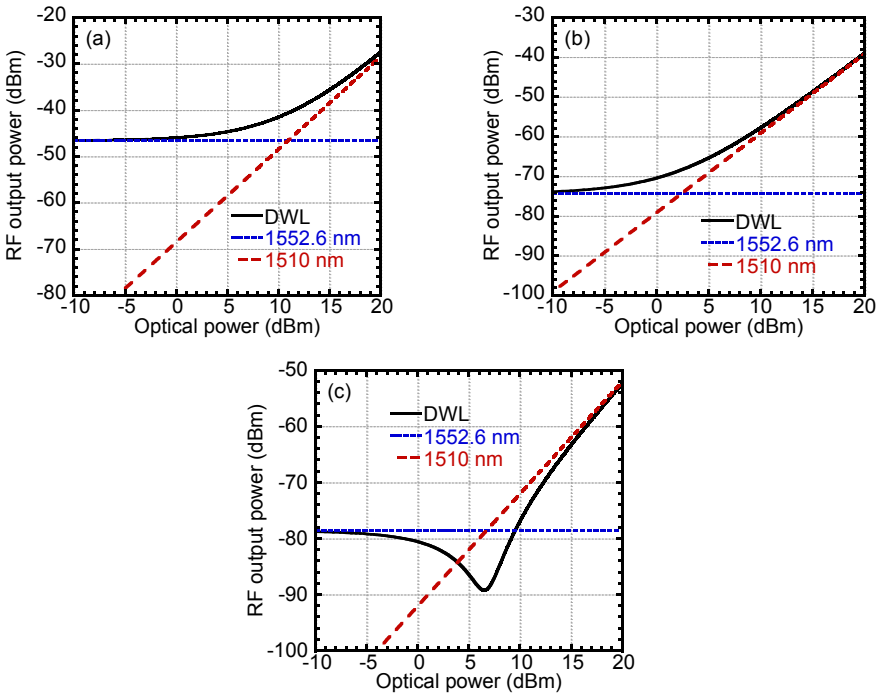

Figure 5-5 Calculated RF output power of (a) the RF signal, (b) HD2, and (c) HD3 using DWL, 1552.6 nm laser, and 1510 nm laser versus the optical power of the 1510 nm laser. V_{DC} = -2 V.

For this case, the bias voltage of the EAM is changed to -2 V to verify the dependence of the bias of DWL technique. RF output power of the 1st, 2nd, and 3rd order components in the RoF transmission system using DWL, 1552.6 nm laser, and 1510 nm laser is calculated and given in Figure 5-5. Figure 5-5 (a) shows that the RF signal is improved by DWL. However, the 2nd order component HD2 is always increased in Figure 5-5 (b). In Figure 5-5 (c), the 3rd order component HD3 is suppressed and it is shown that the two HD3s carried by the two lights are antiphase with each other. So DWL technique is bias dependent for the considered EAM.

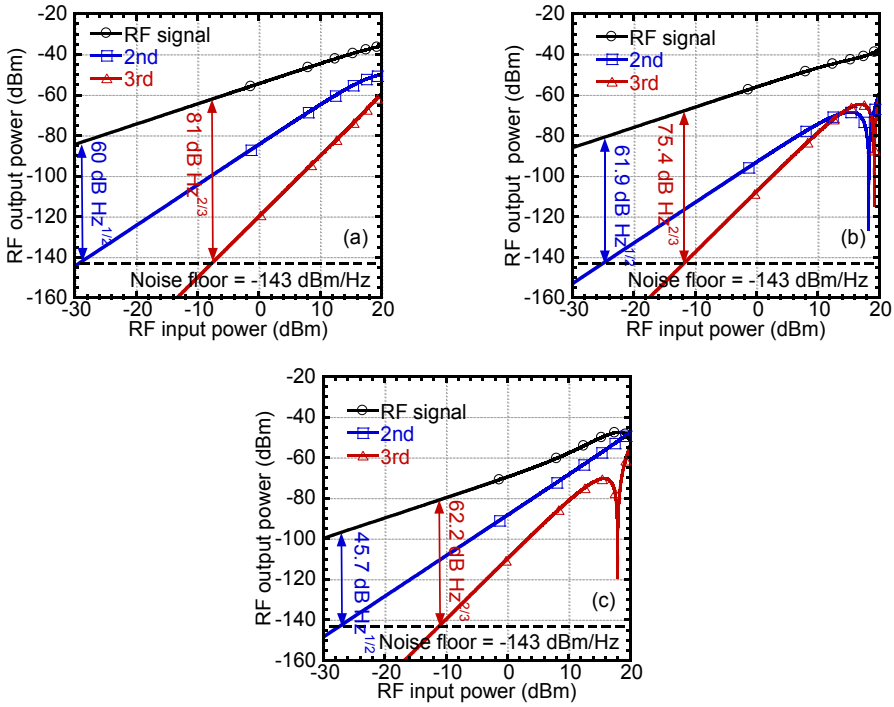

Figure 5-6 Calculated SFDRs of the RoF transmission system using (a) DWL, (b) 1552.6 nm laser, and (c) 1510 nm laser. V_{DC} = -2 V.

The $SFDR_3$ (with respect to HD3) and $SFDR_2$ (with respect to HD2) of the RoF transmission system when the EAM is biased at -2 V are calculated and given in Figure 5-6. The RF output signal power is improved and the 3rd order component HD3 is suppressed so that the $SFDR_3$ is improved by 5.6 dB. But the increase of the HD2 leads to 1.9 dB degradation of the $SFDR_2$. (5.8) shows that m_{n_A} and m_{n_B} have to be in antiphase for the suppression of the n^{th} order component. (5.4) shows that m_{n_A} and m_{n_B} depend on V_{DC} and V_{RF}. However, the calculated SFDRs show that the suppression of the

2^{nd} or 3^{rd} order is independent of V_{RF}. The reason is due to $V_{RF} \ll V_{DC}$ for the used EAM. The RF signal V_{RF} affects power of the RF output signal and nonlinear components only. However, when V_{RF} is increased very high, it may affect the linearization.

5.3.3 Experimental Evaluation

The RF output signals and nonlinear components are measured to evaluate the theory and calculations. Experimental setup is also given in Figure 5-1. The photo of the experimental setup is presented in Figure 5-7. In the experiments, the wavelengths of the two lasers are also 1552.6 nm and 1510 nm. The optical power of the 1552.6 nm laser is 10 dBm. A C-band 40 Gb/s EAM with low chirp is used. Chirp induces phase distortion which degrades the linearization. Two PCs are used to adjust the polarization states because the EAM is polarization dependent. An RF signal generator Hittite HMC-T240 is used to generate a 3.96 GHz RF signal (single tone). A 40 GHz PD with responsivity of 0.6 A/W is employed. A PA ZVA-213+ is used to boost the photocurrent. An SA U3772 is used to measure the RF output power.

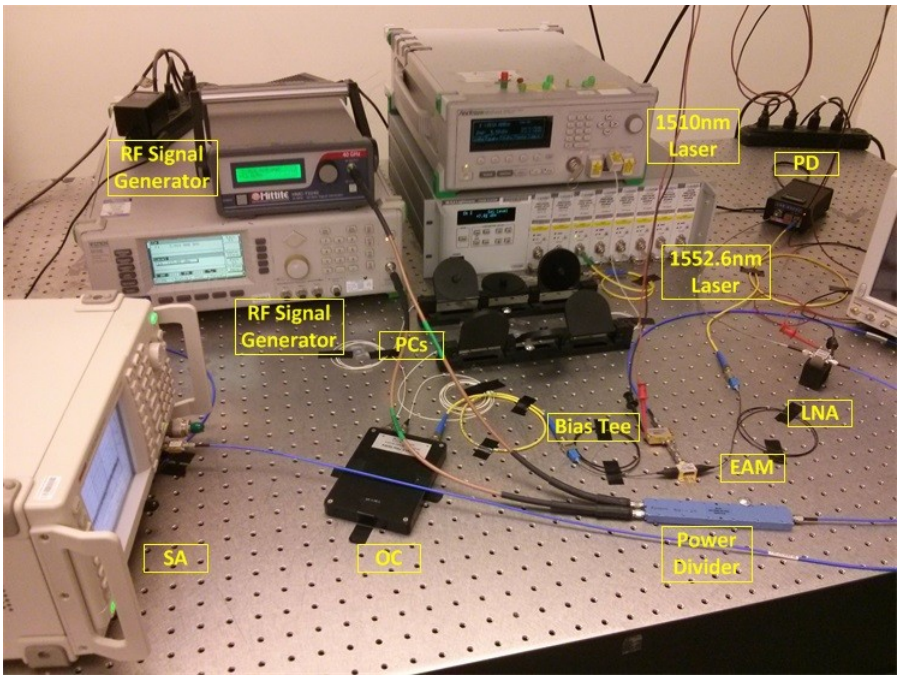

Figure 5-7 Photo of the experimental setup.

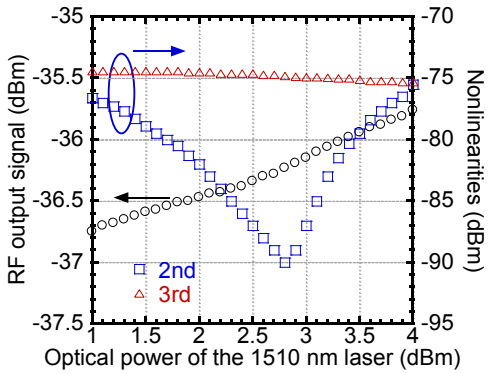

Figure 5-8 Measured RF output signal and HDs using DWL versus the optical power of 1510 nm laser. V_{DC} = -1.5 V.

The optical power of the 1510 nm laser is swept to get the maximal suppression of the HD2. The EAM is biased at -1.5 V. The measured RF output signal and nonlinear components using DWL versus the optical power of the 1510 nm laser is given in Figure 5-8. The RF input power is 10 dBm. Figure 5-8 shows that the RF output signal power is improved with the optical power of the 1510 nm laser because the RF signals carried by the two optical carriers are inphase. Figure 5-8 also shows that the maximal suppression of the HD2 is achieved when the optical power of the 1510 nm laser is 2.8 dBm. The HD3 is slightly decreased when the optical power of the 1510 nm laser is increased. It is illustrated that the maximal suppression of the HD3 can be achieved when the power of the 1510 nm laser is much higher than 4 dBm. In other words, the maximal suppressions of the HD2 and HD3 cannot be achieved at the same time. The measurement results in Figure 5-8 match the calculation results shown in Figure 5-3.

The optical power of the 1510 nm laser is set to 2.8 dBm and the bias voltage of the EAM is swept to obtain the bias dependence of DWL technique. Figure 5-9 (a) shows that the RF signal using DWL is improved independent of the bias voltage of the EAM. It is meant that the RF signals carried by the two optical carriers are inphase for all the bias voltages. When the reverse bias voltage is increased from 0.5 to 3 V, the power of the RF signal for the 1510 nm decreases by 20 dB because the transmission of the EAM for the 1510 nm drops by ~10 dB as shown in Figure 5-2. Figure 5-9 (b) shows that the HD2 is suppressed for reverse bias voltages from 0.6 to 1.7 V and Figure 5-9 (c) shows that the HD3 is suppressed for reverse bias voltages from 1.4 to 2.6 V. It is illustrated that the

HD2s are antiphase for reverse bias voltages from 0.6 to 1.7 V, and the HD3s are antiphase for reverse bias voltages from 1.4 to 2.6 V. So when the reverse bias voltages are in the range of 1.4 to 1.7 V, both the HD2 and HD3 can be suppressed simultaneously.

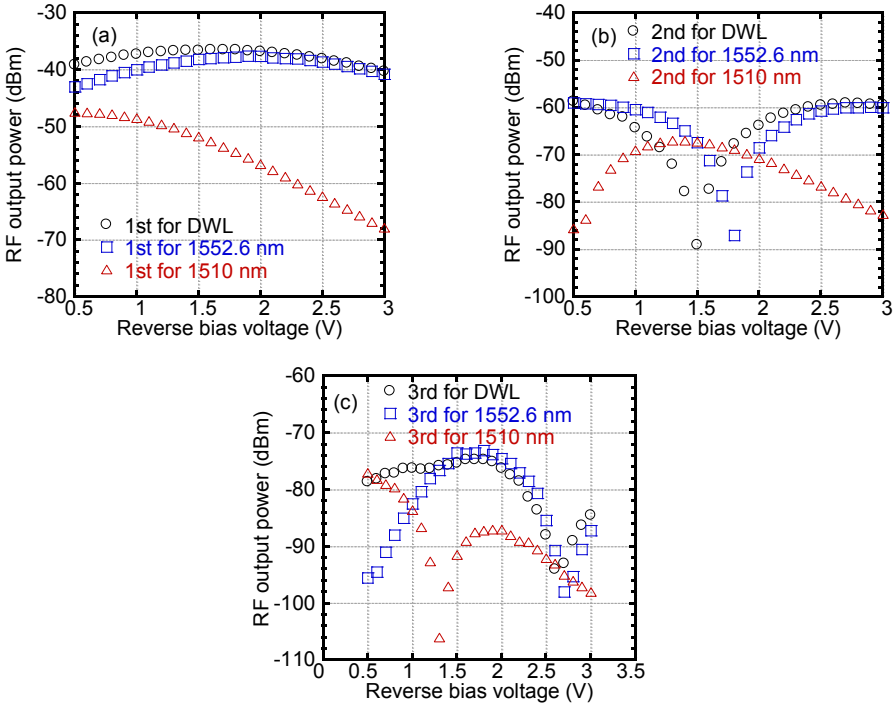

Figure 5-9 Measured (a) RF signals, (b) HD2s, and (c) HD3s versus the reverse bias voltage of the EAM.

The power ratio of the two lasers is also swept to obtain the maximal suppression of either the HD2 or HD3 for different biases. The power ratios of the 1552.6 nm laser and 1510 nm laser for the maximal suppressions are given in Figure 5-10. When the reverse bias voltage is increased, the required power ratio is also increased. In addition, Figure 5-10 (b) shows that the required power ratio for the maximal suppression of the HD3 is 1.5 dB for the reverse bias voltage from 1.7 to 2.1 V. Figure 5-11 shows the measured improvements of the RF signals and maximal suppression of either the HD2 or HD3 versus the reverse bias voltage of the EAM. It can be seen that the maximal suppression of the HD3 is lower than the maximal suppression of the HD2. The reason is due to the fact that higher order component is more susceptible to the dispersion and phase distortion. When the reverse bias voltage is increased, the improvements of the RF signals and maximal suppressions of the nonlinearities both degrade.

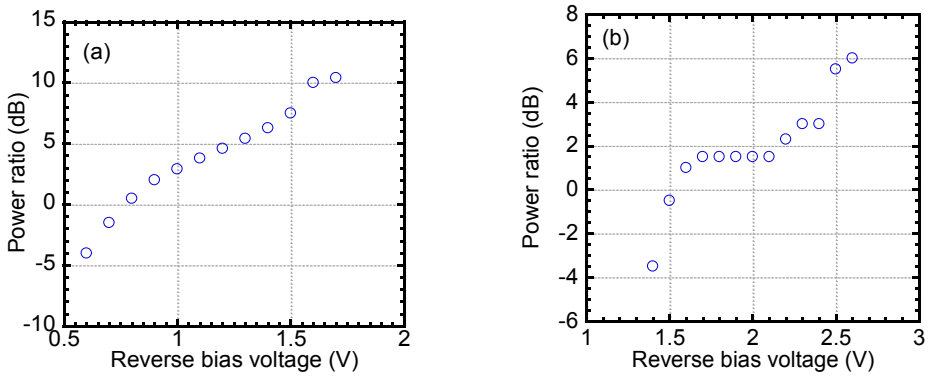

Figure 5-10 The power ratios of the1552.6 nm lasers and 1510 nm laser for the maximal suppression of the (a) HD2 and (b) HD3.

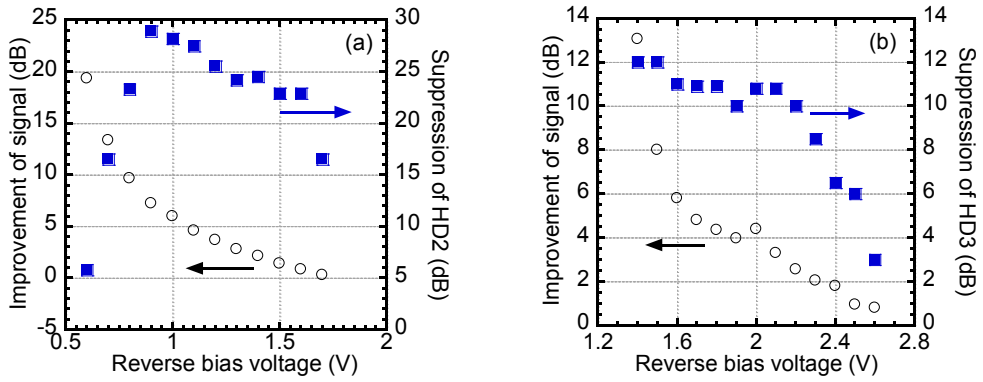

Figure 5-11 Measured improvements of the RF signals and the maximal suppressions of the (a) HD2 and (b) HD3.

Case I: Maximal suppression of 2nd order

The bias voltage is set to -1.5 V and the optical power is set to 10 dBm at the 1552.6 nm and 2.8 dBm at the 1510 nm for the maximal suppression of the HD2. The measured RF spectra of the RF output signals, HD2s, HD3s are given in Figure 5-12. Compared to using the single 1552.6 nm laser, the RF signal is improved by 1.6 dB; the HD2 and HD3 are reduced by 23 and 2.1 dB respectively by using DWL. Moreover, it can be seen that the noise floor is not increased by using one more laser.

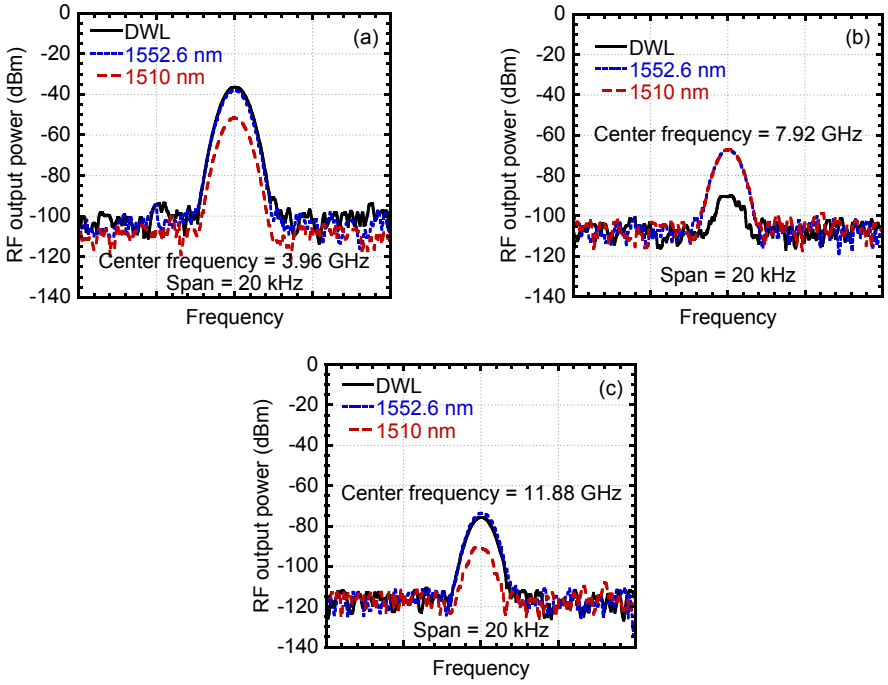

Figure 5-12 Measured RF spectra of the (a) RF output signals, (b) HD2s, and (c) HD3s. V_{DC} = -1.5 V.

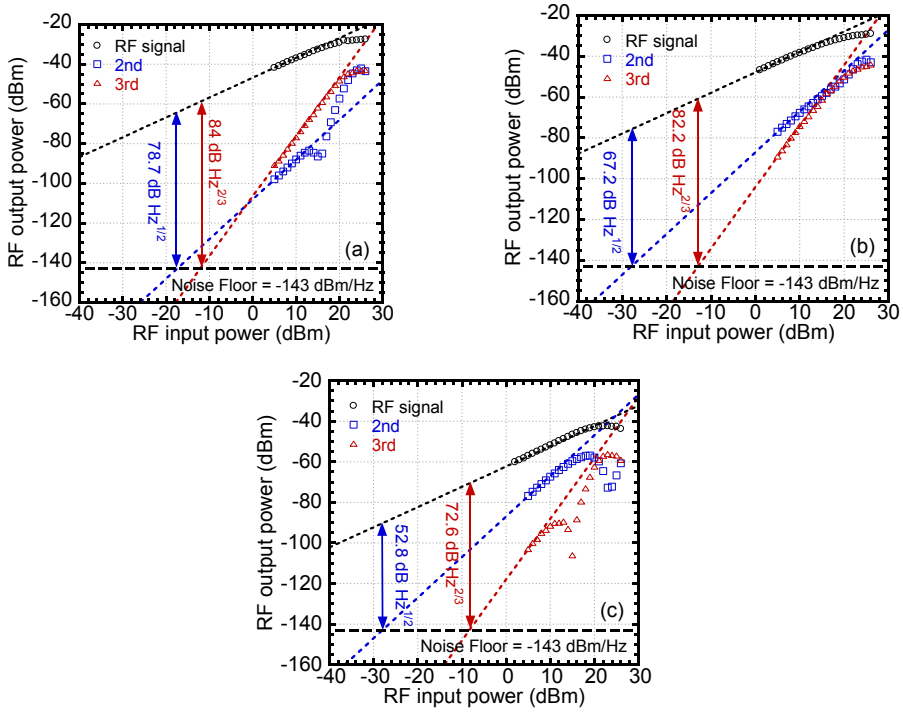

Figure 5-13 Measured SFDRs using (a) DWL, (b) 1552.6 nm laser, and (c) 1510 nm laser. V_{DC} = -1.5 V.

The measured $SFDR_2$ (with respect to HD2) and $SFDR_3$ (with respect to HD3) are given in Figure 5-13. DWL technique increases the $SFDR_2$ from 67.2 and 52.8 to 78.7 dB $Hz^{1/2}$

compared to using the single 1552.6 nm laser and single 1510 nm laser, respectively. Correspondingly, 11.5 and 25.9 dB improvements are achieved. Figure 5-13 also shows that the $SFDR_3$ is improved by 1.8 and 11.4 dB, respectively. Because the power of the 1510 nm laser is adjusted for the maximum suppression of the HD2, the HD3 is only suppressed slightly.

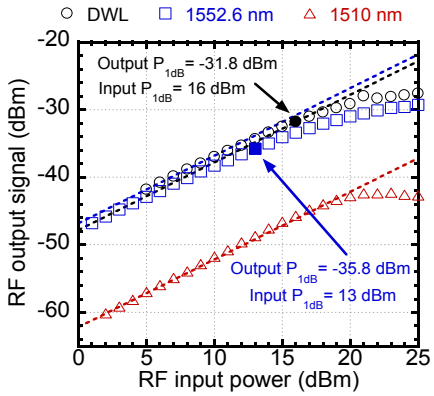

Figure 5-14 Measured RF output signals using DWL, 1552.6 nm laser, and 1510 nm laser. V_{DC} = -1.5 V.

Figure 5-14 presents the measured RF output signal power versus the RF input power of the RoF system using DWL and single laser. Improvements of 3 dB for the input P_{1dB} and 4 dB for the output P_{1dB} are achieved by using DWL. The extensions of the input P_{1dB} and output P_{1dB} illustrate that the system is linearized by the suppression of the HD2.

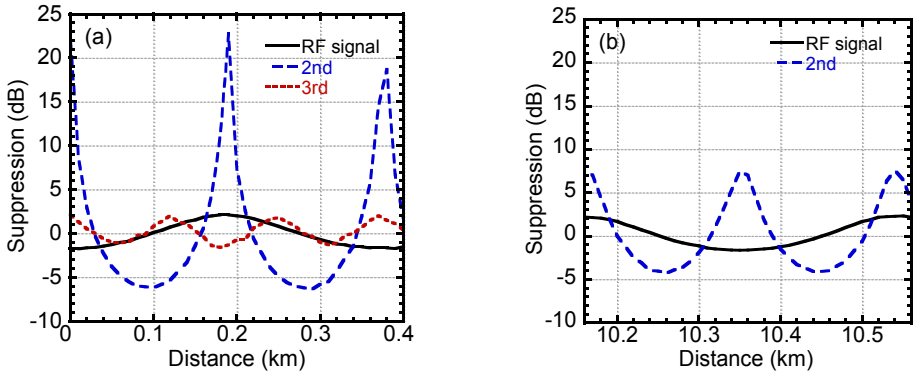

Figure 5-15 Measured suppressions of the RF output signal, HD2, and HD3 versus the transmission distance. V_{DC} = -1.5 V.

Equation (5.7) shows that the magnitudes of the RF signal and nonlinear components are periodic functions of the fiber length because of the delay induced by dispersion. The

dispersion between the two 1510 nm and 1552.6 nm is 644.1 ps/km in SMF. The period corresponding to the subcarrier frequency of 3.96 GHz is 252.5 ps. Thus, the period of the RF signal in (5.7) is 392 m. (5.7) also shows that the periods for the HD2 and HD3 are half and one third of that for the RF signal, respectively. The transmission distance in SMF is swept to check the influence of the dispersion. The fiber length is increased from BTB to 0.4 km with a step of 0.01 km. An additional 10 km SMF is added and the fiber length is swept again. The suppressions of the RF output signal, HD2, and HD3 compared to using the single 1552.6 nm laser are measured. The measured results are given in Figure 5-15. Negative suppression means improvement here. In Figure 5-15 (a), it can be seen that the period of the RF signal is ~380 m. The periods of the HD2 and HD3 are half and one third of the RF signal's. The suppression of the HD2 is 22.7 dB for 190 m and 18.7 dB for 380 m. The suppression of the HD2 at 380 m degrades by 4 dB. The reason is that the optical adapters in the fiber link induce more loss for the 1510 nm. By increasing the optical power of the 1510 nm laser, the suppression can be increased. The measurement is repeated after 10 km transmission. Because the HD3 is almost under the noise level after transmission, it is not included in Figure 5-15 (b). The periods are still 380 m and 190 m for the RF signal and HD2, respectively. However, the suppression of the HD2 degrades to ~7.5 dB at 10.35 km. It is caused by the accumulated loss of the adapters and fibers. 2.4 dB more loss is induced to the 1510 nm laser. When the optical power of the 1510 nm laser is increased to compensate for the additional loss, the suppression can be increased to 21.2 dB. So the performance of DWL is limited substantially by the delay induced by CD. But the delay can be compensated by using DCF. Thus, the linearization performance can be maintained for more than 10 km distance.

For comprehensive study of the linearization performance of DWL technique, two-tone test is now given. All the parameters are the same as the single-tone test. The frequencies in the two-tone test are 3.96 GHz and 3.964 GHz. The RF input power is 10 dBm per channel. The measured IMD2 for DWL, 1552.6 nm laser, and 1510 nm laser are shown in Figure 5-16. It is shown that the IMD2 is suppressed by DWL technique by 12.9 dB compared to using the single 1552.6 nm laser. Moreover, the IMD3 is also suppressed by 0.6 dB and the RF output signal is improved by 1.3 dB compared to using the single

1552.6 nm laser. Note that the IMD3 for the 1510 nm is lower than that for DWL. The reason is that the RF power of the output signal for the 1510 nm is 17 dB lower.

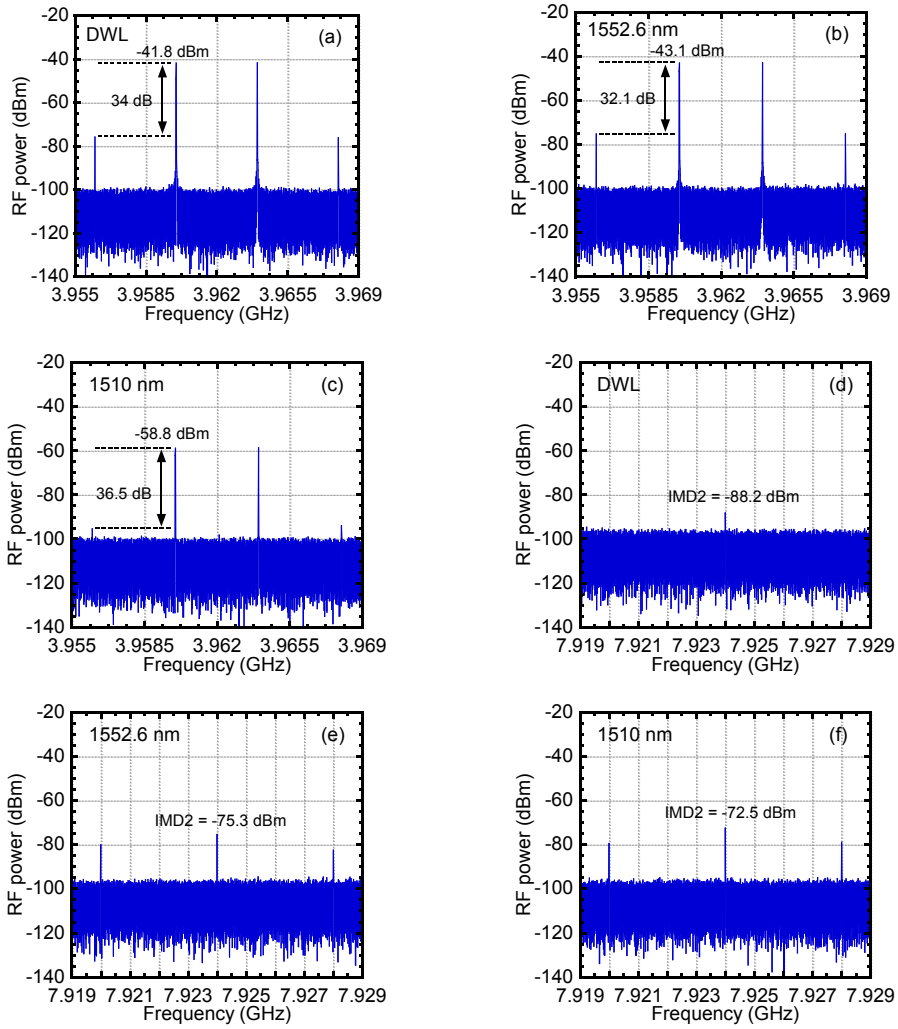

Figure 5-16 Measured spectra of the IMD3s for (a) DWL, (b) 1552.6 nm, and (c) 1510 nm and the IMD2s for (d) DWL, (e) 1552.6 nm, and (f) 1510 nm. V_{DC} = -1.5 V.

$SFDR_2$ (with respect to IMD2) and $SFDR_3$ (with respect to IMD3) for DWL, 1552.6 nm, and 1510 nm are given in Figure 5-17. DWL technique increases the $SFDR_2$ from 66.4 and 48.6 to 74.9 dB $Hz^{1/2}$ compared to using the single 1552.6 nm laser and single 1510 nm laser, respectively. 8.5 and 26.3 dB improvements are obtained. Figure 5-17 also shows that the $SFDR_3$ is improved by 1.3 and 8.1 dB compared to using the single 1552.6 and 1510 nm laser, respectively.

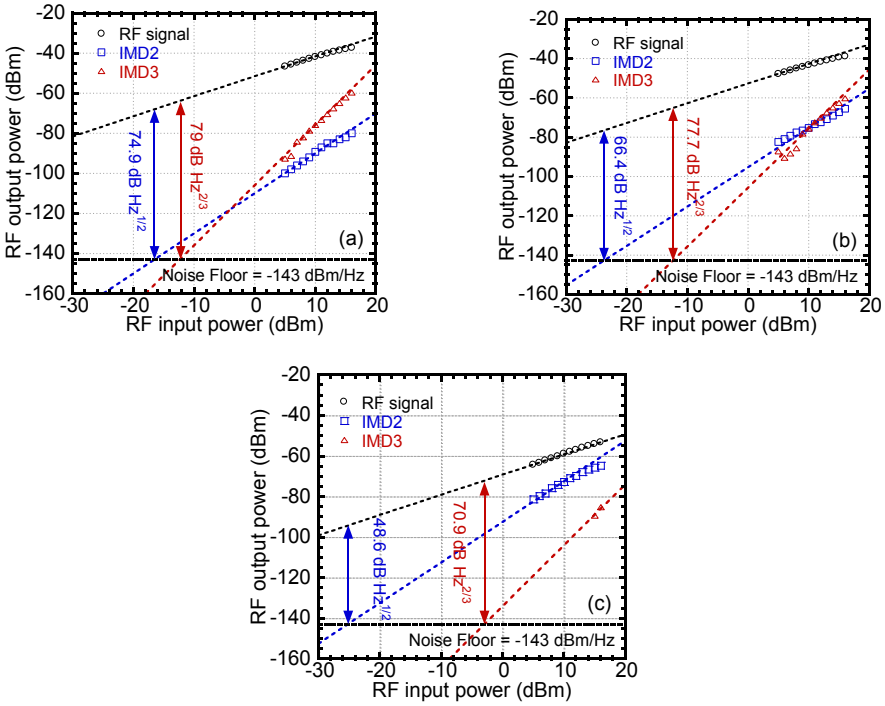

Figure 5-17 Measured SFDRs with respect to the IMDs using (a) DWL, (b) 1552.6 nm laser, and (c) 1510 nm laser. V_{DC} = -1.5 V.

Case II: Maximal suppression of 3rd order

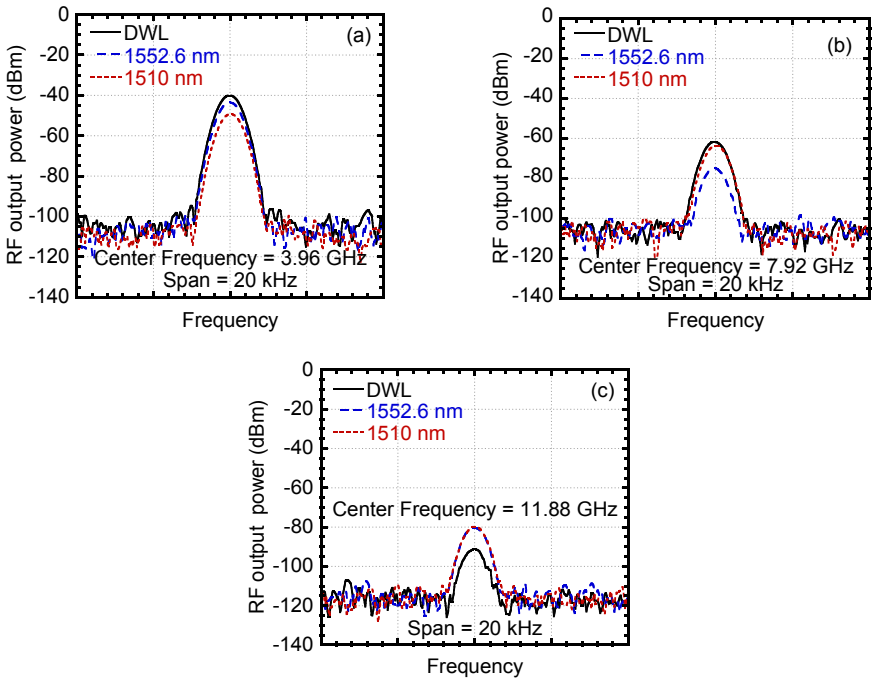

Figure 5-18 Measured spectra of (a) the RF output signals, (b) HD2s, and (c) HD3s. V_{DC} = -2 V.

Similar to the theory, for this case we change the bias voltage of the EAM to -2 V to verify the calculation results. Referring to Figure 5-10 (b), the optical power ratio of 1.5 dB is required for the maximal suppression of the HD3. So the optical power of the 1552.6 nm laser and 1510 nm laser is set to 7 dBm and 5.5 dBm, respectively. Firstly, single-tone test is given. The measured spectra of the RF output signals, HD2s, and HD3s are presented in Figure 5-18. The RF input power is fixed to 10 dBm. Figure 5-18 (a) shows that DWL technique results in an improvement of the RF output signal power by 4 dB compared to using the single 1552.6 nm laser, and by 9.3 dB compared to using the single 1510 nm laser. Figure 5-18 (c) shows that DWL technique results in the suppression of the HD3 by more than 11 dB compared to using the single laser. However, Figure 5-18 (b) shows that the HD2 is increased by 13.2 dB compared to using the single 1552.6 nm laser. These results agree with the calculation results in Figure 5-5.

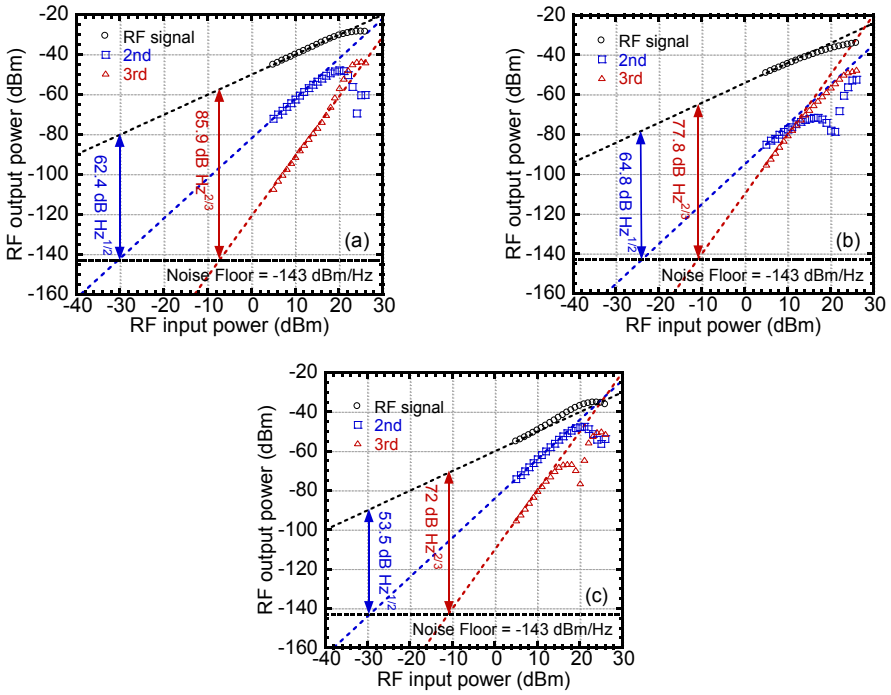

Figure 5-19 Measured SFDRs using (a) DWL, (b) 1552.6 nm laser, and (c) 1510 nm laser. V_{DC} = -2 V.

Figure 5-19 shows that the measured $SFDR_2$ (with respect to HD2) and $SFDR_3$ (with respect to HD3) using DWL and single laser. The $SFDR_3$ is improved by 8.1 dB compared to using the single 1552.6 nm laser. But the $SFDR_2$ is degraded by 2.4 dB. Figure 5-19 illustrates that DWL cannot eliminate the 3rd order completely because of the

phase distortion as mentioned in (5.7). These measured SFDRs match the calculated results. It can be seen that there are some differences between the calculated and measured SFDRs. The difference is caused by the delay induced by the chirp in the EAM. The delay degrades the suppressions of the nonlinearities and the improvement of the RF signal. The delay is assumed to be 4 ps in the calculation. However, the chirp of the EAM is frequency dependent. Moreover, the EAM is sensitive to temperature so that the transmission drifts with the temperature.

The measured RF output signal versus the RF input power of the RoF system using DWL and the single laser is given in Figure 5-20. The RF output signal of the RoF transmission system using DWL is more than 4 dB higher than that of the other two systems. It can be seen that the system using the 1510 nm laser shows an obvious gain expansion for the RF input power from 5 to 19 dBm. So the gain expansion of the 1510 nm laser compensates for the gain compression of the 1552.6 nm laser in DWL technique. Figure 5-20 depicts that the DWL technique results in the improvement of the input P_{1dB} from 14 to 21.7 dBm and the output P_{1dB} from -41.1 to -29.4 dBm. 7.7 dB improvement of the input P_{1dB} and 11.7 dB improvement of the output P_{1dB} are obtained. It also shows that the system is linearized although the HD2 is increased.

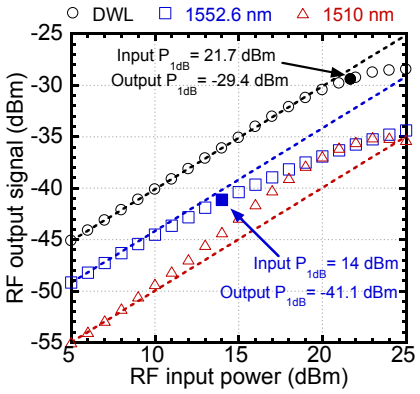

Figure 5-20 Measured RF output signals using DWL, 1552.6 nm laser, and 1510 nm laser. V_{DC} = -2 V.

Now two-tone test is also given to verify the suppression of the IMD3. The RF power is set to 13 dBm per channel because of the low power of the IMD3. The measured IMD3s are given in Figure 5-21. It shows that the IMD3 is suppressed by 23 dB while the RF output signal is improved by 3.7 dB compared to using the single 1552.6 nm laser.

Moreover, the IMD5 is also suppressed by 10.9 dB at the same time. When measuring the IMD5, higher resolution of the SA is used so that the noise shown is lower.

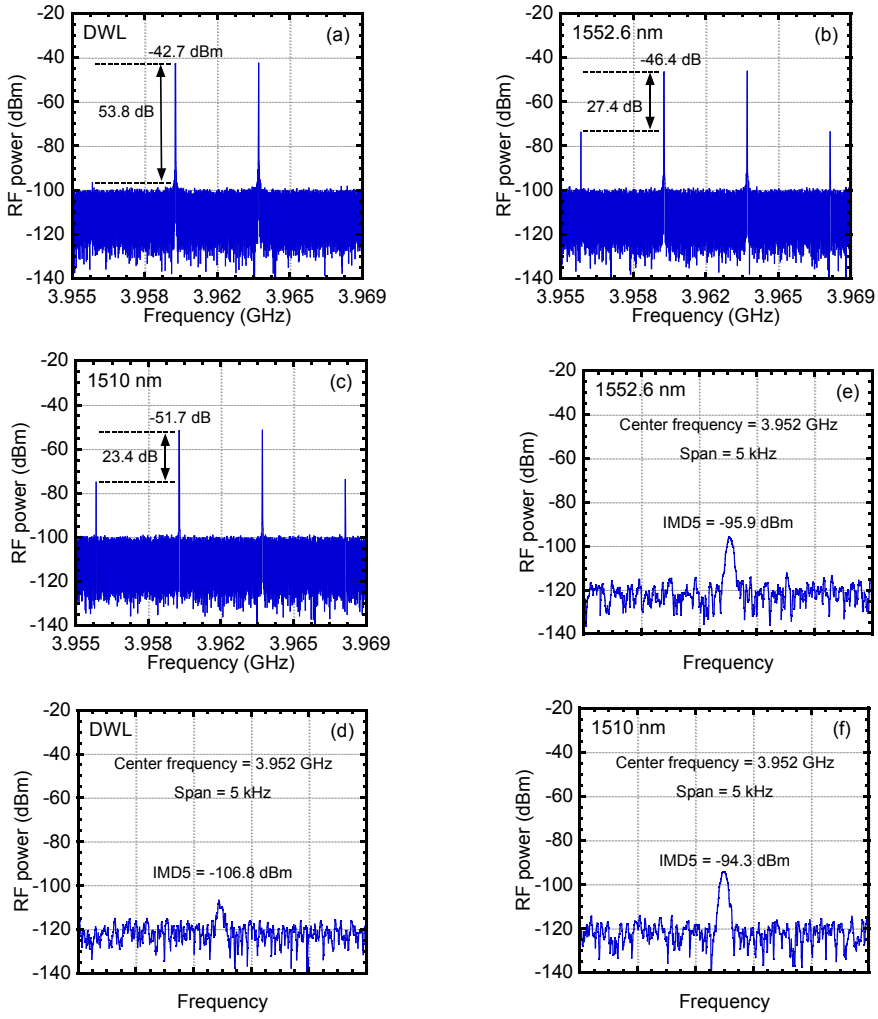

Figure 5-21 Measured spectra of the IMD3s for (a) DWL, (b) 1552.6 nm, and (c) 1510 nm and IMD5s for (d) DWL, (e) 1552.6 nm, and (f) 1510 nm. V_{DC} = -2 V.

$SFDR_3$ (with respect to IMD3) and $SFDR_5$ (with respect to IMD5) for DWL, 1552.6 nm, and 1510 nm respectively are given in Figure 5-22. DWL technique increases the $SFDR_3$ by 20.4 dB compared to using the single 1552.6 nm laser. The $SFDR_5$ is improved by 7.1 dB. It is found that the RoF transmission is 7^{th} order limited, which means that the IMD3 and IMD5 are eliminated so that the 7^{th} order IMD (IMD7) is dominant.

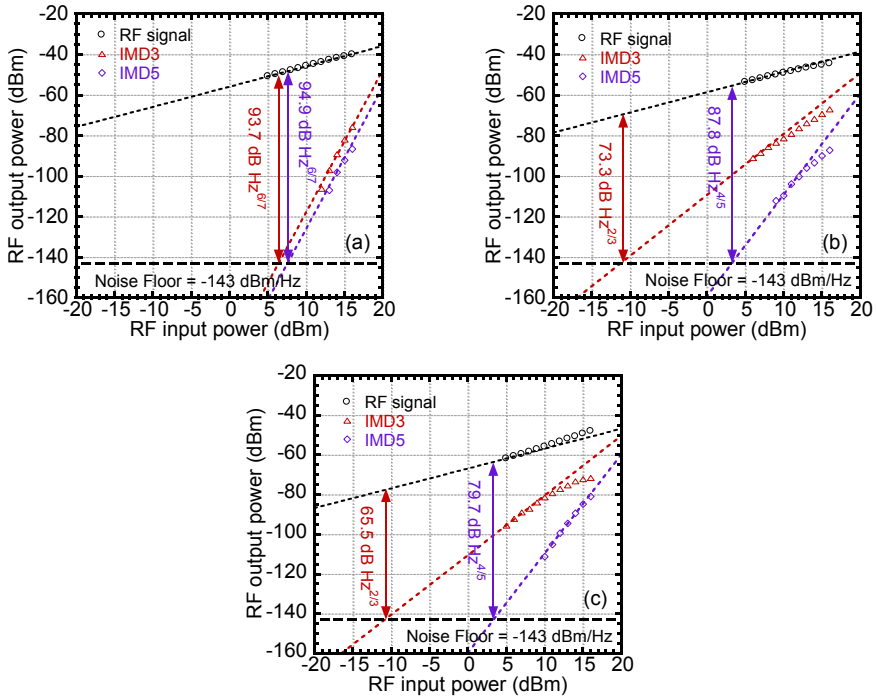

Figure 5-22 Measured SFDRs with respect to IMDs using (a) DWL, (b) 1552.6 nm laser, and (c) 1510 nm laser. V_{DC} = -2 V.

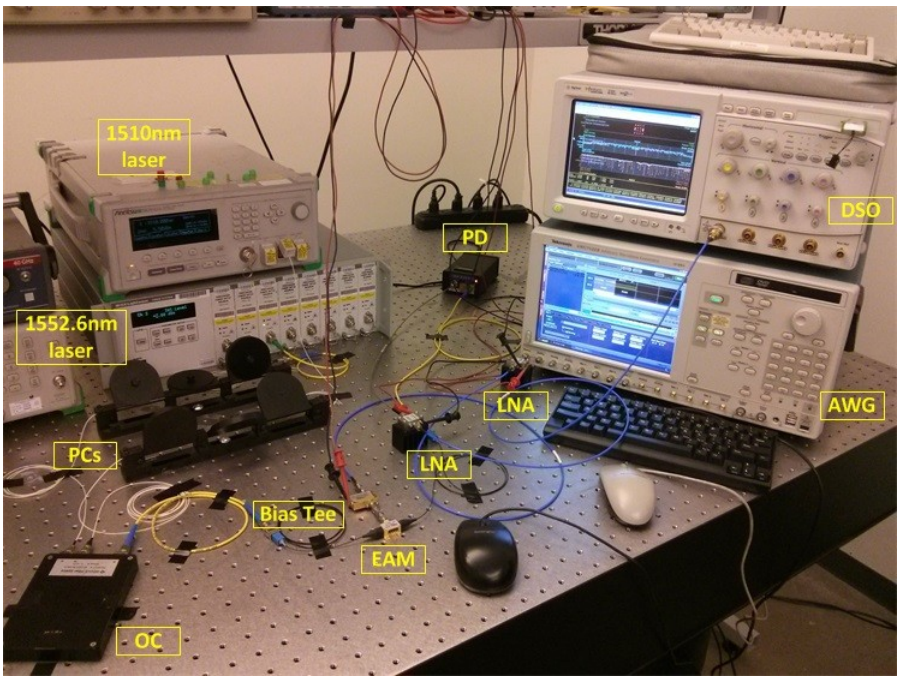

Figure 5-23 Photo of the experimental setup.

Moreover, the RoF transmission for the WiFi signals is linearized to test DWL technique for wideband signals. An AWG 7122B is used to generate the WiFi signals at 2.4 GHz

and 5 GHz compliant with 802.11a whose signal rate is 36 Mbit/s. A PA ZVA-213+ is used to boost the WiFi signals. A DSO 81204B is employed to receive and demodulate the WiFi signals. Other components and devices are as the same as the two-tone test. The photo of the experimental setup is given in Figure 5-23.

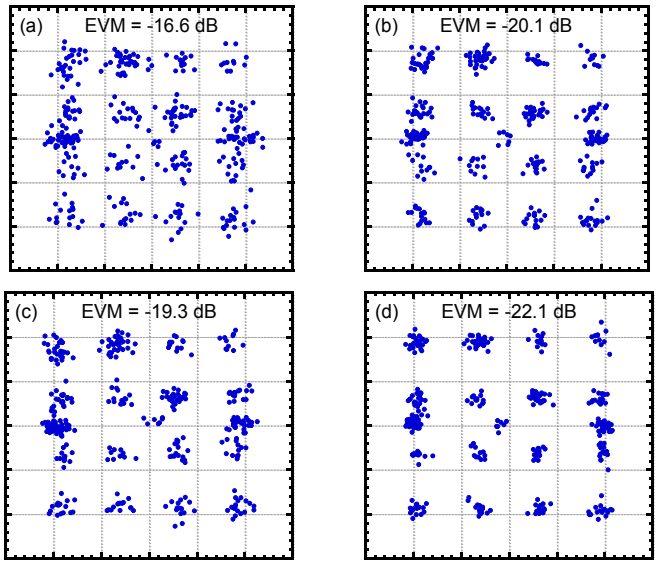

Figure 5-24 Measured constellation diagrams and EVMs for (a) 1552.6 nm at 2.4 GHz, (b) DWL at 2.4 GHz, (c) 1552.6 nm at 5 GHz, and (d) DWL at 5 GHz.

Figure 5-24 presents the measured constellation diagrams and EVMs for using DWL and single 1552.6 nm laser. The RF output power from the AWG is fixed. When DWL technique is used, the optical power of the 1552.6 nm laser and 1510 nm laser is still 7 dBm and 5.5 dBm respectively for the maximum suppression of the IMD3. When the single 1552.6 nm laser is used, the optical power of the laser is adjusted to obtain the same RF received power at the DSO. The RF received power at the DSO is -35.9 dBm for 2.4 GHz and -40.4 dBm for 5 GHz, respectively. The optical power for the single 1552.6 nm laser is 8.75 dBm at 2.4 GHz and 8.5 dBm at 5 GHz, respectively. It can be seen that the EVM at 2.4 GHz is improved from -16.6 to -20.1 dB by DWL in Figure 5-24 (a) and (b). Similarly, the EVM at 5 GHz is improved from -19.3 to -22.1 dB. 3.5 dB at 2.4 GHz and 2.8 dB at 5 GHz improvements are obtained by using DWL technique. The constellation diagrams related to the EVMs are also given and it is obvious that the constellation diagrams are improved by using DWL technique. So DWL technique linearizes the RoF system by using the same optical power ratio for different frequencies.

5.4 DWL for an RoF Transmission System Using an MZM

DWL technique also can linearize an RoF transmission system using an MZM, because MZM is also a wavelength dependent device. Most MZMs are designed for the application for C-band or O-band. But they can still be used in other wavelengths although more insertion loss is induced to the MZMs. So DWL application in an RoF transmission system using an MZM will be studied theoretically and experimentally.

5.4.1 Theory

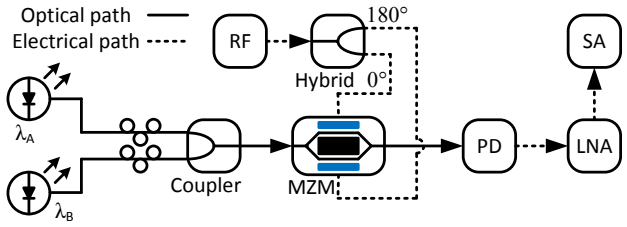

Figure 5-25 Schematic diagram and experimental setup of DWL for an RoF transmission system using an MZM.

The schematic diagram of DWL for an RoF transmission system using an MZM is given in Figure 5-25. The main nonlinear source is assumed to be the MZM and all other components are assumed to be linear. Two lasers emit incoherent lights with different wavelengths which are coupled together and transmitted to an MZM which is used for the optical subcarrier modulation. A 180° hybrid is used for the push-pull modulation in the MZM. MZM is wavelength-dependent so that the two lights experience different modulation characteristics. Thus different signals and nonlinearities are generated and carried by the two optical carriers. In a PD, the two optical carriers are demodulated separately and thus the sums of the signals and nonlinearities are obtained. The total signal and nonlinearities can be changed by adjusting the power ratio of the two lasers. If the nonlinearities carried by the two lights are in antiphase, the nonlinear distortion can be suppressed after the photodetection.

When the MZM is set to push-pull modulation, the transmission of the MZM can be described as

$$T = \frac{P_o}{P_i} = \frac{1}{2L}\left\{1 + \cos\left[\frac{\pi}{V_\pi}(V + V_b)\right]\right\} \tag{5.9}$$

where T is the transmission of the MZM, P_o and P_i are the output and input optical power of the MZM, respectively, L is the insertion loss, V_π is the half-wave voltage, V is the RF signal, and V_b is the bias voltage applied to the MZM. Using Taylor series, (5.9) can be expanded as

$$T = \frac{1}{2L} + \frac{1}{2L}\sum_{n=0}^{\infty}\left[\left(\frac{\pi}{V_\pi}\right)^n \cos\left(\frac{n\pi}{2} + \frac{\pi V_b}{V_\pi}\right)\frac{V^n}{n!}\right] \tag{5.10}$$

Two incident lasers are assumed to be lasers A and B. In DWL technique, if the HD is suppressed, the related IMD will also be suppressed. This is proved in Chapter 5.3.3. So only the single-tone is considered in this part. The half-wave voltages for lasers A and B are different because MZM is wavelength-dependent. We assume the two half-wave voltages for the two lasers are V_{π_A} and V_{π_B}, and $V_{\pi\_A} < V_{\pi\_B}$. The two lasers are incoherent so that they can be demodulated separately in a PD. After photodetection, the total photocurrent can be given as follows:

$$\begin{aligned} I = \frac{RP_A}{2L} + \frac{RP_B}{2L} + \sum_{n=0}^{\infty}\left\{\left[\frac{RP_A}{2L}m_A^n \cos\left(\frac{n\pi}{2} + m_A V_b\right)\right.\right. \\ \left.\left. + \frac{RP_B}{2L}m_B^n \cos\left(\frac{n\pi}{2} + m_B V_b\right)\right]\frac{V^n}{n!}\right\} \end{aligned} \tag{5.11}$$

where P_A and P_B are the optical input power for lasers A and B, respectively, and R is the responsivity of the PD. m_A and m_B are the modulation indexes of the MZM for lasers A and B, respectively, i.e., $m_A = \frac{\pi}{V_{\pi\_A}}$ and $m_B = \frac{\pi}{V_{\pi\_B}}$. The n^{th} order component in the photocurrent can be eliminated when the following condition is met.

$$\frac{P_A}{P_B} = -\left(\frac{m_B}{m_A}\right)^n \frac{\cos\left(\frac{n\pi}{2} + m_B V_b\right)}{\cos\left(\frac{n\pi}{2} + m_A V_b\right)} \tag{5.12}$$

The power and modulation indices are positive and the power ratio of the two lasers is adjustable. For the even order components, (5.12) can be achieved when ${V_{\pi\_A}}/{2} < V_b <$

$V_{\pi\_B}/_2$. Then the even order components carried by the two optical carriers can cancel each other. And it can be found that the odd order components are increased in the meantime. When $V_{\pi\_A} < V_b < V_{\pi\_B}$, odd order can be eliminated by properly adjust the power ratio of the two lasers. So it can be seen that the odd and even order components cannot be eliminated simultaneously.

5.4.2 Experiments

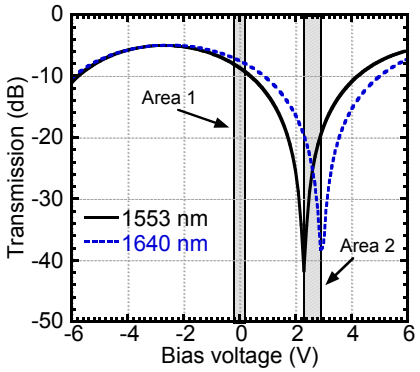

Figure 5-26 Measured transmissions of the MZM.

RF output signals, HD2s and HD3s of an RoF transmission system are measured to verify the performance of DWL. The experimental setup is given in Figure 5-25. A 40 Gb/s MZM which is designed for C-band is used. Two PCs are used and adjusted to get the maximum optical output power of the MZM for each laser. The two lasers are combined and transmitted to the MZM through a 3 dB OC. An RF signal generator is used to generate an RF signal. The MZM is set to push-pull modulation using a 180° hybrid. A 40 GHz PD with responsivity of 0.6 A/W is employed. A wideband PA ZVA-213+ is used to boost the photocurrent. An SA is used to measure the RF output power. The two wavelengths of the lasers are 1553 nm and 1640 nm. Measured transmissions of the MZM for the two wavelengths are shown in Figure 5-26. The maximum transmission points of the MZM are -2.7 V for 1553 nm and -2.5 V for 1640 nm. The minimum transmission points are 2.3 V for 1553 nm and 2.9 V for 1640 nm, respectively. So the half-wave voltages are 5 V for 1553 nm and 5.4 V for 1640 nm. Referring to the requirements of (5.12), the even order nonlinearities can be suppressed when -0.2 V < V_b < 0.2 V and it is marked as Area 1 in Figure 5-26. The odd order nonlinearities can be

suppressed when 2.3 V < V_b < 2.9 V and it is marked as Area 2. The two Cases, maximal suppressions of the HD2 or HD3, are studied separately as follows.

Case I: Maximal suppression of 2nd order

The RF signal generator is set to 7 GHz and 10 dBm. The bias voltage is swept. Optical power of the 1553 nm laser is set to 0 dBm and optical power of the 1640 nm laser is adjusted to obtain the maximum suppression of the HD2. In the experiment, it is found that the HD2 can be suppressed for the bias voltages from -0.2 to 0.1 V. The measurement results agree with the theories.

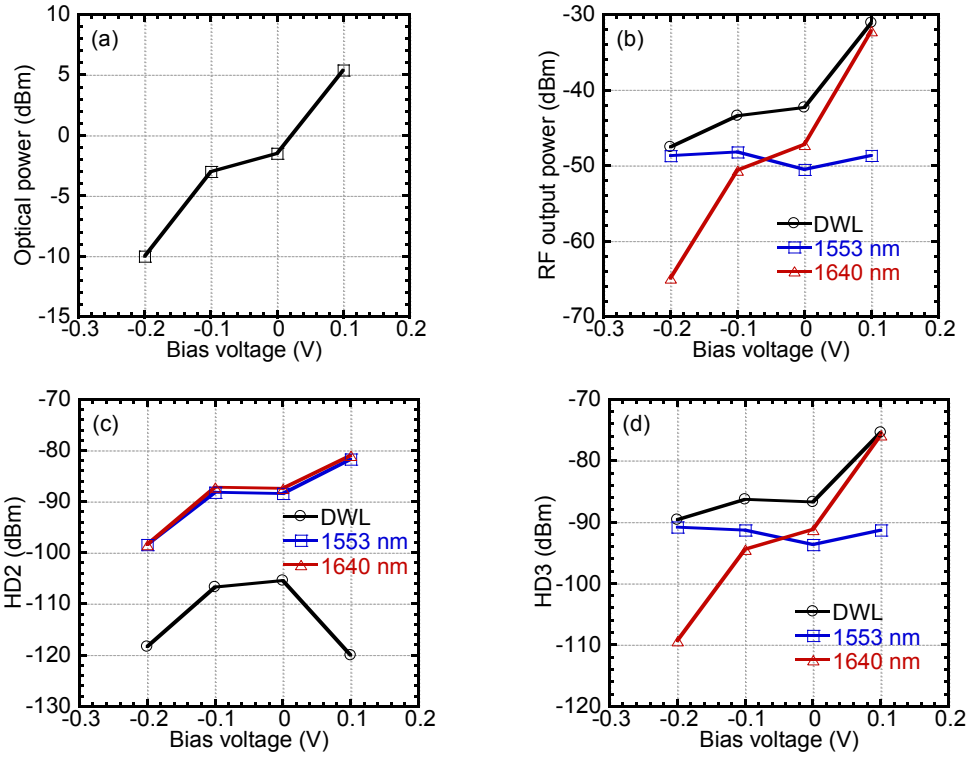

Figure 5-27 (a) Measured optical power of the 1640 nm laser for the maximum suppression of the HD2. (b) The RF power of the RF output signals, (c) HD2s, (d) HD3s for DWL, 1553 nm and 1640 nm, respectively. The HD2 is maximally suppressed.

The required optical power of the 1640 nm laser for the maximum suppression of the HD2 is given in Figure 5-27 (a). When the bias voltage of the MZM is increased, the required optical power of the 1640 nm laser is also increased. From -0.2 to 0.1 V, the required optical power of the 1640 nm laser is increased from -10 to 5.4 dBm. The reason

is that the HD2 is the minimum when the MZM is biased at $V_\pi/2$. When the MZM is biased at -0.2 V, the HD2 for 1553 nm is the minimum. And the HD2 for 1640 nm is the minimum when the MZM is biased at 0.2 V. When the bias voltage is increased from -0.2 to 0.2 V, the HD2 for 1553 nm is increased and for 1640 nm is decreased. So the optical power of the 1640 nm laser has to be increased to make the power of the two HD2s the same. Figure 5-27 (b) shows the measured RF output signals for DWL, 1553 nm, and 1640 nm, respectively. The power of the RF output signal for DWL is higher than that for 1553 nm and 1640 nm from -0.2 to 0.1 V. This is because the odd order components for the two wavelengths are inphase in this bias range. So the RF signal is improved by DWL. Figure 5-27 (c) presents the HD2. The HD2 for DWL is suppressed when the power of the HD2s for 1553 nm and 1640 nm is the same. It illustrates that the HD2s carried by the two optical carriers are in antiphase from -0.2 to 0.1 V. It also shows that the HD2 for the 1553 nm laser is increased with the bias voltage. Figure 5-27 (d) presents the measured HD3. It can be seen that it is increased by DWL. Moreover, when the bias voltage is increased, the optical power of the 1640 nm laser has to be increased as shown in Figure 5-27 (a). So the odd order components such as 1st and 3rd order components are also increased with the bias voltage.

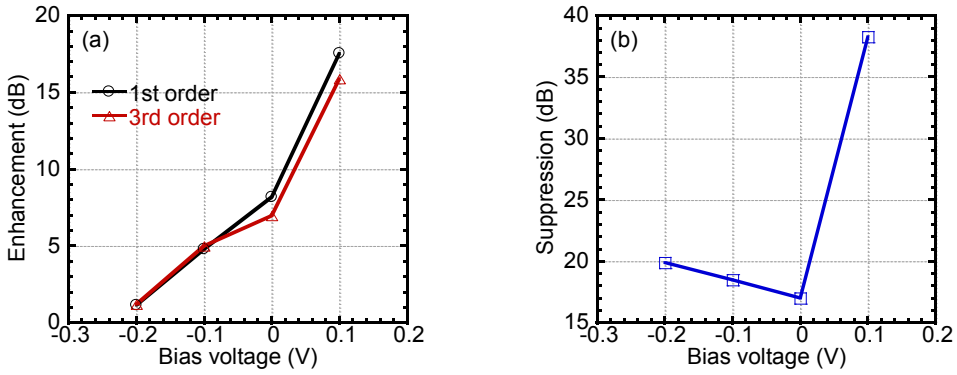

Figure 5-28 (a) Enhancements of the RF output signal and HD3 by DWL. (b) Suppression of the HD2.

The improvements of the RF output signal and the HD3 and suppression of the HD2 by DWL are given in Figure 5-28. It shows that the RF output signal and HD3 are increased by the same level by DWL in Figure 5-28 (a). This illustrates the SFDR with respect to the HD3 can be improved by DWL in this bias voltage range. When the bias voltage is 0.1 V, the improvement of the RF output signal is 17.6 dB. Figure 5-28 (b) shows the

suppression of the HD2 is higher than 17 dB for the bias voltage from -0.2 to 0.1 V. And the highest suppression is 38.3 dB at 0.1 V bias voltage.

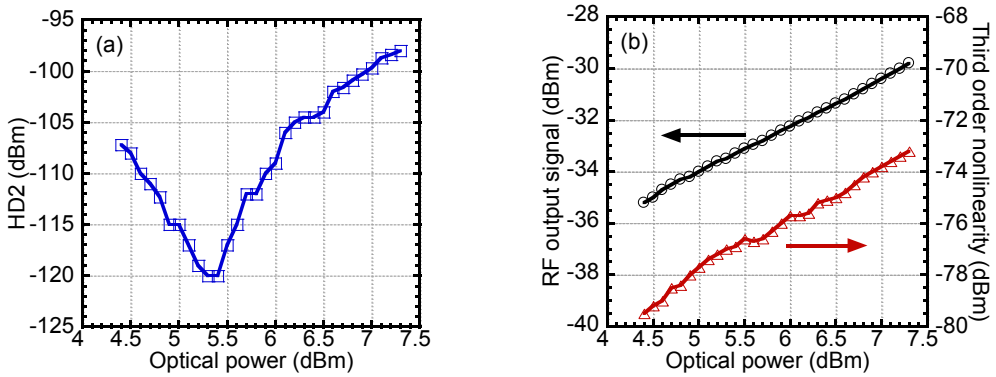

Figure 5-29 (a) RF power of the HD2 and (b) RF power of the RF output signal and the HD3 using DWL versus the optical power of the 1640 nm laser.

To verify the dependence of the optical power ratio, the power of the 1640 nm laser is swept. The power of the 1553 nm laser is fixed at 0 dBm. The RF input power is 10 dBm and the bias voltage is set to 0.1 V for the maximum suppression of the HD2. Figure 5-29 shows the HD2, RF output signal, and HD3 using DWL technique versus the optical power of the 1640 nm laser. In Figure 5-29 (a), the maximum suppression of the HD2 is achieved at 5.4 dBm. When the optical power is shifted to 4.6 or 5.9 dBm, the suppression degrades by 10 dB. Figure 5-29 (b) shows that the RF output signal and HD3 are increased in power with the power of the 1640 nm laser. This is because the odd order components carried by the two optical carriers are inphase with each other. And it can be seen that 1 dB increase of optical power causes ~2 dB increase of RF power.

Here, to simplify the explanation, the SFDRs with respect to the HD2 and HD3 are defined as $SFDR_2$ and $SFDR_3$. Then the SFDRs at 0.1 V bias voltage are measured and given in Figure 5-30 with respect to the HD2 and HD3 respectively for DWL, 1553 nm, and 1640 nm. Figure 5-30 (a) shows that the HD2 is 4^{th} order limited that means the HD2 is suppressed by DWL. It also can be seen that the RF signal and the HD3 are both increased. Figure 5-30 (b) and (c) present the SFDRs for 1553 and 1640 nm, respectively. Compared to Figure 5-30 (b), the $SFDR_2$ is improved by 38.4 dB and the $SFDR_3$ is improved by 12.1 by DWL technique. Despite the fact that the HD3 is increased by DWL,

the $SFDR_3$ is still improved. The reason is that the power of the RF signal and the HD3 is increased by the same power level by DWL. So the $SFDR_3$ is improved by the increase of the RF output signal. Compared to Figure 5-30 (c), the $SFDR_2$ and $SFDR_3$ are improved by 11.3 dB and 0.7 dB respectively. It can be seen that the HD2 in Figure 5-30 (c) is 3rd order limited. This is because the even order nonlinearities for 1640 nm are suppressed when the MZM is biased at its quadrature point. So the measured 2nd order nonlinearity in Figure 5-30 (c) is a combination of the suppressed even order nonlinearities and optical beating of odd order nonlinearities in the PD.

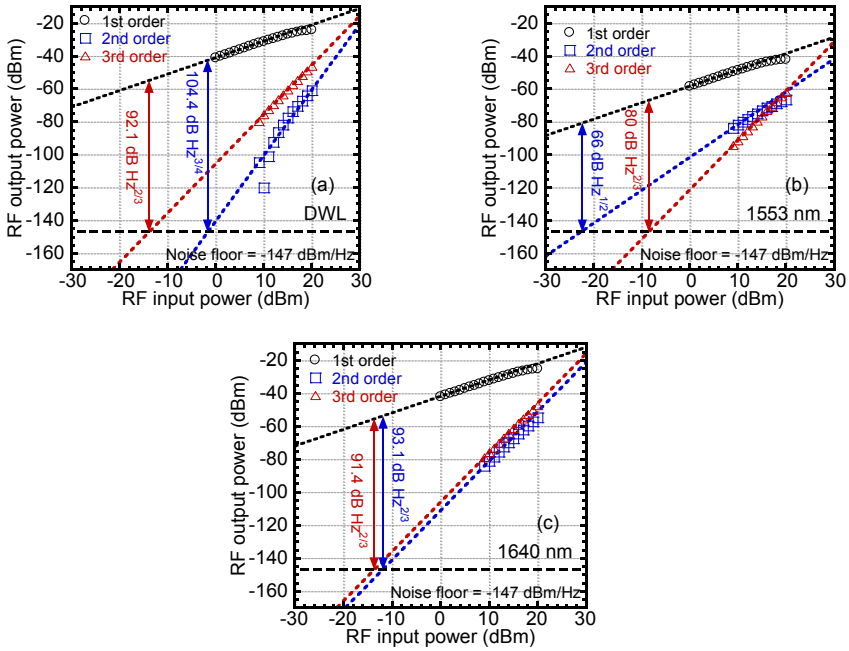

Figure 5-30 Measured SFDRs with respect to HD2 and HD3 for (a) DWL, (b) 1553 nm, and (c) 1640 nm. V_b = 0.1 V.

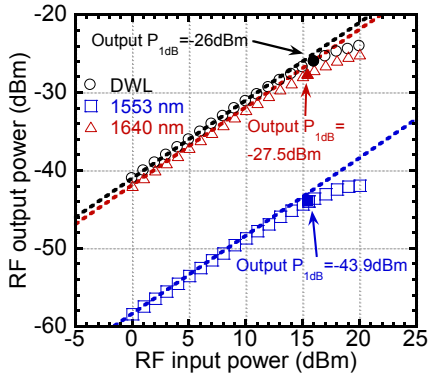

Figure 5-31 Measured P_{1dB}s for DWL, 1553 nm, and 1640 nm. V_b = 0.1 V.

Measured input and output P_{1dB}s for DWL, 1553 nm, and 1640 nm at the bias voltage of 0.1 V are given in Figure 5-31. The input P_{1dB}s for DWL, 1553 nm, and 1640 nm are 16, 15.5, and 15.4 dBm, respectively. So the input P_{1dB} is improved by 0.5 and 0.6 dB. The output P_{1dB}s for DWL, 1553 nm, and 1640 nm are -26, -43.9, and -27.5 dBm, respectively. It can be seen that the RF output signal power is improved by the 1640 nm laser. The output P_{1dB} is improved by 17.9 and 1.5 dB respectively. This illustrates that the system is linearized by DWL technique.

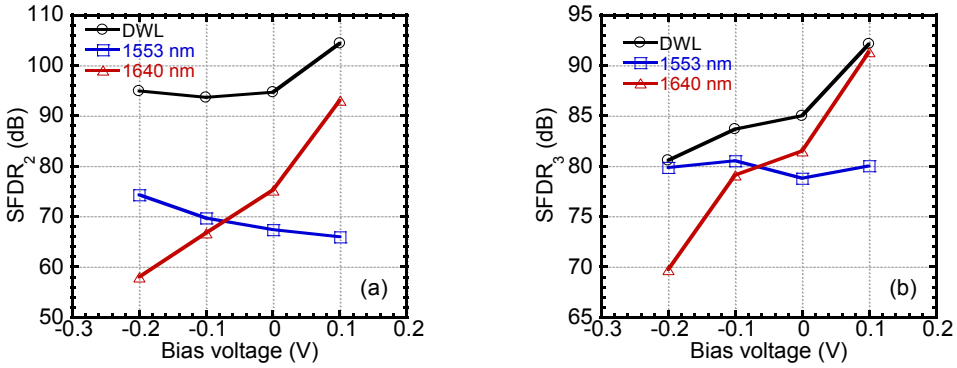

Figure 5-32 (a) Measured $SFDR_2$s and (b) $SFDR_3$s versus the bias voltage. The HD2 is maximally suppressed.

Figure 5-28 (b) shows that DWL can suppress the HD2 by more than 17 dB for bias voltage from -0.2 to 0.1 V. To verify the range of the bias voltage, the SFDRs and P_{1dB}s are measured for bias voltage from -0.2 to 0.1 V. The measured SFDRs versus the bias voltage of the MZM are given in Figure 5-32. The optical power of the 1553 nm laser is fixed at 0 dBm. In Figure 5-32 (a), the $SFDR_2$ for 1553 nm drops with the increase of the bias voltage because the HD2 for 1553 nm achieves the minimum at its quadrature point of -0.2 V. For the same reason, the HD2 for 1640 nm achieves the minimum at its quadrature point of 0.1 V. And the optical power of the 1640 nm laser is increased for the maximum suppression of the HD2. So the $SFDR_2$ for 1640 nm increases from -0.2 to 0.1 V. Compared to using a single laser, the $SFDR_2$ is improved for the bias voltage from -0.2 to 0.1 V by DWL. And the $SFDR_2$ achieves the maximum at 0.1 V. Figure 5-32 (b) presents that the $SFDR_3$s. The HD3 is increased by DWL, but the $SFDR_3$ is also improved. So it means that the $SFDR_3$ is improved by the increase of the improvement of the RF output signal. When the bias voltage is increased, the optical power of the 1640 nm laser is enhanced so that the $SFDR_3$ for 1640 nm is improved. The power of the RF

output signal is improved much more at 0.1 V than other bias voltages by DWL as shown in Figure 5-27 (b). So the $SFDR_3$ achieves the maximum at 0.1 V.

Figure 5-33 presents the measured output P_{1dB}s for DWL, 1553 nm laser, and 1640 nm laser versus the bias voltage. The output P_{1dB} using DWL increases with the bias voltage. It is enhanced by the increase of the optical power of the 1640 nm laser. For the system using the 1553 nm laser, the output P_{1dB} changed little while the bias voltage is swept. And it can be seen that the output P_{1dB} using DWL is higher than that using a single laser for the range of bias voltage.

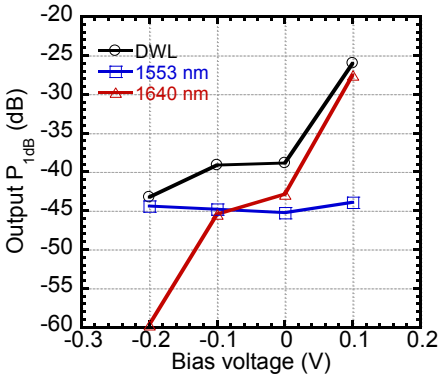

Figure 5-33 Measured output P_{1dB}s for DWL, 1553 nm laser, and 1640 nm laser.

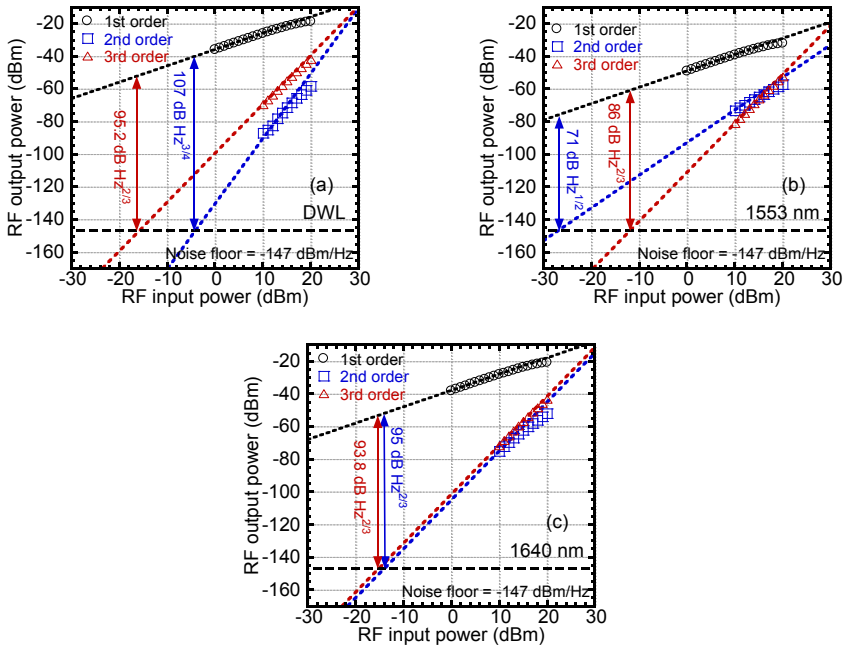

Figure 5-34 Measured SFDRs at 4 GHz for (a) DWL, (b) 1553 nm, and (c) 1640 nm. Vb = 0.1 V.

To verify the frequency dependence of the DWL technique, the SFDRs at 4 GHz and 0.1 V are also measured and given in Figure 5-34. The experimental setup is the same to that for 7 GHz. The measurement results show that the linearization performance for 4 GHz is similar to that for 7 GHz. Compared to using single 1553 nm laser, the $SFDR_2$ is improved by 36 dB and the $SFDR_3$ is improved by 9.2 dB. Compared to using single 1640 nm laser, the $SFDR_2$ is improved by 12 dB and the $SFDR_3$ is improved by 1.4 dB. Therefore, Figure 5-34 illustrates that DWL technique is independent of RF frequency.

Case II: Maximal suppression of 3rd order

To comprehensively study the linearization of the MZM using DWL technique, the HD3 is also maximally suppressed by sweeping the bias voltage of the MZM and the optical power ratio. It is found that the suppression can be obtained for the bias voltages from 2.3 to 2.8 V. The range of the bias voltage agrees with the calculation given in (5.12) and Figure 5-26. The optical power of the 1553 nm laser is 0 dBm and the optical power of the 1640 nm is swept to achieve the maximum suppression of the HD3. The HD3s carried by the two optical carriers need to have the same power to cancel each other referring to (5.11). The required optical power of the 1640 nm laser for the maximum suppression of the HD3 is given in Figure 5-35 (a). The required optical power is increased from -9 to 6.5 dBm while the bias voltage is increased from 2.3 to 2.8 V. The reason is that the HD3 carried by the 1640 nm laser drops to the minimum at its minimum transmission point of 2.9 V. And the HD3 carried by the 1553 nm laser increases from its minimum transmission point of 2.3 V. So the optical power of the 1640 nm laser has to be enhanced to make the RF power of the two HD3s carried by the two optical carriers the same. Figure 5-35 (b) shows that the RF output signal power is reduced by ~10 dB by DWL because the odd order components are suppressed in this range of bias voltage. Because of the same reason, Figure 5-35 (d) shows that the HD3 is suppressed by more than 15 dB. It also shows that the two HD3s carried by the two optical carriers are almost in the same power level. However, it can be seen that the HD2 is increased by DWL in Figure 5-35 (c).

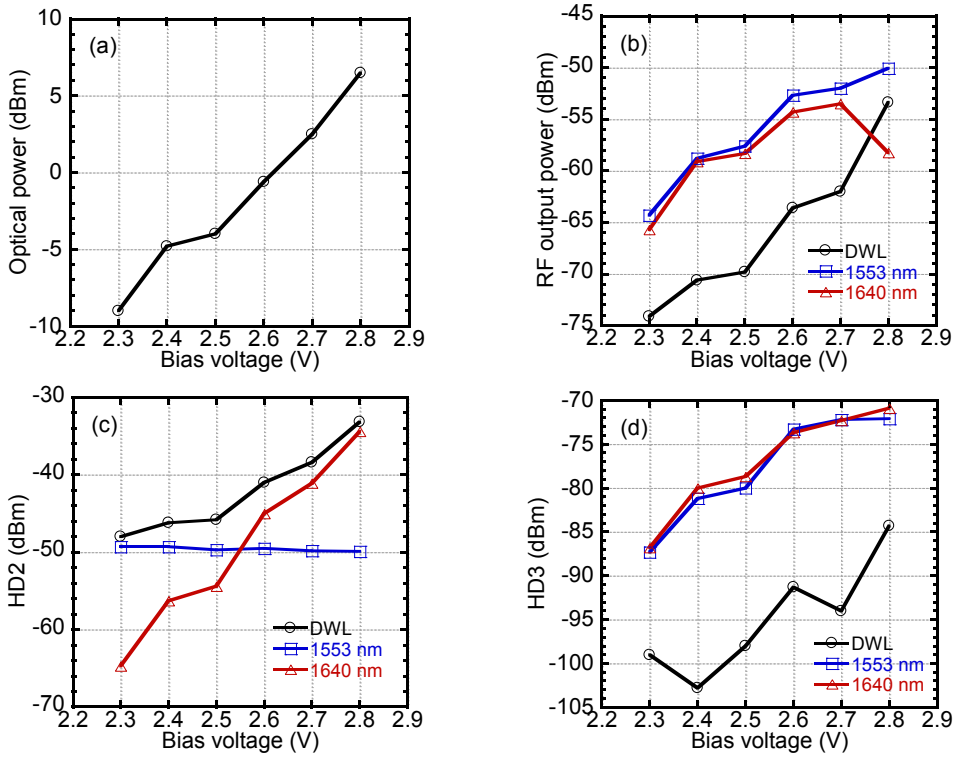

Figure 5-35 (a) Measured optical power of the 1640 nm laser for the maximum suppression of HD3. (b) RF power of the RF output signals, (c) HD2, (d) HD3 for DWL, 1553 nm and 1640 nm, respectively. The HD3 is maximally suppressed.

The suppressions of the RF signal and HD3 by DWL compared to using the 1553 nm laser are given in Figure 5-36 (a). The RF signal power is suppressed by more than 9.8 dB for bias voltages from 2.3 to 2.7 V and 3.3 dB at 2.8 V. The HD3 is suppressed by more than 11.7 dB and the maximum suppression is 21.8 dB at 2.7 V. However, Figure 5-36 (b) shows that the HD2 is increased by using DWL technique. The enhancement of the HD2 is increased with the bias voltage because the optical power of the 1640 nm laser is increased with the bias voltage as shown in Figure 5-35 (a). The minimum enhancement of the HD2 is 1.3 dB at 2.3 V and the maximum enhancement is 16.8 dB at 2.8 V.

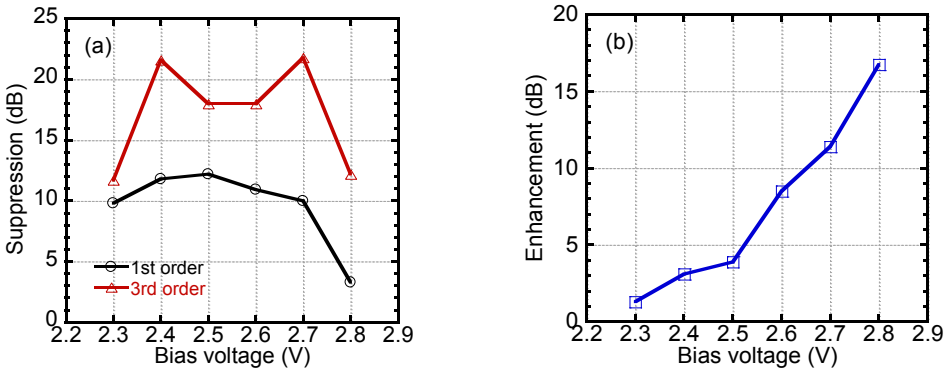

Figure 5-36 (a) Suppressions of the RF signal and HD3 compared to using the 1553 nm laser. (b) Enhancement of the HD2 compared to using the 1553 nm laser.

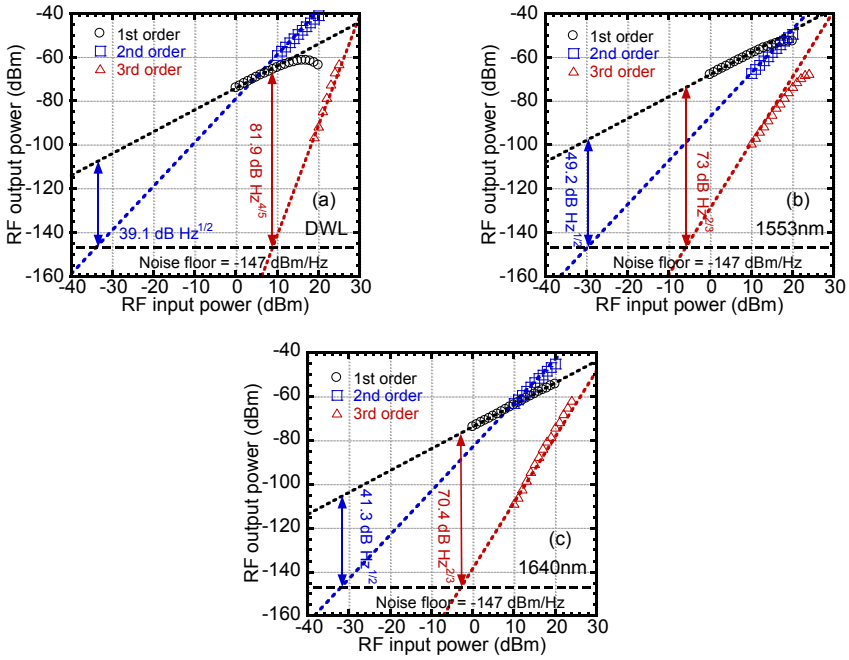

Figure 5-37 Measured SFDRs for (a) DWL, (b) 1553 nm, and (c) 1640 nm. V_b = 2.6 V.

The measured SFDRs when the MZM is biased at 2.6 V are given in Figure 5-37. The HD3 is maximally suppressed by adjusting the optical power of the 1640 nm laser. It can be seen that the $SFDR_3$ is improved from 73 and 70.4 dB $Hz^{2/3}$ to 81.9 dB $Hz^{4/5}$ by DWL compared to using a single laser, although the RF signal power is also suppressed by DWL. It shows that the HD3 is 5th order limited when DWL technique is employed. But the $SFDR_2$ is reduced because the HD2 is increased by DWL. And Figure 5-37 shows that the power of the RF output signals is low because the MZM is biased near its

minimum transmission point. So although the $SFDR_3$ can be improved, high loss is induced to the RF signal.

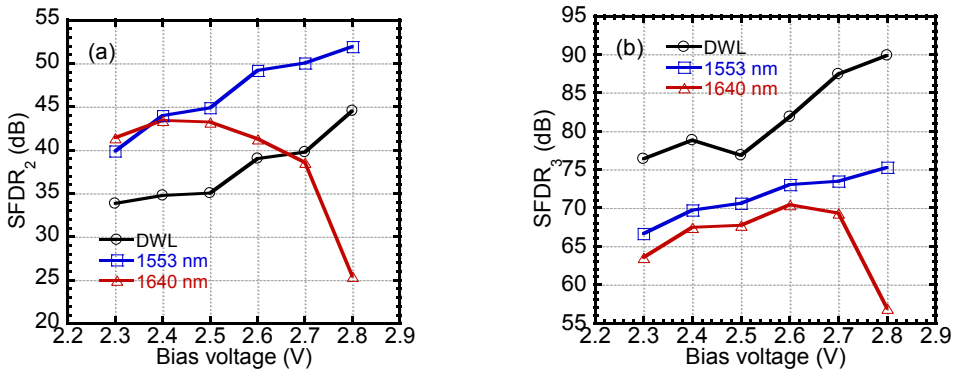

Figure 5-38 Measured (a) $SFDR_2$s and (b) $SFDR_3$s versus the bias voltage. The HD3 is maximally suppressed.

Figure 5-38 presents the measured SFDRs versus the bias voltage. In Figure 5-38 (a), the $SFDR_2$ degrades when DWL is used. The reason is that the HD2 is increased in this range of the bias voltage. And it can be seen that the $SFDR_2$s are lower than 52 dB in this range of bias voltage. This is because the bias voltage is near the minimum transmission point of the MZM. So the RF signal is weak and the HD2 is strong. Figure 5-38 (b) shows that the $SFDR_3$ is improved by using DWL compared to using a single laser. And more than 6.3 dB improvement is achieved for the bias voltages from 2.3 to 2.8 V. The maximal $SFDR_3$ using DWL is obtained at 2.8 V. Moreover, it should be noted that the P_{1dB} degrades by using DWL for this range of bias voltage because the RF output signal is reduced.

5.5 Summary

In this chapter, DWL technique using two lasers with different wavelengths to improve the RF signal power and suppress the 2^{nd} and 3^{rd} order nonlinearities simultaneously in RoF transmission systems has been comprehensively studied theoretically and experimentally. DWL technique is proved to linearize externally modulated RoF transmission systems when the 2^{nd} and 3^{rd} order nonlinearities are both considered at the same time. EAM or MZM can be linearized by using DWL technique. HDs and IMDs can also be suppressed at the same time.

Firstly, an RoF transmission system using an EAM which has wavelength dependent transmission and nonlinear characteristics is linearized by DWL. The theory is presented and the dependence of the optical power ratio of the two lasers and the SFDRs are calculated based on the theory and verified by the experiments for the EAM. Both the calculation and experimental results show that in addition to the enhanced RF signal power, the 2^{nd} and 3^{rd} as well as 5^{th} order nonlinearities are suppressed.

When the 2^{nd} order nonlinearity is maximally suppressed, 11.5 and 1.8 dB improvements of the $SFDR_2$ and $SFDR_3$ with respect to HDs respectively are achieved by using DWL. 8.5 and 1.3 dB improvements of the $SFDR_2$ and $SFDR_3$ with respect to IMDs respectively are achieved. Correspondingly, 3 and 4 dB improvements of the input P_{1dB} and output P_{1dB} respectively are obtained.

When the 3^{rd} order nonlinearity is maximally suppressed, the $SFDR_3$ with respect to HD3 and IMD3 is improved by 8.1 and 20.4 dB, respectively, and corresponding 7.7 and 11.7 dB improvements of the input P_{1dB}, and output P_{1dB} respectively are achieved. It is found that IMD5 is also suppressed, and $SFDR_5$ with respect to IMD5 is improved by 7.1 dB. Moreover, the RoF transmissions of WiFi signals at 2.4 GHz and 5 GHz are also linearized by using DWL technique. 3.5 dB at 2.4 GHz and 2.8 dB at 5 GHz improvements of the EVM are obtained by using DWL technique when the optical power ratio of the 1552.6 nm laser and 1510 nm laser is the same to that for single-tone and two-tone tests.

Then DWL technique is also studied to linearize an RoF transmission system using an MZM. Theories are given to predict the bias dependence of DWL technique for the MZM. Single-tone test is used in the experiments. The theories and experiments both prove that DWL can be used to suppress the odd or even order nonlinearities in the system. But the odd and even order nonlinearities cannot be suppressed at the same time. And if one is suppressed, the other one will be increased. Unfortunately, when the odd order nonlinearities are suppressed, the RF signal is also suppressed. However, in the experiments, it is found that the $SFDR_2$ and $SFDR_3$ are both improved simultaneously when the even order nonlinearities are suppressed. The reason is that the RF signal is

improved. Compared to using a single 1553 nm laser, the $SFDR_2$ is improved by 38.4 dB and the $SFDR_3$ is improved by 12.1 dB when the bias voltage is 0.1 V.

Chapter 6 Conclusion

6.1 Conclusion

RoF transmission systems are transparent infrastructures to support various wireless access technologies. They are susceptible to the nonlinearities, and the optical subcarrier modulation is the main nonlinear source in RoF transmission systems. Not only the IMD3, but also the HDs and even order IMDs need to be suppressed for the broadband application of RoF transmission systems. In this thesis, three linearization technologies are proposed to linearize RoF transmission systems. Two low-cost broadband analog PDCs are proposed to suppress the IMD3 of directly and externally modulated RoF transmission systems. Moreover, DWL technique is investigated and verified to linearize externally modulated RoF transmission systems when 2nd and 3rd order nonlinearities are considered as the main nonlinearities at the same time. The detailed conclusions of these linearization technologies are given as below:

1. A low-cost analog broadband PDC is designed and experimentally verified. Two zero bias beam lead GaAs Schottky diodes are used as the predistorter. Zero bias diode leads to lower bias current which is lower than 3 mA so that lower power consumption is achieved. The zero bias diode has high series resistance so that no broadband multi-section matching network is required. Thus the size and parasitics of the circuit are significantly reduced. The bandwidth of the PDC from 7 to 18 GHz is obtained. Using the proposed PDC, the input P_{1dB} of an RoF transmission system using an MZM is improved by 0.4 and up to 2.2 dB from 7 to 18 GHz. The measured SFDRs are improved by more than ~10 dB from 7 to 14 GHz and more than ~6 dB from 15 to 18 GHz. Moreover, the proposed PDC is also verified in an RoF transmission system using an EAM. The simulation shows that the EAM can be linearized by the PDC for the bias voltages from -0.9 to -1.9 V. As a result, the EAM is biased at -1.5 V. The measured input P_{1dB} of the system is also improved by 0.8 and up to 3.8 dB from 8 to 17 GHz. And the measured SFDR is improved by more than ~9 dB from 7 to 14 GHz and ~4 dB from 15 to 18 GHz by the PDC. Compared to the previous work [43], this PDC has many advantages: lower bias

currents and thus lower power consumption, no matching network required and thus further smaller size and lower parasitics, and higher bandwidth.

2. A novel ultra broadband low-cost analog PDC is proposed and designed to linearize RoF transmission systems. A dual anti-parallel Schottky diode is used as a predistorter. Push-pull operation using only one DC bias is obtained, further no quarter-wavelength transmission line and power divider are needed. The PDC is adjusted by tuning the bias current. The bandwidth from 10 MHz to 30 GHz is achieved. The dimension of the PDC is 2.4×1 cm^2. The RoF transmission systems with both direct modulation and external modulation are linearized in the experiments. In two-tone test, a directly modulated RoF transmission system is linearized and the IMD3 is suppressed. The SFDR at 8 GHz is improved by 11.9 dB. The PDC is also evaluated in an RoF transmission system using an EAM. In two-tone test, it is found that the IMD3 is suppressed by the PDC. The input and output P_{1dB}s are both improved. The measurements show that the SFDR is improved by more than 10 dB from 1 to 5 GHz and more than 5 dB from 1 to 30 GHz by the PDC. The low SFDR improvement at higher frequency is due to the enhanced noise and accumulated loss. Moreover, WiFi signals at 2.4 and 5 GHz are transmitted in the RoF transmission system to test the PDC. The measurements show that the EVM is improved by 1 dB at both 2.4 and 5 GHz by the PDC. For an externally modulated RoF transmission using an MZM, the SFDR is improved by more than 12 dB from 2 to 5 GHz and more than 5 dB from 2 to 30 GHz. The IMD3 is suppressed and the IMD5 is dominant. Moreover, WiFi signal at 2.4 GHz is verified in the RoF transmission system for BTB and 20 km SMF transmission. For the RF input power to the MZM from -11 to 8 dBm, the EVM is improved by more than 0.4 dB. The maximal improvements of the EVMs are 5.1 dB for BTB and 3.5 dB for 20 km SMF transmission. It is proved that the low-cost ultra broadband PDC can linearize RoF transmission systems with direct modulation and external modulation. To our knowledge, the proposed PDC has the broadest bandwidth among the reported PDCs. The comparison of the PDCs is shown in Table 6-1.

Table 6-1 Comparison of the PDCs.

Parameters	PDC in Chapter 4	PDC in Chapter 3	Previous Work [43]
Bandwidth	10 MHz to 30 GHz	7 to 18 GHz	3.1 to 4.8 GHz
Bias Current	< 6 mA	< 3 mA	13.3 mA
Dimension	2.4×1 cm^2	3.5×1.6 cm^2	13.2×7.7 cm^2
Bias	1	2	2

3. DWL technique using two lasers with different wavelengths to improve the RF signal power and suppress the 2nd and 3rd order nonlinearities simultaneously in externally modulated RoF transmission systems are comprehensively studied theoretically and experimentally. EAM and MZM can be both linearized by using DWL technique. HDs and IMDs can also be suppressed at the same time. Firstly, an RoF transmission system using an EAM which has wavelength dependent transmission and nonlinear characteristics is linearized by DWL. The theory is presented and the dependence of the optical power ratio of the two lasers and the SFDRs are calculated based on the theory and verified by the experiments. Both the calculation and experimental results show that in addition to the enhanced RF signal power, the 2nd and 3rd as well as 5th order nonlinearities are suppressed. When the 2nd order nonlinearity is maximally suppressed, 11.5 and 1.8 dB improvements of the $SFDR_2$ and $SFDR_3$ with respect to HDs respectively are achieved by using DWL. 8.5 and 1.3 dB improvements of the $SFDR_2$ and $SFDR_3$ with respect to IMDs respectively are achieved. Correspondingly, 3 and 4 dB improvements of the input and output P_{1dB}s respectively are obtained. When the 3rd order nonlinearity is maximally suppressed, the $SFDR_3$s with respect to HD3 and IMD3 are improved by 8.1 and 20.4 dB, respectively, and corresponding 7.7 and 11.7 dB improvements of the input and output P_{1dB}s respectively are achieved. The IMD5 is also suppressed, and the $SFDR_5$ with respect to the IMD5 is improved by 7.1 dB. Moreover, the RoF transmissions of WiFi signals at 2.4 and 5 GHz are also

linearized by using DWL technique. 3.5 dB at 2.4 GHz and 2.8 dB at 5 GHz improvements of the EVMs are obtained by using DWL technique when the optical power ratio of the 1552.6 nm laser and 1510 nm laser is 1.5 dB. DWL technique is also studied to linearize an RoF transmission system using an MZM. Theories are given to predict the bias dependence of DWL technique for MZM. Single-tone test is used in the experiments. Theories and experiments prove that DWL can be used to suppress the odd or even order nonlinearities in the system. But the odd and even order nonlinearities cannot be suppressed at the same time. When one is suppressed, the other one is increased. Unfortunately, when the odd order nonlinearities are suppressed, the RF signal is also suppressed. However, in the experiments, it is found that the $SFDR_2$ and $SFDR_3$ are both improved at the same time when the even order nonlinearities are suppressed. The RF signal and 3^{rd} order nonlinearity are improved by the same level by DWL, so the $SFDR_3$ can be improved while the 3^{rd} order nonlinearity is increased. Compared to using a single 1553 nm laser, the $SFDR_2$ is improved by 38.4 dB and the $SFDR_3$ is improved by 12.1 dB when the bias voltage is 0.1 V.

6.2 Future Work

One of the future studies about the linearization technologies will focus on the simultaneous suppressions of several nonlinearities. Chapters 3 and 4 show that the PDC can suppress the IMD3, but the IMD5 is also strong when the RF input power is high enough. So the PDC will be designed to suppress both IMD3 and IMD5 at the same time.

One drawback of the PDC is that the PDC cannot reduce the memory effect. Also presently, digital linearization cannot reach high bandwidth. So one of the future works is the study on the broadband linearization by using the analog PDC with digital filter to suppress nonlinearities and reduce memory effect.

DWL technique can suppress 2^{nd} and 3^{rd} order nonlinearities simultaneously, but the additional laser increases the cost. So low-cost optical linearization technologies need to be studied, which only uses more passive optical components for linearization instead of active components.

Although digital linearization is limited by the low bandwidth, it has the best performance compared to the analog and optical linearization technologies. So high-efficiency digital linearization is also a topic for future studies.

Reference

[1] J. H. Winters, R. D. Gitlin, and S. Kasturia, "Reducing the effects of transmission impairments in digital fiber optic systems," *IEEE Commun. Mag.*, vol. 31, no. 6, pp. 68-76, Jun. 1993.

[2] T. Terahara, T. Naito, N. Shimojoh, T. Chikarna and M. Suyama, "85 Gbit/s WDM transmission of 16 5.3 Gbit/s RZ data signals over 7931 km using accurate gain-equalisation and precompensation of group-velocity-dispersion," *Electron. Lett.*, vol.33, no. 7, pp. 603-605, Mar. 1997.

[3] R. A. de A. Lima, M. C. R. Carvalho, and L. F. M. Conrado, "Digital optical transmission links with in-line erbium doped fiber amplifier chains," *IEEE MTT-S Int. Microw. Symp.*, vol. 1, pp. 374-378, Aug. 1997.

[4] H. Asada, T. Yamada, N. A. Rabou, H. Ikeda, and Y. Shimodaira, "Optical fiber digital transmission of multiplexed video and audio signals suitable for multimedia applications," *IEEE Trans. Consum. Electron.*, vol. 44, no. 2, pp. 273-279, May 1998.

[5] R. E. Schuh, E. Sundberg, B. Verri, and T. Arkner, "Penalty free simultaneous 1 Gbit/s digital and GSM-1800 radio signal transmission over 600 m multimode fibre using 850 nm VCSEL sources," *IEEE Int. Symp. Pers. Indoor Mobile Radio Commun.*, vol. 5, pp. 2274-2276, Sept. 2002.

[6] J. Yu, X. Zhou, M. F. Huang, Y. Shao, D. Qian, T. Wang, M. Cvijetic, P. Magill, L. Nelson, M. Birk, S. Ten, H. B. Mathew, and S. K. Mishra, "17 Tb/s (161×114 Gb/s) PolMux-RZ-8PSK transmission over 662 km of ultra-low loss fiber using C-band EDFA amplification and digital coherent detection," *European Conf. Opt. Commun.*, Sept. 2008.

[7] D. van den Borne, V. A. J. M. Sleiffer, M. S. Alfiad, S. L. Jansen, and T. Wuth, "POLMUX-QPSK modulation and coherent detection: The challenge of long-haul 100G transmission," *European Conf. Opt. Commun.*, Sept. 2009.

[8] K.-I. Kitayama, A. Maruta, and Y. Yoshida, "Digital Coherent Technology for Optical Fiber and Radio-Over-fiber Transmission Systems," *J. Lightw. Technol.*, vol. 32, no. 20, pp.3411-3420, Mar. 2014.

[9] G. Raybon, A. Adamiecki, S. Randel, and P. J. Winzer, "Single-carrier and dual-carrier 400-Gb/s and 1.0-Tb/s transmission systems," *Opt. Fiber Commun. Conf. Expo.*, Mar. 2014.

[10] M. G. Larrode and A. M. J. Koonen, "All-Fiber Full-Duplex Multimode Wavelength-Division-Multiplexing Network for Radio-Over-Multimode-Fiber Distribution of Broadband Wireless Services," *IEEE Trans. Microw. Theory Techn.*, vol. 56, no. 1, pp. 248-255, Jan. 2008.

[11] N. Pleros, K. Vyrsokinos, K. Tsagkaris, and N. D. Tselikas, "A 60 GHz Radio-Over-Fiber Network Architecture for Seamless Communication With High Mobility," *J. Lightw. Technol.*, vol. 27, no. 12, pp. 1957-1967, May 2009.

[12] C.-T. Lin, J. Chen, P.-C. Peng, C.-F. Peng, W.-R. Peng, B.-S. Chiou, and S. Chi, "Hybrid Optical Access Network Integrating Fiber-to-the-Home and Radio-Over-Fiber Systems," *IEEE Photon. Technol. Lett.*, vol. 19, no. 8, pp. 610-612, Apr. 2007.

[13] G. Kalfas and N. Pleros, "An Agile and Medium-Transparent MAC Protocol for 60 GHz Radio-Over-Fiber Local Access Networks," *J. Lightw. Technol.*, vol. 28, no. 16, pp. 2315-2326, Mar. 2010.

[14] F. Brendel, J. Poette, B. Cabon, T. Zwick, F. Van Dijk, F. Lelarge, and A. Accard, "Chromatic Dispersion in 60 GHz Radio-Over-Fiber Networks Based on Mode-Locked Lasers," *J. Lightw. Technol.*, vol. 29, no. 24, pp. 3810-3816, Oct. 2011.

[15] T. P. C. de Andrade, N. L. S. da Fonseca, L. B. Oliveira, and O. C. Branquinho, "MAC protocols for wireless sensor networks over radio-over-fiber links," *IEEE Int. Conf. Commun.*, pp. 254-259, Jun. 2012.

[16] A. Haddad, E. A. Doumith, and M. Gagnaire, "Impairment-aware radio-over-fiber control plane for LTE antenna backhauling," *IEEE Int. Conf. Commun.*, pp. 2816-2821, Jun. 2012.

[17] Y. Yang, F. Li, C. Lim, and A. Nirmalathas, "Radio-over-fiber technologies for future mobile backhaul supporting cooperative base stations," *IEEE MTT-S Int. Microw. Symp.*, Jun. 2013.

[18] G. S. D. Gordon, M. J. Crisp, R. V. Penty, T. D. Wilkinson, and I. H. White, "Feasibility Demonstration of a Mode-Division Multiplexed MIMO-Enabled Radio-Over-Fiber Distributed Antenna System," *J. Lightw. Technol.*, vol. 32, no. 20, pp. 3521-3528, Mar. 2014.

[19] M. Morant, J. Prat, and R. Llorente, "Radio-Over-Fiber Optical Polarization-Multiplexed Networks for 3GPP Wireless Carrier-Aggregated MIMO Provision," *J. Lightw. Technol.*, vol. 32, no. 20, pp. 3721-3727, Apr. 2014.

[20] J. Park, W. V. Sorin, and K. Y. Lau, "Elimination of the fiber chromatic dispersion penalty on 1550 nm millimeter-wave optical transmission," *Electron. Lett.*, vol. 33, issue 6, pp. 512-513, Mar. 1997.

[21] G. H. Smith, D. Novak, and Z. Ahmed, "Overcoming chromatic-dispersion effects in fiber-wireless systems incorporating external modulators," *IEEE Trans. Microw. Theory Techn.*, vol. 45, issue 8, pp. 1410–1415, Aug. 1997.

[22] G. H. Smith, D. Novak, and Z. Ahmed, "Technique for optical SSB generation to overcome dispersion penalties in fiber-radio systems," *Electron. Lett.*, vol. 33, no. 1, pp. 74-75, Jan. 1997.

[23] A. Bjarklev, T. Rasmussen, O. Lumholt, K. Rottwitt, and M. Helmer, "Optimal design of single-cladded dispersion-compensating optical fibers," *Opt. Lett.*, vol. 19, issue 7, pp. 457–459, Apr. 1994.

[24] A. J. Antos and D. K. Smith, "Design and characterization of dispersion compensating fiber based on the LP01 mode," *J. Lightw. Technol.*, vol. 12, issue 10, pp. 1739–1745, Oct. 1994.

[25] K. Nishimura, R. Inohara, M. Tsurusawa, and M. Usami, "80 Gbit/s wavelength conversion using MQW electro-absorption modulator in delayed-interferometric configuration," *Electron. Lett.*, vol. 39, no. 10, pp. 792–794, May 2003.

[26] C. Sui, B. Hraimel, X. Zhang, L. Wu, Y. Shen, K. Wu, T. Liu, T. Xu and Q. Nie, "Impact of electro-absorption modulator integrated laser on MB-OFDM ultra-wideband signals over fiber systems," *J. Lightw. Technol.*, vol.28, no24. pp. 3548-3555, Nov. 2010.

[27] S. Højfeldt and J.Mørk, "Modeling of carrier dynamics in quantum-well electroabsorption modulators," *IEEE J. Sel. Topics in Quantum Electron.*, vol. 8, no. 6, pp. 1265-1276, Nov. 2002.

[28] T. Mori and H. Kawaguchi, "Characteristics of nondegenerate four-wave mixing in electro-absorption modulator," *Appl. Phys. Lett.*, vol. 85, no. 6, pp. 869–871, Aug. 2004.

[29] H. Kuwatsuka, T. Simoyama, and H. Ishikawa, "Enhancement of third-order nonlinear optical susceptibilities in compressively strained quantum wells under the population inversion condition," *IEEE J. Quantum Electron.*, vol. 35, no. 12, pp. 1817–1825, Dec. 1999.

[30] A. D'Ottavi, P. Spano, G. Hunziker, R. Paiella, R.Dall'Ara, G.Guekos, and K. J. Vahara, "Wavelength conversion at 10 Gb/s by four-wave mixing over a 30-nm interval," *IEEE Photon. Technol. Lett.*, vol. 10, no. 7, pp. 952–954, Jul. 1997.

[31] E. S. Awad, P. S. Cho, and J. Goldhar, "Simultaneous four-wave mixing and cross-absorption modulation inside a single EAM for high-speed optical demultiplexing and clock recovery," *IEEE Photon. Technol. Lett.*, vol. 17, no. 7, pp. 1534-1536, Jun. 2005.

[32] C. S. Park, C. K. Oh, C. G. Lee, D.-H. Kim, and C. S. Park, "A photonic up-converter for a WDM radio-over-fiber system using cross-absorption modulation in an EAM," *IEEE Photon. Technol. Lett.*, vol. 17, no. 9, pp. 1950-1952, Sept. 2005.

[33] C. S. Park, Y. Guo, Y. K. Yeo, Y. Wang, L. C. Ong, and S. Kato, "Fiber-Optic 60-GHz Wireless Downlink Using Cross-Absorption Modulation in an EAM," *IEEE Photon. Technol. Lett.*, vol. 20, no. 8, pp. 557-559, Apr. 2008.

[34] Q. Lin and G. P. Agrawal, "Vector theory of cross-phase modulation: role of nonlinear polarization rotation," *IEEE J. Quantum Electron.*, vol. 40, no. 7, pp. 958-964, Jul. 2004.

[35] G. Meloni, A. Bogoni, and L. Poti, "Real-time ps-resolution optical sampler based on XPM-induced polarization rotation in 1-meter-long bismuth oxide fibre," *European Conf. Opt. Commun.*, vol. 1, pp. 63-64, Sept. 2005.

[36] J. H. Lee, T. Nagashima, T. Hasegawa, S. Ohara, N. Sugimoto, and K. Kikuchi, "Wide-band tunable wavelength conversion of 10-gb/s nonreturn-to-zero signal using cross-phase-Modulation-induced polarization rotation in 1-m bismuth oxide-based nonlinear optical fiber," *IEEE Photon. Technol. Lett.*, vol. 18, no. 1, pp. 1041-1135, Jan. 2006.

[37] R. Zhu, B. Hraimel, and X. Zhang, "Analysis of simultaneous photonic frequency downconversion and optical subcarrier modulation in an electroabsorption modulator," *J. Lightw. Technol.*, vol. 30, no. 3, pp. 344–354, Feb. 2012.

[38] A. Georgiadis, "Gain, phase, imbalance, and phase noise effects on error vector magnitude," *IEEE Trans. Veh. Technol.*, vol. 53, no. 2, pp. 443-449, Mar. 2004.

[39] R. B. Ellis and M. H. Capstick, "Feedback control of a linearised Mach-Zehnder modulator for SCM applications," *High Freq. Postgraduate Student Colloq.*, pp. 33-38, Sept. 1996.

[40] G. C. Wilson, T. H. Wood, M. Gans, J. L. Zyskind, J. W. Sulhoff, J. E. Johnson, T. Tanbun-Ek, and P. A. Morton, "Predistortion of electroabsorption modulators for analog CATV systems at 1.55 μm," *J. Lightw. Technol.*, vol. 15, no. 9, pp. 1654-1662, Sept. 1997.

[41] H. Matsubara, K. Ishihara, N. Miyadai, and T. Nojima, "A Novel 3rd-and-5th-Order Predistortion Circuit for 2 GHz Band W-CDMA Amplifier," *Asia-Pacific Microw. Conf.*, Dec. 2007.

[42] A. Katz, R. Gray, and R. Dorval, "Truly wideband linearization," *IEEE Microw. Mag.*, vol. 10, no. 7, pp. 20-27, Dec. 2009.

[43] Y. Shen, B. Hraimel, X. Zhang, G. E. R. Cowan, K. Wu, and T. Liu, "A Novel Analog Broadband RF Predistortion Circuit to Linearize Electro-Absorption Modulators in Multiband OFDM Radio-Over-Fiber Systems," *IEEE Trans. Microw. Theory Techn.*, vol. 58, no. 11, pp. 3327-3335, Sept. 2010.

[44] B. Hraimel and X. Zhang, "Low-cost broadband predistortion-linearized single-drive x-cut Mach–Zehnder modulator for radio-over-fiber systems," *IEEE Photon. Technol. Lett.*, vol. 24, no. 18, pp. 1571–1573, Sept. 2012.

[45] B.-H. Son, K.-J. Kim, Y. Li, C.-I. Park, and Y.-W. Choi, "Simple electrical predistortion method using Schottky diode for radio-over-fiber systems," *IEEE Photon. Technol. Lett.*, vol. 27, no. 8, pp. 907–910, Apr. 2015.

[46] R. Sadhwani and B. Jalali, "Adaptive CMOS predistortion linearizer for fiber-optic links," *J. Lightw. Technol.*, vol. 21, no. 12, pp. 3180-3193, Dec. 2003.

[47] T.-Y. Huang, Y.-H. Lin, and H. Wang, "A K-band adaptive-bias power amplifier with enhanced linearizer using 0.18-μm CMOS process," *IEEE MTT-S Int. Microw. Symp.*, May 2015.

[48] Y.-H. Chen, K.-Y. Kao, C.-Y. Chao, and K.-Y. Lin, "A 24 GHz CMOS power amplifier with successive IM2 feed-forward IMD3 cancellation," *IEEE MTT-S Int. Microw. Symp.*, May 2015.

[49] L. Ding and G. T. Zhou, "Effects of even-order nonlinear terms on predistortion linearization," *IEEE Digit. Signal Process. Workshop*, Oct. 2002.

[50] R. I. Killey, P. M. Watts, V. Mikhailov, M. Glick, and P. Bayvel, "Electronic dispersion compensation by signal predistortion using digital Processing and a dual-drive Mach-Zehnder Modulator," *IEEE Photon. Technol. Lett.*, vol. 17, no. 3, pp. 714-716, Mar. 2005.

[51] L. C. Vieira, N. J. Gomes, A. Nkansah, and F. Van Dijk, "Behavioral modeling of radio-over-fiber links using memory polynomials," *Int. Topical Meeting Microw. Photon.*, pp. 85-88, Oct. 2010.

[52] L. C. Vieira, N. J. Gomes, and A. Nkansah, "An experimental study on digital predistortion for radio-over-fiber links," *Asia Commun. Photon. Conf. Exhibition*, pp. 126-127, Dec. 2010.

[53] Y. Zhao, X. Pang, L. Deng, X. Yu, X. Zheng, H. Zhang, and I. T. Monroy, "Digital predistortion of 75-110 GHz W-band frequency multiplier for fiber wireless short range access systems," *European Conf. Opt. Commun.*, Sept. 2011.

[54] Z. Liu, M. A. Violas, and N. B. Carvalho, "Transmission of four channels SCM over fiber and nonlinear compensation for RSOA external modulators," *IEEE GLOBECOM Workshops*, pp. 147-151, Dec. 2011.

[55] A. Awoye, M. S. Leeson, and R. J. Green, "Neural network based adaptive predistortion for radio over fiber links," *Int. Conf. Transparent Opt. Netw.*, Jul. 2012.

[56] D. Lam, A. M. Fard, and B. Jalali, "Digital broadband linearization of analog optical links," *IEEE Photon. Conf.*, pp. 370-371, Sept. 2012.

[57] O. Omomukuyo, M. P. Thakur, and J. E. Mitchell, "Experimental demonstration of digital predistortion for linearization of Mach-Zehnder modulators in direct-detection MB-OFDM ultra-wideband over fiber systems," *Asia Commun. Photon. Conf.*, Nov. 2012.

[58] Y. Zhao, L. Deng, X. Pang, X. Yu, X. Zheng, H. Zhang, and I. T. Monroy, "Digital predistortion of 75-110 GHz W-band frequency multiplier for fiber wireless short range access systems," *Opt. Exp.*, vol. 19, no. 26, pp. B18-B25, Dec. 2012.

[59] Y. Pei, K. Xu, J. Li, A. Zhang, Y. Dai, Y. Ji, and J. Lin, "Complexity-reduced digital predistortion for subcarrier multiplexed radio over fiber systems transmitting sparse multi-band RF signals," *Opt. Exp.*, vol. 21, no. 3, pp. 3708-3714, Feb. 2013.

[60] Y. Zhang, J. Li, H. Chen, C. Yin, Y. Dai, F. Yin, and K. Xu, "Clip-and-Filter-Based Crest Factor Reduction and Digital Predistortion for WLAN-Over-Fiber Links," *IEEE Photon. Technol. Lett.*, vol. 26, no. 23, pp. 2315-2318, Sept. 2014.

[61] C. H. Lee, V. Postoyalko, and T. O'Farrell, "Enhanced performance of RoF link for cellular mobile systems using postdistortion compensation," *IEEE Int. Symp. Pers. Indoor Mobile Radio Commun.*, pp. 2772-2776, Sept. 2004.

[62] J. Basak and B. Jalali, "Photodetector linearization using adaptive electronic post-distortion," *Opt. Fiber Commun. Conf. Expo.*, *Nat. Fiber Opt. Eng. Conf. (OFC/NFOEC)*, vol. 4, Mar. 2005.

[63] R. Duan, K. Xu, J. Dai, Q. Lv, Y. Dai, J. Wu, and J. Lin, "Digital linearization technique for IMD3 suppression in intersity-modulated analog optical links," *Int. Topical Meeting Microw. Photon., Asia Pacific Microw. Photon. (MWP/APMP)*, pp. 234-237, Oct. 2011.

[64] R. Duan, K. Xu, J. Dai, Y. Cui, J. Wu, Y. Li, Y. Dai, and J. Li, "Linearity improvement based on digital signal processing in intensity-modulated analog optical links incorporating photonic frequency downconversion," *Opt. Fiber Commun. Conf. Expo.*, *Nat. Fiber Opt. Eng. Conf. (OFC/NFOEC)*, JW2A, Mar. 2012.

[65] P. Li, R. Shi, M. Chen, H Chen, S. Yang, and S. Xie, "Linearized photonic if downconversion of analog microwave signals based on balanced detection and digital signal post-processing," *Int. Topical Meeting Microw. Photon. (MWP)*, pp. 68-71, Sept. 2012.

[66] X. Xie, Y. Dai, K. Xu, J. Niu, Y. Li, R. Wang, Y. Ji, and J. Lin, "Digital nonlinearities compensation based on forward distortion information acquisition in channelized RF photonic links," *Int. Topical Meeting Microw. Photon. (MWP)*, pp. 88-91, Sept. 2012.

[67] Y. Pei, J. Li, K. Xu, Y. Dai, Y. Ji, and J. Lin, "Digital multi-channel post-linearization for uplink in multi-band radio-over-fiber systems," *Opt. Fiber Commun. Conf. Expo.*, Mar. 2014.

[68] C. Yu, A. Zhu, "Single feedback loop-based digital predistortion for linearizing concurrent multi-band transmitters," *IEEE MTT-S Int. Microw. Symp. (IMS)*, Jun. 2014.

[69] L. M. Johnson and H. V. Roussell, "Reduction of intermodulation distortion in interferometric optical modulators," *Opt. Lett.*, vol. 13, issue 10, pp. 928-930, 1988.

[70] L. M. Johnson and H. V. Roussell, "Linearization of an interferometer modulator at microwave frequencies by polarization mixing," *IEEE Photon. Technol. Lett.*, vol. 2, issue 11, pp. 810-811, Nov. 1990.

[71] B. M. Haas and T. E. Murphy, "A simple, linearized, phase-modulated analog optical transmission system," *IEEE Photon. Technol. Lett.*, vol. 19, no. 10, pp. 729-731, May. 2007.

[72] B. Masella, B. Hraimel, and X. Zhang, "Enhanced spurious-free dynamic range using mixed polarization in optical single sideband Mach-Zehnder modulator," *J. Lightw. Technol.*, vol. 27, no. 15, pp. 3034–3041, Aug. 2009.

[73] B. Hraimel, X. Zhang, W. Jiang, K. Wu, T. Liu, T. Xu, Q. Nie, and K. Xu, "Experimental demonstration of mixed-polarization to linearize electro-absorption modulators in radio-over-fiber links," *IEEE Photon. Technol. Lett.*, vol. 23, no. 4, pp. 230-232, Feb. 2011.

[74] B. Hraimel and X. Zhang, "Performance improvement of radio-over fiber links using mixed-polarization electro-absorption modulators," *IEEE Trans. Microw. Theory Techn.*, vol. 59, issue 12, pp. 3239–3248, Dec. 2011.

[75] B. Hraimel and X. Zhang, "Characterization and compensation of AM-AM and AM-PM distortion in mixed polarization radio over fiber systems," *IEEE MTT-S Int. Microw. Symp. Dig.*, Jun. 2012.

[76] B. Hraimel, X. Zhang, T. Liu, T. Xu, Q. Nie, and D. Shen, "Performance enhancement of an OFDM ultra-wideband transmission-over-fiber link using a linearized mixed-polarization single-drive x-cut Mach-Zehnder modulator," *IEEE Trans. Microw. Theory Techn.*, vol. 60, issue 10, pp. 3328–3338, Oct. 2012.

[77] X. Chen, W. Li, and J. Yao, "Microwave photonic link with improved dynamic range using a polarization modulator," *IEEE Photon. Technol. Lett.*, vol. 25, no. 14, pp. 1373-1376, Jun. 2013.

[78] Y. Cui, Y. Dai, F. Yin, J. Dai, K. Xu, J. Li, and J. Lin, "Intermodulation distortion suppression for intensity-modulated analog fiber-optic link incorporating optical carrier band processing," *Opt. Exp.*, vol. 21, no. 20, pp. 23433-23440, Oct. 2013.

[79] D. H. Jeon, H. D. Jung, and S. K. Han, "Mitigation of dispersion-induced effects using SOA in analog optical transmission," *IEEE Photon. Technol. Lett.*, vol. 14, issue 8, pp. 1166-1168, Aug. 2002.

[80] J. Palaci, J. Herrera, and J. Marti, "EAM-SOA based millimeter-wave frequency up-conversion for radio-over-fiber applications," *Int. Topical Meeting Microw. Photon. (MWP)*, Oct. 2009.

[81] B. Hraimel and X. Zhang, "Suppression of radio over fiber system nonlinearity using a semiconductor optical amplifier and mixed polarization," *Opt. Fiber Commun. Conf. Expo. Nat. Fiber Opt. Eng. Conf. (OFC/NFOEC)*, OTHR2, Mar. 2013.

[82] D. J. M. Sabido, IX, M. Tabara, T. K. Fong, C. L. Lu, and L. G. Kazovsky, "Improving the dynamic range of a coherent am analog optical link using a cascaded linearized modulator," *IEEE Photon. Technol. Lett.*, vol. 7, no. 7, pp. 813-815, Jul. 1995.

[83] W. K. Burns, "Linearized optical modulator with fifth order correction," *J. Lightw. Technol.*, vol. 13, no. 8, pp. 1724–1727, Aug. 1995.

[84] J. D. Farina, B. R. Higgins, and J. P. Farina, "New linearization technique for analog fiber-optic links," *Opt. Fiber Commun.*, pp. 283-285, Mar. 1996.

[85] G. E. Betts and F. J. O'Donnell, "Microwave analog optical links using suboctave linearized modulators," *IEEE Photon. Technol. Lett.*, vol. 8, no. 9, pp. 1273-1275, Sept. 1996.

[86] E. I. Ackerman, "Broad-band linearization of a Mach–Zehnder electrooptic modulator," *IEEE Trans. Microw. Theory Techn.*, vol. 47, no. 12, pp. 2271-2279, Dec. 1999.

[87] A. Karim and J. Devenport, "High dynamic range microwave photonic links for RF signal transport and RF-IF conversion," *J. Lightw. Technol.*, vol. 26, no. 15, pp. 2718–2724, Aug. 2008.

[88] D. Marpaung, C. Roeloffzen, and W. van Etten, "Push-pull modulated analog photonic link with enhanced SFDR," *Int. Topical Meeting Microw. Photon.*, Oct. 2009.

[89] V. R. Pagan, B. M. Haas, and T. E. Murphy, "Linearized electrooptic microwave downconversion using phase modulation and optical filtering," *Opt. Exp.*, vol. 19, no. 2, pp. 883-895, Jan. 2011.

[90] J. Dai, K. Xu, R. Duan, Y. Cui, J. Wu, and J. Lin, "Optical linearization for intensity-modulated analog links employing equivalent incoherent combination technique," *Int. Topical Meeting Microw. Photon., Asia Pacific Microw. Photon. (MWP/APMP)*, pp. 230-233, Oct. 2011.

[91] Y. Cui, K. Xu, J. Dai, X. Sun, Y. Dai, Y. Ji, and J. Lin, "Overcoming chromatic-dispersion-induced power fading in rof links employing parallel modulators," *IEEE Photon. Technol. Lett.*, vol. 24, no. 14, pp. 1173-1175, Apr. 2012.

[92] H. Zhang, S. Pan, M. Huang, and X. Chen, "Linear analog photonic link based on cascaded polarization modulators," *Asia Commun. Photon. Conf.*, Nov. 2012.

[93] F. Wei, S. Li, X. Zheng, H. Zhang, and B. Zhou, "Improvement of optically generated adjacent channel interference in RoF systems," *IEEE Photon. Technol. Lett.*, vol. 25, no. 12, pp. 1137-1140, May 2013.

[94] K. K. Loi, J. H. Hodiak, X. B. Mei, C. W. Tu, and W. S. C. Chang, "Linearization of 1.3-μm MQW electroabsorption modulators using an all-optical frequency-insensitive technique," *IEEE Photon. Technol. Lett.*, vol. 10, no. 7, pp. 964-966, Jul. 1998.

[95] B. M. Hass, V. J. Urick, J. D. McKinney, and T. E. Murphy, "Dual-wavelength linearization of optical-modulated analog microwave signals," *J. Lightw. Technol.*, vol. 26, no. 15, pp. 2748–2753, Aug. 2008.

[96] Z. Wu, K. Xu, J. Niu, Q. Lv, Y. Dai, and J. Lin, "Third-order intermodulation distortion improvement radio-over-fiber link using dual-wavelength intensity modulation," *High Speed Intell. Commun. Forum*, May 2012.

[97] T. Iwai, K. Sato, and K. Suto, "Reduction of dispersion-induced distortion in SCM transmission systems by using predistortion-linearized MQW-EA modulators," *J. Lightwave Technol.*, vol. 15, issue 2, pp. 169–178, Feb. 1997.

[98] C. Lim, M. Attygalle, A. Nirmalathas, D. Novak, and R. Waterhouse, "Analysis of optical carrier-to-sideband ratio for improving transmission performance in fiber-radio links," *IEEE Trans. Microw. Theory Techn.*, vol. 54, no. 5, pp. 2181-2187, May 2006.

[99] C. Lim, A. Nirmalathas, K.-L. Lee, D. Novak, and R. Waterhouse, "Intermodulation distortion improvement for fiber–radio applications incorporating OSSB+C modulation in an optical integrated-access environment," *J. Lightw. Technol.*, vol. 25, no. 6, pp. 1602-1612, Jun. 2007.

[100] A. Ferreira, T. Silveira, D. Fonseca, R. Ribeiro, and P. Monteiro, "Highly linear integrated optical transmitter for subcarrier multiplexed systems," *IEEE Photon. Technol. Lett.*, vol. 21, no. 7, pp. 438-440, Feb. 2009.

[101] S. Li, X. Zheng, H. Zhang, and B. Zhou, "Highly linear radio-over-fiber system incorporating a single-drive dual-parallel Mach–Zehnder modulator," *IEEE Photon. Technol. Lett.*, vol. 22, no. 24, pp. 1775-1777, Sept. 2010.

[102] A. Agarwal, T. Banwell, P. Toliver, and T. K. Woodward, "Predistortion compensation of nonlinearities in channelized RF photonic links using a dual-port optical modulator," *IEEE Photon. Technol. Lett.*, vol. 23, no. 1, pp. 24-26, Nov. 2010.

[103] Q. Lv, K. Xu, Y. Dai, Y. Li, J. Wu, and J. Lin, "Nonlinear intermodulation distortion suppression in digital photonic link using polarization modulator," *Int. Topical Meeting Microw. Photon., Asia Pacific Microw. Photon. (MWP/APMP)*, pp. 262-265, Oct. 2011.

[104] G Zhang, S Li, X Zheng, H Zhang, B Zhou, and P Xiang, "Dynamic range improvement strategy for Mach-Zehnder modulators in microwave/millimeter-wave RoF links," *Opt. Exp.*, vol. 20, no. 15, pp. 17214-17219, Jul. 2012.

[105] W. Li and J. Yao, "Dynamic range improvement of a microwave photonic link based on bi-directional use of a polarization modulator in a Sagnac loop," *Opt. Exp.*, vol. 21, no. 13, pp. 15692-15697, Jul. 2013.

[106] Z. Chen, L. Yan, W. Pan, B. Luo, X. Zou, Y. Guo, H. Jiang, and T. Zhou, "SFDR enhancement in analog photonic links by simultaneous compensation for dispersion and nonlinearity," *Opt. Exp.*, vol. 21, no. 18, pp. 20999-21009, Aug. 2013.

[107] R. Zhu, X. Zhang, B. Hraimel, D. Shen, and T. Liu, "Broadband Predistortion Circuit Using Zero Bias Diodes for Radio over Fiber Systems," *IEEE Photon. Technol. Lett.*, vol. 25, no. 21, pp. 2101-2104, Nov. 2013.

[108] R. Zhu and X. Zhang, "Broadband Predistortion Circuit Design for Electro-Absorption Modulator in Radio over Fiber System," *Opt. Fiber Commun. Conf. Expo*., Mar. 2014.

[109] R. Zhu, Z. Xuan, and X. Zhang, "Novel broadband analog predistortion circuit for radio-over-fiber systems," *IEEE MTT-S Int. Microw. Symp.*, May 2015.

[110] R. Zhu and X. Zhang, "Linearization of radio-over-fiber systems by using two lasers with different wavelengths," *IEEE MTT-S Int. Microw. Symp.*, Jun. 2014.

Publications

Journal:

1. R. Zhu, X. Zhang, D. Shen, and T. Liu, "Analysis of dual wavelengths linearization technique for radio-over-fiber system with electro-absorption modulator," *IEEE Trans. Microw. Theory Tech.*, no. 99, pp. 1-11, Jun. 2015.
2. R. Zhu, X. Zhang, B. Hraimel, D. Shen, and T. Liu, "Broadband predistortion circuit using zero bias diodes for radio over fiber systems," *IEEE Photon. Technol. Lett.*, vol. 25, no. 21, pp. 2101-2104, Nov. 2013.
3. R. Zhu, B. Hraimel, and X. Zhang, "Analysis of simultaneous photonic frequency downconversion and optical subcarrier modulation in an electroabsorption modulator," *J. Lightw. Technol.*, vol. 30, no. 3, pp. 344–354, Feb. 2012.
4. X. Zhang, R. Zhu, D. Shen, and T. Liu, "Linearization technologies for broadband radio-over-fiber transmission systems," *MDPI Photonics*, vol. 10, no. 3390, pp. 455-472, Nov. 2014.
5. R. Zhu, Y. Zhang, X. Zhang, and D. Shen, "Ultra broadband predistortion circuit for radio-over-fiber transmission systems," submitted to *IEEE Trans. Microw. Theory Tech.*, Jul. 2015.
6. R. Zhu, Y. Zhang, X. Zhang, and D. Shen, "SFDR improvement of radio-over-fiber transmission system using dual wavelength linearization," to be submitted to *IEEE J. Opt. Commun. Netw.*. Aug. 2015.

Conference:

1. R. Zhu, Z. Xuan, and X. Zhang, "Novel broadband analog predistortion circuit for radio-over-fiber systems," *IEEE MTT-S Int. Microw. Symp.*, May 2015.
2. R. Zhu and X. Zhang, "Linearization of radio-over-fiber systems by using two lasers with different wavelengths," *IEEE MTT-S Int. Microw. Symp.*, Jun. 2014.
3. R. Zhu and X. Zhang, "Broadband predistortion circuit design for electro-absorption modulator in radio over fiber system," *Opt. Fiber Commun. Conf. Expo*., Mar. 2014.
4. X. Zhang, B. Hraimel, R. Zhu, D. Shen, and T. Liu, "Linearization techniques for broadband radio over fiber transmission," *Progress Electromagn. Res. Symp. Proc.*, pp. 1315-1320, Aug. 2013.